Research Report

Weld Reliability Analysis

FINAL REPORT

AISC RESEARCH REPORT NO. 02
AUGUST 2024

Project Title:	**Weld Reliability Analysis**
Primary Investigator(s):	**Bo Dowswell, Clayton Cox**
Research Organization(s):	**Arc International, LLC** **Hoar Construction**

DISCLAIMER

The material contained herein has been developed by researchers based on their research findings and is for general information only. The information in it should not be used without first securing competent advice with respect to its suitability for any given application. The publication of the information is not intended as a representation or warranty on the part of the American Institute of Steel Construction (AISC) or of any other person named herein, that the information is suitable for any general or particular use or of freedom from infringement of any patent or patents. Anyone making use of the information assumes all liability arising from such use.

PREFACE

The American Institute of Steel Construction (AISC), headquartered in Chicago, is a non-partisan, not-for-profit technical institute and trade association established in 1921 to serve the structural steel design community and construction industry in the United States. As part of its technical activities, AISC actively funds and supports research related to structural steel design and construction. AISC members primarily come from the structural steel construction community, including producers, fabricators, and engineers.

Many AISC members are engineers, so much of our research supports the engineering community, including maintaining and updating our technical publications such as Design Guides, The Steel Construction Manual, and our Specifications and Provisions. We distribute our specifications free for their use. The primary goal of those specifications is the reliability of structures and, through that, the safety of the public.

AISC does not use the results of research for profit, nor do we sell reports of the research or derivatives from it. Our work is performed in the interest of public safety. As such, we fund projects to, in part, support the development of next-generation steel systems for enhanced performance, safety, sustainability, and economy.

It is reasonably common for AISC research projects to receive additional direct, indirect, or in-kind support from external organizations such as federal or state agencies or member companies . As such, the partial or complete contents of this Report may also reside in the public domain of these external funding agencies.

WELD RELIABILITY ANALYSIS

FINAL REPORT

Submitted to

AMERICAN INSTITUTE OF STEEL CONSTRUCTION

August 31, 2024

by

Bo Dowswell, P.E., Ph.D.
ARC International, LLC
Birmingham, AL
bo@arcstructural.com

Clayton Cox
Hoar Construction
Birmingham, AL
ccox@hoar.com

TABLE OF CONTENTS

CHAPTER 1
INTRODUCTION

This report uses data from existing research to calculate appropriate resistance factors for various welded joints using a first-order reliability analysis. The AISC *Specification* (AISC, 2022) is the primary basis for the analysis, however, design methods in the AISC *Manual* (AISC, 2023) and AWS D1.1 (AWS, 2020) were used where necessary. The following joint types were included in the analysis:

1. Concentrically loaded, normal strength fillet welds
    a. Longitudinally loaded fillet welds
    b. Transversely loaded fillet welds
    c. Fillet welds with skewed load angles
    d. Multi-orientation fillet weld groups
    e. Welds with skewed dihedral angles
    f. Single-sided fillet welds
2. Partial-joint-penetration (PJP) welds
    a. Longitudinally loaded PJP welds
    b. Transversely loaded PJP welds
3. Concentrically loaded, high strength fillet welds
    a. High strength longitudinally loaded fillet welds
    b. High strength transversely loaded fillet welds
4. Eccentrically loaded fillet weld joints

CHAPTER 2
SPECIFICATIONS, CODES AND MANUALS

In this chapter, the design methods in various specifications, codes and manuals are reviewed.

AISC *SPECIFICATION* (AISC, 2022)

The strength of welded joints is defined by Equation J2-3 in AISC *Specification* Section J2.4(a). For each condition, the weld metal nominal stresses, F_{nw}, are listed in Table J2.5 along with the corresponding values for ϕ (LRFD) and Ω (ASD).

For partial-joint-penetration (PJP) welds

$$R_n = F_{nw}A_{we} \qquad \text{(}Spec.\text{ Eq. J2-3)}$$

For PJP welds that are subjected to shear or tension normal to the weld axis, Table J2.5 specifies $F_{nw} = 0.60F_{EXX}$. For shear loading, $\phi = 0.75$ (LRFD) and $\Omega = 2.00$ (ASD). For tension loading normal to the weld axis, $\phi = 0.80$ (LRFD) and $\Omega = 1.88$ (ASD). The effective area, A_{we}, of groove welds is defined in Section J2.1a as the length times the effective throat, E. The effective throat is based on the welding process, the welding position and the groove type according to Table J2.1. For example, for FCAW in the flat (F) or horizontal (H) position with a 45° bevel groove, the effective throat is equal to the groove depth, S.

For fillet welds

$$R_n = F_{nw}A_{we}k_{ds} \qquad \text{(}Spec.\text{ Eq. J2-4)}$$

For fillet welds, Table J2.5 specifies $F_{nw} = 0.60F_{EXX}$ and $\phi = 0.75$ (LRFD) and $\Omega = 2.00$ (ASD). The effective area, A_{we}, of fillet welds is defined in Section J2.2a as the effective length times the effective throat, E. The effective throat is the shortest distance from the root to the face of the diagrammatic weld. When strain compatibility of the various weld elements is considered, the directional strength increase factor is

$$k_{ds} = 1.0 + 0.50\sin^{1.5}\theta \qquad \text{(}Spec.\text{ Eq. J2-5)}$$

For all other conditions, including fillet welds at the ends of rectangular HSS loaded in tension, $k_{ds} = 1.0$.

where

A_{we} = effective area of the weld, in.^{2}
E = effective throat of the weld, in.
F_{EXX} = filler metal classification strength, ksi
F_{nw} = nominal stress of the weld metal, ksi
k_{ds} = directional strength increase factor

θ = angle between the line of action of the required force and the weld longitudinal axis as shown in Figure 2.1, degrees

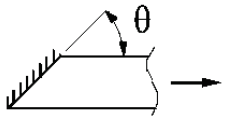

Fig. 2.1. Loading angle for fillet welds.

For concentrically loaded joints consisting of both longitudinal and transverse fillet welds with a uniform leg size, the strength is permitted to be calculated with *Specification* Equation J2-6. Alternatively, the strength of these weld groups can be calculated by summing the individual weld strengths with k_{ds} = 1.0 used in lieu of 1.5 for the transverse welds.

$$R_n = 0.85F_{nw}A_{wel} + 1.5F_{nw}A_{wet} \quad \text{(}Spec.\text{ Eq. J2-6)}$$

where

A_{wel} = effective area of longitudinally loaded fillet welds, in.^{2}
A_{wet} = effective area of transversely loaded fillet welds, in.^{2}

Design requirements for end loaded fillet welds with high l/w ratios are in AISC *Specification* Section J2.2b(d). When $l/w \leq 100$, the effective length is equal to the actual length. When $100 < l/w \leq 300$, the effective length is calculated by multiplying the actual length by the reduction factor, β, according to Equation J2-1. When $l/w > 300$, the effective length is $180w$.

$$\beta = 1.2 - 0.002\left(\frac{l}{w}\right) \leq 1.0 \quad \text{(}Spec.\text{ Eq. J2-1)}$$

where

l = actual length of end-loaded weld, in.
w = weld leg size, in.

AWS D1.1 (AWS, 2020)

The requirements for concentrically loaded fillet and PJP weld strengths in AWS D1.1 are similar to the ASD provisions in the AISC *Specification*. Equations 2.1 through 2.6 are required to calculate the strength of eccentrically loaded fillet weld groups with the instantaneous center of rotation (ICR) method according to AWS D1.1 Subclause 4.6.4.3.

$$F_{vi} = 0.3F_{EXX}(1.0 + 0.50\sin^{1.5}\theta)F(\rho) \quad (2.1)$$

$$F(\rho) = [\rho(1.9 - 0.9\rho)]^{0.3} \quad (2.2)$$

$$\rho = \frac{\Delta_i}{\Delta_m} \tag{2.3}$$

$$\Delta = 0.209w(\theta + 6)^{-0.32} \tag{2.4}$$

$$\Delta_u = 1.087w(\theta + 6)^{-0.65} < 0.17w \tag{2.5}$$

$$\Delta_i = \Delta_u \frac{r_i}{r_{crit}} \tag{2.6}$$

where

F_{vi} = allowable stress of the weld metal, ksi
r_{crit} = distance from the instantaneous center of rotation to the weld element with the minimum Δ_u/r_i ratio, in.
r_i = distance from the instantaneous center of rotation to element i, in.
Δ_m = deformation of weld element at maximum stress, in.
Δ_u = deformation of weld element at ultimate stress (rupture), in.
Δ_i = deformation of weld element at intermediate stress levels, in.

Butler et al (1972) originally developed the ICR method based on the empirical load-deformation curves from Butler and Kulak (1971), who tested concentrically loaded linear fillet welds at angles of 0°, 30°, 60° and 90° from the loading direction. The equations in AWS D1.1 Subclause 4.6.4.3 were primarily developed by Lesik and Kennedy (1990), except that their polynomial function for $F(\rho)$ was replaced by the simpler empirical approximation of Equation 2.2. Also, an upper limit of $0.17w$ was added to the original equation for Δ_u, resulting in Equation 2.5. Lesik and Kennedy (1990) used linear regression to develop the load-deformation curves with the data from Miazga and Kennedy (1989), who tested 70 ksi concentrically loaded linear fillet welds with varying load angles from 0 to 90° in 15° increments.

For multi-orientation fillet weld groups, Section 4.6.4.4 specifies an allowable load equal to the sum of the strengths of each weld, ΣF_{vi}, where $F_{vi} = 0.30CF_{EXX}$. Values for coefficient C are listed in Table 4.4 for various weld orientation combinations. These coefficients were calculated using the equations in Subclause 4.6.4.3. For joints that combine longitudinal ($\theta = 0°$) and transverse ($\theta = 90°$) welds, $C = 0.825$ for the longitudinal welds and $C = 1.50$ for the transverse welds. For joints that combine welds with load angles of 45° and 90°, $C = 1.29$ for the skewed welds and $C = 1.50$ for the transverse welds. The coefficients in Table 4.4 are reproduced in Table 8-1 of the AISC *Manual*.

When the fillet weld dihedral angle, ψ, is between 80° and 100°, Subclause 4.4.2.6 allows the effective throat to be calculated using $\psi = 90°$. For other conditions, Subclause 4.4.3 requires the effective throat the calculated busing the actual geometry, considering the effect of the Z loss dimension when $30° \le \psi < 60°$. The Z loss dimension addresses the potential area of incomplete fusion near the weld root. The values for Z are listed in D1.1 Table 4.2 for various dihedral angles,

welding processes and welding positions. AWS D1.1 Annex A provides further information on the calculation of effective throat dimensions in skewed T-joints.

AISC *MANUAL* (AISC, 2023)

Eccentrically loaded weld groups are discussed in Part 8 of the AISC *Manual*. Figure 2.2a shows a fillet weld group with eccentricity in the plane of the faying surface. These welds can be analyzed with either the ICR method or the elastic method.

Figure 2.2b shows a fillet weld group with eccentricity perpendicular to the plane of the faying surface. Several methods are available to analyze these welds, including the ICR method, the elastic method and the plastic method. Additionally, these joints can be designed using the bearing strength of the connecting elements on the compression side of the neutral axis and the weld strength on the tension side of the neutral axis.

When the plastic method is used, two options are available for combining the normal force and moment. For the conventional plastic method, the stresses caused by the normal force and the moment are summed as shown in Figure 2.3a. The optimum plastic method is based on the traditional plastic stress distribution shown in Figure 2.3b.

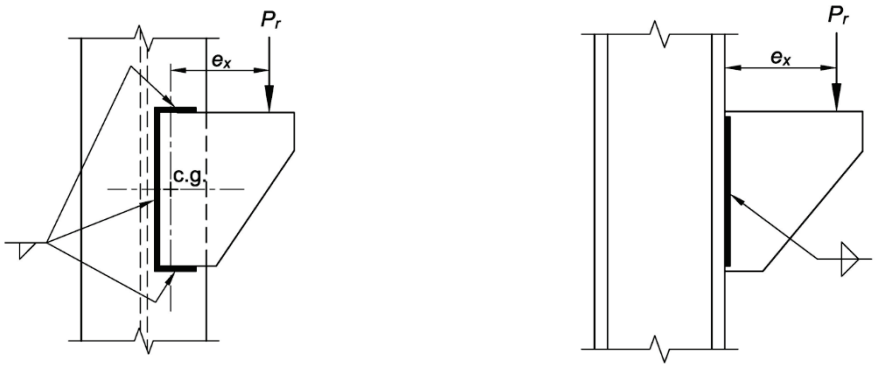

a. In-plane eccentricity *b. Out-of-plane eccentricity*

Fig. 2.2. Eccentrically loaded weld groups.

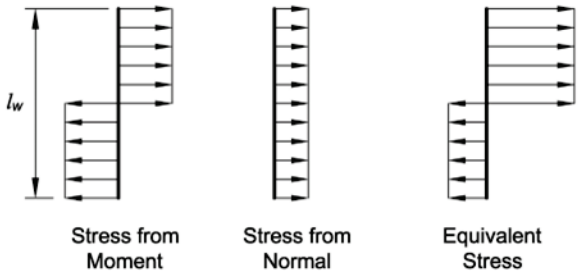

a. Conventional plastic method

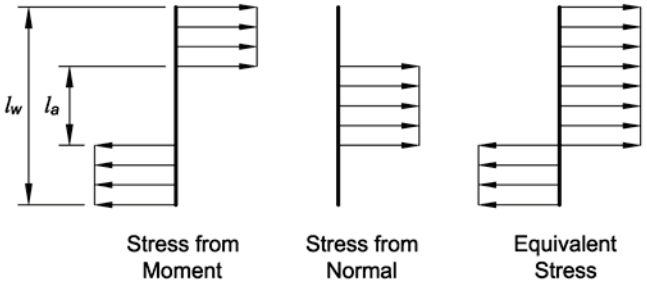

b. Optimum plastic method

Fig. 2.3. Plastic method normal stresses.

CANADIAN STANDARD S16-14 (CSA, 2014)

Canadian Standard S16-14 (CSA, 2014) specifies Equation 2.7 for the strength of concentrically loaded linear fillet weld groups. Equation 2.8 defines M_w, which is a coefficient that accounts for any differences in the weld deformation capacity that are caused by their orientation. In the case of a single fillet weld, $M_w = 1.0$.

$$R_n = 0.67 F_{EXX} (1.0 + 0.50 \sin^{1.5}\theta) A_{we} M_w \tag{2.7}$$

$$M_w = \frac{0.85 + \theta_1/600}{0.85 + \theta_2/600} \tag{2.8}$$

where

ϕ = 0.67

θ_1 = angle between the line of action of the required force and the weld longitudinal axis for the weld segment under consideration, degrees

θ_2 = angle between the line of action of the required force and the weld longitudinal axis for the weld segment in the group that is oriented nearest to 90°

EN 1993-1-8 (CEN, 2005)

Eurocode 3 Part 1-8 (CEN, 2005) is limited to steel grades S235 up to and including S460. Section 4 allows two design methods for welded connections: the directional method and the simplified method. According to Section 4.2(2), "the ultimate tensile strength of the filler metal should be equivalent to, or better than that specified for the base material." The directional method is applicable to both fillet and PJP welds. Both Equation 2.9 and 2.10 must be satisfied.

$$\sqrt{\sigma_T^2 + 3\left(\tau_T^2 + \tau_L^2\right)} \le \frac{F_u}{\beta_w \gamma_{M2}} \tag{2.9}$$

$$\sigma_T \le \frac{0.9F_u}{\gamma_{M2}} \tag{2.10}$$

For the simplified method, which is applicable only to fillet welds, the available stress at the theoretical effective throat is calculated with Equation 2.11.

$$F_{nw} \le \frac{F_u}{\sqrt{3}\beta_w \gamma_{M2}} \tag{2.11}$$

where

F_u = specified minimum tensile strength of the base metal, ksi
β_w = correlation factor according to Table 2.1
γ_{M2} = partial safety factor, = 1.25
σ_T = normal stress perpendicular to the plane of the throat, ksi.
τ_L = shear stress in the plane of the throat, parallel to the weld axis, ksi.
τ_T = shear stress in the plane of the throat, perpendicular to the weld axis, ksi.

Table 2.1. Correlation factors for fillet welds in EN 1993-1-8 (CEN, 2005).

Steel Grade	F_u (MPa)	F_u (ksi)	β_w
S235	340-360	49.3-52.2	0.80
S275	360-430	52.2-62.4	0.85
S355	450-510	65.3-74.0	0.90
S420	500-540	72.5-78.3	1.0
S460	530-570	76.9-82.7	1.0

The Section 4.11 design requirements for fillet welds with high *l*/*w* ratios are similar to those in AISC *Specification* Section J2.2b(d), except the effective throat is used instead of the weld leg size. For lap joints longer than 150*E*, Equation 2.12 is applicable.

$$\beta = 1.2 - \frac{0.2l}{150E} \le 1.0 \tag{2.12}$$

Section 4.12 is applicable to eccentrically loaded single-sided fillet and PJP welds. Welds are required to be "designed according to elastic design rules" when flexure about the weld longitudinal axis results in tension stress at the root. Section 4.12(1) requires that "local eccentricity should be avoided where possible." Section 4.12(1) allows local eccentricity to be neglected for welds around the perimeter of HSS shapes.

EN 1993-1-12 (CEN, 2007)

Eurocode 3 Part 1-12 (CEN, 2007) provides additional requirements for steel grades from S460 up to and including S700. For undermatched electrodes, Section 4.5.3.2(6) requires the joint strength to be based on the strength of the filler metal. For longitudinal fillet welds in lap joints, Section 4.11 requires the effect of uneven stress distribution to be considered when the length is greater than 50*E*.

PREN 1993-1-8 (CEN, 2021)

The latest draft of Eurocode 3 Part 1-8 (CEN, 2021) is applicable to all steel grades from S235 up to and including S700 unless otherwise stated in individual clauses. Section 4 lists revised correlation factors and provides new correlation factors for high strength steels according to Table 2.2.

Table 2.2. Correlation factors for fillet welds in prEN 1993-1-8 (CEN, 2021).

Steel Grade	F_u (MPa)	F_u (ksi)	β_w
S235	340-360	49.3-52.2	0.80
S275	360-430	52.2-62.4	0.85
S355	450-510	65.3-74.0	0.90
S420	500-540	72.5-78.3	0.88
S450	550	79.8	1.05
S460	530-570	76.9-82.7	0.85
S500	550	79.8	0.90
S550	590-640	85.6-92.8	0.95
S620	650-700	94.3-101	1.05
S690	710-770	103-112	1.10

For steel grades higher than S460 with mismatched filler metals, the strength of fillet welds can be calculated with Equations 2.10 and 2.13 for the directional method and Equation 2.14 for the simplified method.

$$\sqrt{\sigma_T^2 + 3\left(\tau_T^2 + \tau_L^2\right)} \le \frac{0.25F_u + 0.75F_{EXX}}{\sqrt{3}\beta_{wm}\gamma_{M2}} \tag{2.13}$$

$$F_{nw} \le \frac{0.25F_u + 0.75F_{EXX}}{\sqrt{3}\beta_{wm}\gamma_{M2}} \tag{2.14}$$

where

β_{wm} = modified correlation factor according to Table 2.3

Table 2.3. Modified correlation factors for filler metals in prEN 1993-1-8 (CEN, 2021).			
Strength Class	F_{EXX} **(MPa)**	F_{EXX} **(ksi)**	β_{wm}
42	500	72.5	0.89
46	530	76.9	0.85
69	770	112	1.09
89	940	136	1.19

For long lap joints connected by fillet welds, Equation 2.12 remains unchanged. However, for steel grades equal to or higher than S460, the length of longitudinal fillet welds in lap joints is limited to 150*E*.

AIJ RECOMMENDATIONS (AIJ, 2012)

The Architectural Institute of Japan *Recommendations for Design of Connections in Steel Structures* (AIJ, 2012) specifies Equation 2.15 for calculating the strength of fillet welds. Equations 2.16 and 2.17 are applicable to longitudinal and transverse PJP welds, respectively. Because Equation 2.17 is based on the tensile strength of the base metal, it is valid only when matching or overmatching weld metal is used.

$$F_{nw} \le \frac{F_{EXX}}{\sqrt{3}}\left(1.0 + 0.40\sin\theta\right) \tag{2.15}$$

$$F_{nw} \le \frac{F_{EXX}}{\sqrt{3}} \tag{2.16}$$

$$F_{nw} = F_u \tag{2.17}$$

where

F_u = specified minimum tensile stress of the weaker base metal joined, ksi

CHAPTER 3
LITERATURE REVIEW

This chapter provides a review of the available literature on weld strength. Although the review focuses on the research with experimental test data, design methods and supplementary information are also included.

FILLET WELDS

In this section, the available literature related to concentrically loaded, normal strength fillet welds is reviewed.

ABW (1931)

ABW (1931) reported a comprehensive series of experimental tests on many different configurations for both fillet and groove welds. The specified tensile strength of the weld metal was 56 ksi. The tensile strength was measured using 20 specimens each for the 34 primary welders in the study using a complete penetration welded coupon subjected to tension. This resulted in a weighted average rupture strength of 53.7 ksi. The average shear rupture strength on the throat of the concentrically loaded fillet weld specimens was 42.5 ksi and the average strength of butt welds in tension was 49.6 ksi.

AWS (1937)

The early research on fillet welded connections was primarily concerned with the elastic stress distributions, both along the weld length and in the weld cross section. The available research on fillet-welded joints prior to 1937, consisting of 150 references, was summarized in AWS (1937). The research shows highly nonlinear stresses along the length and in the weld cross section, even for the simplest configurations.

Rosenthal and Levray (1939)

Rosenthal and Levray (1939) tested longitudinally loaded fillet welds in double-lap joints. The primary objective of the research was to determine the elastic stress distribution in the joints; however, ten specimens were tested to destruction. Only four of these specimens ruptured along the weld throat. The specimens were fabricated using the SMAW process. The measured weld metal tensile strength, σ_{uw}, was 57.0 ksi. The specified weld sizes were ⅛ in. and the welds were machined to the specified triangular cross section and length before testing. For the four specimens that ruptured along the weld throat, the mean rupture stress was 47.5 ksi, which is $0.833\sigma_{uw}$.

Godfrey and Mount (1940)

Godfrey and Mount (1940) tested fillet welds in single-lap, double-lap and tee joints. The testing program included longitudinal specimens, transverse specimens and specimens with combined longitudinal and transverse welds. The specimens were fabricated with ASTM Grade 10 electrodes using the SMAW process. The electrodes had a specified minimum tensile strength of 60 ksi. The actual tensile strength, measured with all-weld-metal specimens, σ_{uw}, was 78.25 ksi. The measured tensile strength of the base metals was approximately 75% of the measured weld metal tensile

strength. The specified weld sizes were 5⁄16, ½ and ¾ in.; however, measured weld dimensions were not reported.

The nine longitudinally loaded specimens ruptured along the weld throat at a mean stress of 51.5 ksi, which is $0.658\sigma_{uw}$. The nine transversely loaded double-lap joint specimens ruptured along the weld throat at a mean stress of 76.4 ksi, which is $0.976\sigma_{uw}$. The transverse-to-longitudinal strength ratio is 1.48.

The three transversely loaded T-joint specimens ruptured along the weld throat at a mean stress of 61.6 ksi, which is $0.787\sigma_{uw}$. Compared to the transversely loaded double-lap specimens, the rupture stress of the T-joint specimens was 19.4% lower.

For the nine transversely loaded single-lap single weld specimens, "the specimens became distorted…and considerable bending took place in the fillet welds." Compared to the transversely loaded double-lap specimens, the rupture stress of the single-lap specimens was 27.6% lower.

For the three specimens with combined longitudinal and transverse welds, the strengths can be accurately calculated by summing the individual strengths, including the 50% directional strength increase for the transverse welds and no reduction for the longitudinal welds.

Spraragen and Claussen (1942)

Spraragen and Claussen (1942) reviewed 77 references on fillet welds that were published between 1932 and 1939. For longitudinally loaded fillet welds, the rupture stress at the throat is between 0.64 and 0.84 times the uniaxial tensile strength. Although longitudinally loaded fillet welds had high elastic stress concentrations at the end, it was shown that the rupture strength of short welds (l/w between 1.4 and 19), is unaffected by the weld length.

Tests on double-lap specimens with transversely loaded fillet welds showed that the specimens with tensile loads were approximately 20% higher than for compression-loaded specimens. Also, several research projects showed that the rupture strength of transversely loaded T-joints varies between 75% and 100% of the strength of double-lap specimens. This effect was caused by the constraint provided by the transverse contact force at the faying surfaces as well as the friction resulting from these forces. A gapped T-joint specimen designed by Kist (1936) to eliminate the transverse force at the faying surfaces had only 64% of the strength of a double-lap transverse tension specimen with similar welds. Hankins and Brown (1938) tested double-lap specimens with a cutout in the middle plate to eliminate any contact between the outer plates and the inner plates. Compared to otherwise identical specimens without the cutouts, the specimens with the cutouts had 25% reduction in strength. It was concluded that the rupture stress at the throat of transversely loaded fillet welds was slightly higher than the uniaxial tensile strength measured with all-weld-metal coupons.

Wilson et al. (1949)

The primary objective of the research by Wilson et al. (1949) was to determine the fatigue performance of welded joints; however, the static testing of joints with various weld group configurations was also documented. The static testing program included four longitudinal

specimens, eight transverse specimens and ten specimens with combined longitudinal and transverse welds.

The specimens were fabricated with E6010 electrodes using the SMAW process. Although the weld metal tensile strength was not measured, the expected tensile strength of the weld metal can be calculated with the values from Table 4.1, where $\sigma_{uw} \approx \rho_{MI} F_{EXX}$. = (1.06)(60 ksi) = 63.6 ksi.

The specified weld sizes were ¼, 5⁄16 and ½ in. The throat dimensions were measured prior to testing and the rupture surfaces were measured after testing. Although the measured throat dimensions were "slightly oversize," the rupture surfaces were "slightly less" than the measured throat dimensions. This indicates that the "penetration was not quite perfect."

Eb (1952)

Eb (1952) tested transversely loaded fillet welds in double-lap, tee and gapped tee joints. The gapped T-joint specimens, which were similar to those tested by Kist (1936), eliminated the transverse force on the faying surface. The T-joint specimens had only 68% of the strength of a double-lap transverse tension specimens with similar welds. The gapped T-joint specimens had only 61% of the strength of a double-lap transverse tension specimens with similar welds.

Vreedenburgh (1954)

Vreedenburgh (1954) continued the work of Kist (1936) with supplementary tests and analyses. Although Kist assumed the rupture plane was always defined by the theoretical throat, Vreedenburgh found out that the rupture planes were not always coincident with the theoretical throat. Additionally, Vreedenburgh found that the experimental behavior was not compatible with any of the available failure theories. Because of this, an empirical solution was adopted. As shown in Figure 3.1, the shear strength of the weld was assumed to be 0.75 times the weld metal uniaxial tensile strength. For transversely loaded equal-leg welds, the weld throat is oriented 45° from the load and the strength is $0.84\sigma_t$. Based on this approach, the ratio of the transverse fillet weld strength to longitudinal fillet weld strength is 0.84/0.75 = 1.12. Also, according to Figure 3.1, welds subjected to compression at the effective throat are 70% stronger than welds subjected to tension at the effective throat.

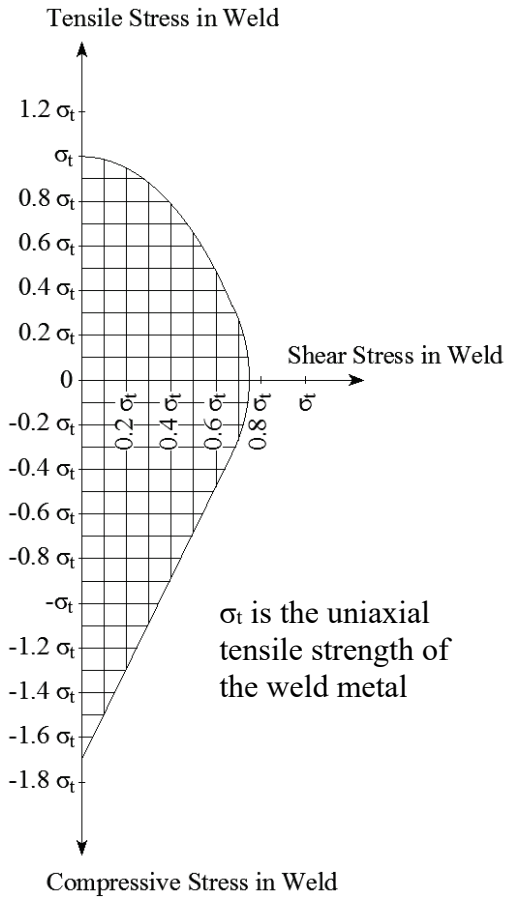

Fig. 3.1. Fillet weld critical limiting stress according to Vreedenburgh (1954).

Wastlund and Ostlund (1956)

Wastlund and Ostlund (1956) tested 30 longitudinally loaded fillet weld specimens. Only 28 of the specimens were tested to destruction. Each end of the specimen had four 80 mm long fillet welds and the connected bar heights varied from 20 to 45 mm to determine the effect of eccentricity. The specimens were fabricated with Philips Ph 48 electrodes using the SMAW process. The electrodes had a measured tensile strength, σ_{uw}, of 5,750 kg/cm^2 (81.8 ksi). The specified throat was 3.5 mm, and the welds were ground to obtain the proper throat within ± 0.2 mm. Because all 30 specimens had similar strengths, the effect of the bar height is negligible. The mean rupture stress was $0.686\sigma_{uw}$.

Three additional longitudinally loaded fillet weld specimens were tested to destruction. For this group, the weld lengths (70, 70 and 140 mm) and throat dimensions (3.5, 6.0 and 3.0 mm) varied. The mean rupture stress for these three specimens was $0.748\sigma_{uw}$ and the mean rupture stress for all 33 specimens was $0.692\sigma_{uw}$.

Archer et al. (1964)

Archer et al. (1964) compared different failure theories with experimental results to determine which one best represents the actual strength of fillet welds. The failure theories included

maximum principal stress, maximum shear stress and von-Mises. The comparisons also included calculations that considered the moments at the weld legs that were caused by the small eccentricity between the load and the resisting force; however, the results were more accurate when these moments were neglected. The authors determined that the maximum shear stress method, while neglecting the moment in the weld, provides the best fit. The predicted orientation angle of the rupture plane compared well with the experimental results. Nevertheless, the calculated weld strength using maximum shear stress slightly underestimated the experimental strength that was determined using double-lap specimens with longitudinal welds.

Douwen and Witteveen (1966)
Douwen and Witteveen (1966) recommended combining the normal and shear stresses on the theoretical effective throat using von Mises equation. Because von Mises yield criterion was found to be conservative, the resulting effective stress was multiplied by a correlation factor, β_{dw}, that is dependent on the base metal strength. The authors recommended $\beta_{dw} = 0.7$ for St 37 steel and 0.85 for St 51 steel. Both the International Institute of Welding (IIW, 1976) and Eurocode 3 (CEN, 2005) adopted this approach later.

Bornscheuer and Feder (1966)
Bornscheuer and Feder (1966) tested 21 longitudinal and 8 transverse fillet welded joints with leg sizes between 0.18 and 0.63 in. For the longitudinal welds, the weld length varied from 3.94 to 11.8 in. The specimens were fabricated with 70 ksi electrodes; however, the weld metal tensile strength was not measured. The expected tensile strength of the weld metal can be calculated with the value from Table 4.1, which results in $\sigma_{uw} \approx (1.04)(70 \text{ ksi}) = 72.8 \text{ ksi}$. Li et al. (2007) provides further information on these tests.

Swannell (1968)
To obtain a uniform shear distribution along the weld length, Swannell (1968) subjected 15 round specimens with circular fillet weld groups to torsional moments. The original 5⁄16-in. fillet welds were machined to equal-leg ¼-in. welds. Post-test inspections of the rupture surfaces indicated "very little root penetration in any of the welds." The measured weld metal uniaxial tensile strength was 64.4 ksi and the mean rupture stress at the throat was 57.0 ksi, resulting in an average shear strength equal to 88.5% of the tensile strength.

Preece (1968), Higgins and Preece (1969)
Preece (1968) and Higgins and Preece (1969) documented 168 tests on double-lap specimens with either longitudinal or transverse fillet welds. The variables were weld size (¼, ⅜ and ½-in.), electrode strength (60, 70, 90 and 110 ksi), weld length (1.5, 2, 3 and 4 in.) and base metal (ASTM A36, A441 and A514). Although the weld metal tensile strength was not measured, the expected tensile strength of the weld metal can be calculated with the values from Table 4.1, where $\sigma_{uw} \approx \rho_{M1} F_{EXX}$.

The experimental rupture stress increased slightly with length; however, the increase of 3% was deemed negligible. All specimens ruptured in the weld metal "even when the mechanical properties of the weld metal exceeded those of the base metal by a substantial amount." The transverse welds averaged 1.57 and 1.44 times stronger than longitudinal welds for 70 and 110 ksi electrodes, respectively.

For the ¼-in. fillet welds, the average measured weld size was 20% greater than the specified size. For the ⅜ and ½-in. fillet welds, the average measured weld sizes were 13 and 5% greater than the specified sizes, respectively.

Ligtenburg (1968)

Ligtenburg (1968) compiled the data from a series of experiments where fillet-welded joints were tested in nine different countries. The specimens were double- and single-lap joints with longitudinal, transverse and combined longitudinal/transverse welds. All specimens were welded with the SMAW process. The weld sizes and plate material properties varied. Only the results from double-lap specimens were used in this report. Several of the specimens ruptured in the plates; however, only the specimens that ruptured in the welds were included in the data. The results are based on the measured weld lengths and leg sizes, as well as the measured tensile strength of the weld metal.

The results were compared to the "ISO formula," which is Equation 3.1. This results in $F_{nw} = 0.745F_{EXX}$ for longitudinal welds, $F_{nw} = 0.845F_{EXX}$ for transverse welds and $k_{ds} = 1.13$. Using a regression analysis, the authors showed that the "ISO formula" is conservative. The proposed rupture stresses are $F_{nw} = 0.84\sigma_c$ for longitudinal welds (standard deviation = 14.5%) and $F_{nw} = 1.37\sigma_c$ for transverse welds (standard deviation = 10%), resulting in $k_{ds} = 1.63$.

$$\sqrt{\sigma_T^2 + 1.8\left(\tau_T^2 + \tau_L^2\right)} \le \sigma_c \tag{3.1}$$

$$\sigma_c \le \frac{F_{EXX} + F_u}{2} \tag{3.2}$$

For joints with multi-orientation fillet weld groups, the total weld strength is the sum of the transverse and longitudinal weld strengths with a reduction in the regression coefficients: $F_{nw} = 0.78\sigma_c$ for longitudinal welds and $F_{nw} = 1.25\sigma_c$ for transverse welds. This results in a standard deviation of 11.7%.

Strating (1971)

Strating (1971) tested 38 different specimens with three duplicates each for a total of 114 tests. The specimens were similar to Lightenburg's double-lap specimens; however, the FCAW, GMAW and SAW processes were used instead of SMAW. Both self-shielded and gas-shielded (CO_2) FCAW was used. The GMAW shielding gases were CO_2 and Argon/CO_2/O_2.

The authors recommended that the weld rupture strength calculations should be based on the average tensile stress of the base metal and the weld metal. A linear regression analysis showed that the strength of longitudinally and transversely loaded welds can be predicted with Equations 3.3 and 3.4, respectively. A conclusion from the tests on joints with combined longitudinal and transverse welds is that failure of the transverse welds always precludes failure of the longitudinal welds at loads that are less than the sum of the independent strengths.

$$R_n = 0.83F_{EXX}A_{we} \tag{3.3}$$

$$R_n = 1.33F_{EXX}A_{we} \tag{3.4}$$

The design recommendations were based on weld areas that were calculated using pre-test throat dimensions measured 45° from the connected plates. Therefore, the effect of any convexity or concavity was considered. Although the effect of penetration was not considered in the recommendations, several specimens were sectioned after testing for penetration measurements. The results are listed in Table 3.1. As expected, the SAW welds had the largest mean penetration depth (0.130 in.).

Table 3.1. Penetration measurements by Starting (1971).

Process	Shielding Gas	Penetration (in.)		
		Mean	Min.	Max.
FCAW-S		+0.0381	–0.0197	+0.110
FCAW-G	CO_2	+0.00504	–0.0197	+0.0307
GMAW	CO_2	+0.0689	+0.0256	+0.118
GMAW	Argon/CO_2/O_2	+0.0500	–0.0394	+0.110
SAW		+0.130	+0.0354	+0.197

Butler and Kulak (1969, 1971)

Butler and Kulak (1969, 1971) measured the load-deformation of fillet welds in 23 concentrically loaded double-lap joints. 60 ksi SMAW electrodes were specified to deposit ¼ in. fillet welds at angles of 0°, 30°, 60° and 90° from the loading direction. The authors found that the strength and ductility is dependent on the loading direction and developed empirical equations 3.5 through 3.9 to describe the load-deformation behavior of the specific welds that were tested. These equations are plotted in Figure 3.2 for θ = 0°, 30°, 60° and 90°. Equation 3.5 results in k_{ds} = 15.8/10.9 = 1.45 when θ = 90°. Additionally, eight eccentrically loaded connections were tested.

$$R = R_u(1 - e^{-\mu\Delta})^{\lambda} \tag{3.5}$$

$$R_u = \frac{10 + \theta}{0.92 + 0.0603\theta} \tag{3.6}$$

$$\Delta_u = 0.225(\theta + 5)^{-0.47} \tag{3.7}$$

$$\mu = 75e^{0.0114\theta} \tag{3.8}$$

$$\lambda = 0.4e^{0.0146\theta} \tag{3.9}$$

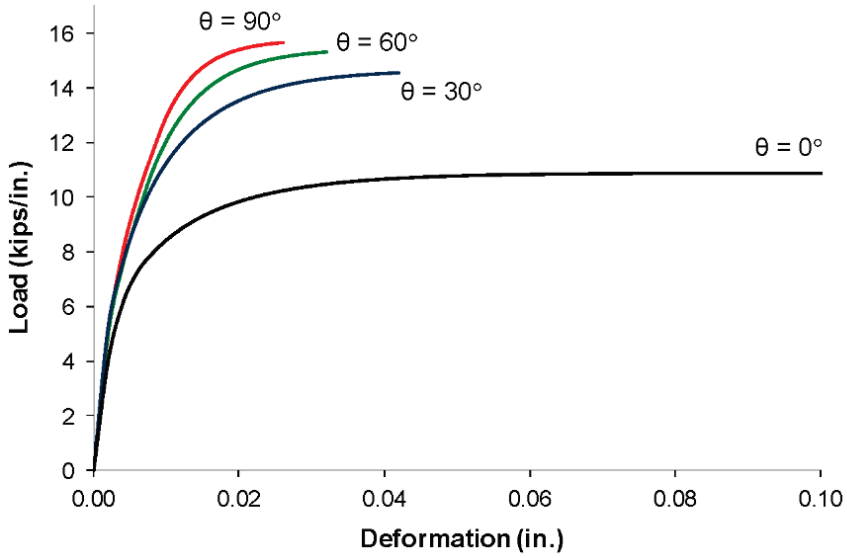

Fig. 3.2. Load-deformation curves for ¼ in. E60 fillet welds.

Clark (1971)

Clark (1971) tested 18 concentrically loaded double-lap specimens with a specified fillet weld size of 5⁄16 in. and load angles of 0°, 30°, 60° and 90°. The specimens were fabricated using the SMAW process with 60 ksi electrodes; however, the weld metal tensile strength was not measured. The expected tensile strength of the weld metal can be calculated with the value from Table 4.1, which results in $\sigma_{uw} \approx (1.06)(60\text{ ksi}) = 63.6\text{ ksi}$. Li et al. (2007) provides further information on these tests.

Kato and Morita (1974)

Kato and Morita (1974) calculated the strength of transverse fillet welds using the theory of elasticity and determined that the rupture plane is 22.5° from the loading direction. Based on this critical rupture plane, they developed a directional strength factor of

$$k_{ds} = \frac{1.0 - \pi/4}{\sin^2(22.5°)} = 1.46 \tag{3.10}$$

The authors compared their theoretical findings with the results from finite element models and 15 experimental tests, which verified the rupture plane orientation. The experimental specimens were double-lap joints. Although the stress distribution along the critical section was shown to be non-uniform, the proposed equations were shown reasonably accurate.

Swannell (1974)

Swannell (1974) tested 13 double-lap fillet weld specimens, including five specimens with longitudinally loaded welds, one transversely loaded specimen and seven multi-orientation specimens that combined both longitudinal and transverse welds. The welds were oversized and

machined to an ideal triangular shape with a weld leg size of ¼ in. The specimens were fabricated with the SMAW process using E6013 electrodes. The weld metal tensile strength, σ_w, from all-weld-metal coupons was 69.1 ksi and the elongation at rupture was 28.5%.

Higgs (1981), Biggs et al. (1981)

Based on cruciform specimens loaded in both directions as shown in Figure 3.3, Higgs (1981) and Biggs et al. (1981) recommended a circular interaction between the normal stresses and shear stresses on the critical section of fillet welds. Figure 3.4 shows that the orientation of the critical section varies with the load ratio, f_y/f_x. The stress interaction on the critical section is shown in Figure 3.5. Figure 3.6 shows the interaction between x- and y-direction loads, f_x and f_y, respectively. It is interesting to note that f_y increases with an increase in f_x up to approximately f_x/f_y.= 0.6.

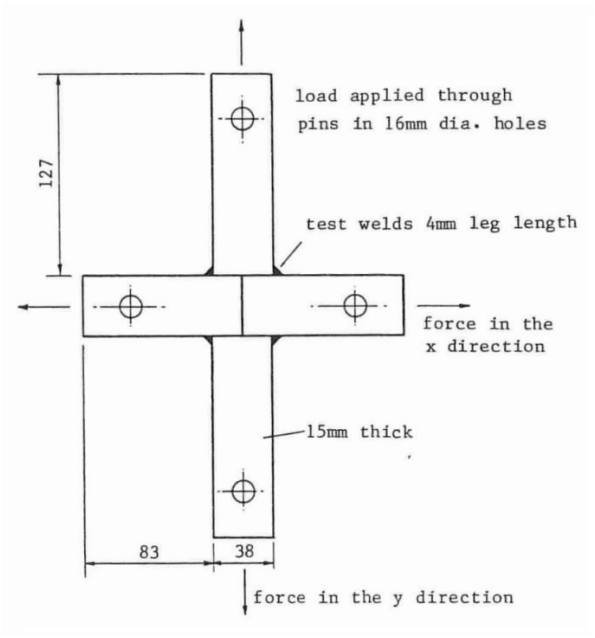

Fig. 3.3. Experimental specimens tested by Higgs. (1981).
(from Biggs et al., 1981)

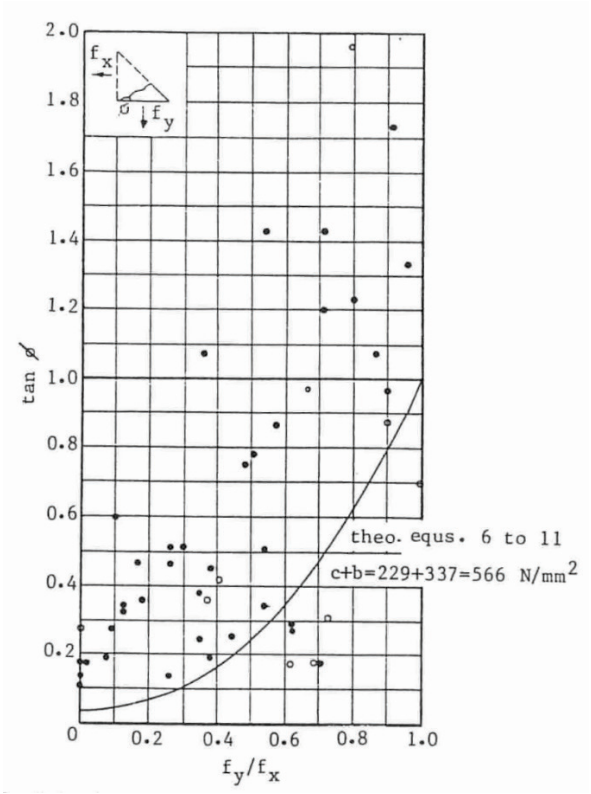

Fig. 3.4. Orientation of the critical section versus the load ratio, f_x/f_y. (from Biggs et al., 1981)

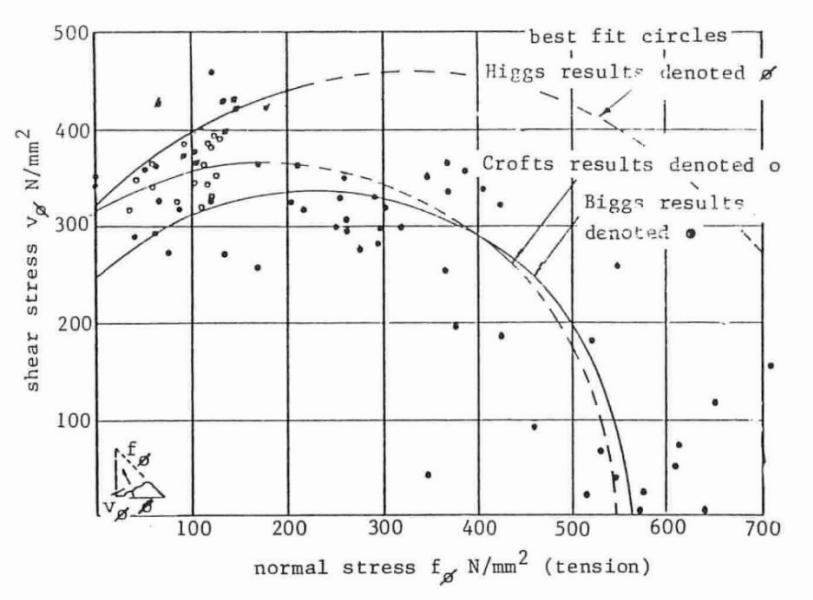

Fig. 3.5. Stress interaction on the critical section. (from Biggs et al., 1981)

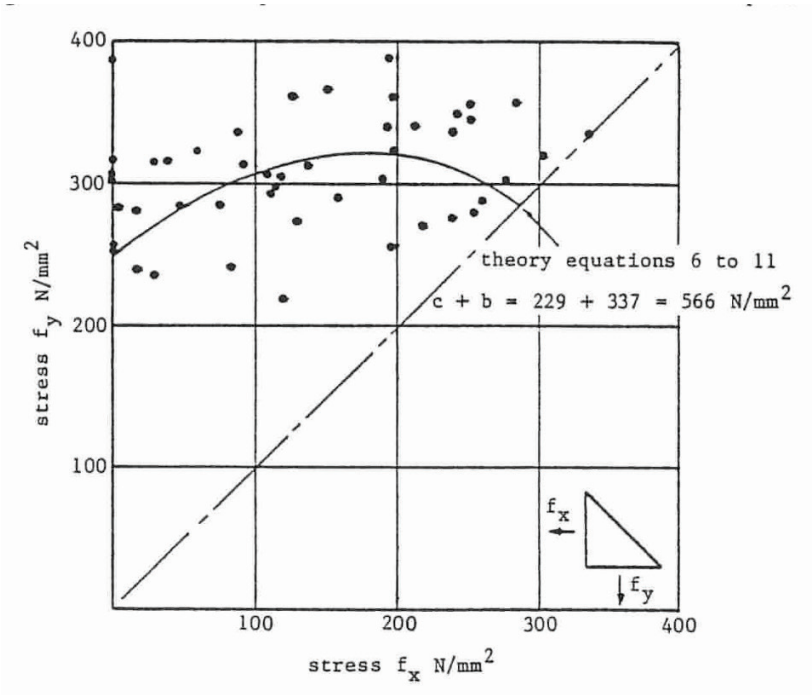

Fig. 3.6. Interaction between x- and y-direction loads.
(from Biggs et al., 1981)

Kamtekar (1982), Kamtekar (1987)
Based on von Mises yield criterion, Kamtekar (1982) derived equations to calculate the strength of longitudinally- and transversely loaded fillet welds. The same theory was used by Kamtekar (1987) to derive equation 3.11 for the full range of loading angles ($0° < \theta < 90°$). The theory predicts that transverse welds rupture along the leg (fusion zone) at a 41% higher load than longitudinal welds.

$$k_{ds} = \sqrt{2 - \cos^2 \theta} \tag{3.11}$$

Pham (1983)
Pham (1983) documented a series of 36 tests on transversely loaded T-joints connected with fillet welds using the FCAW and SAW welding processes. Macro-etches showed that the theoretical throat increased by 30% for FCAW welds and 50% for SAW welds with a coefficient of variation of 0.20 for both processes. Many of the welds ruptured along the fusion zone; however, the experimental loads exceeded the expected strengths due to oversized welds and overstrength weld metals.

Neis (1985)
Neis (1985) used plasticity theory to derive the ultimate strength and maximum displacement of fillet welds. Although several simplifying assumptions were required, limited comparisons with

experimental results showed “an acceptable fit.” The ultimate (rupture) force and deformation are calculated with Equations 3.12 and 3.13 respectively.

$$R_u = \sigma_{tu} w L \sqrt{\frac{1+15\sin^2\alpha_d}{6\left(1+7\sin^2\alpha_d\right)}} \tag{3.12}$$

$$\delta_u = \varepsilon_u \sqrt{\frac{3}{2\left(1+7\sin^2\alpha_d\right)}} \tag{3.13}$$

The complete load-deformation curve can be plotted with Equations 3.14 through 3.16.

$$R_i = R_u \frac{f_i}{f_u} \tag{3.14}$$

$$f_i = 1 - \frac{e^{-25\delta_i} + e^{-75\delta_i}}{2} \tag{3.15}$$

$$f_u = 1 - \frac{e^{-25\delta_u} + e^{-75\delta_u}}{2} \tag{3.16}$$

where

R_i = strength at deformation Δ_i, kips
α_d = angle between the weld longitudinal axis and the weld displacement direction
δ_i = Δ_i/w
δ_u = Δ_u/w
ε_u = uniaxial engineering tensile rupture strain
σ_{tu} = true tensile rupture stress, ksi
σ_{uw} = uniaxial engineering tensile rupture stress, ksi

As a conservative estimate, the authors noted that the true tensile rupture stress can be calculated with Equation 3.17.

$$\sigma_{tu} = \sigma_u(1 + 0.75\varepsilon_u) \tag{3.17}$$

Equation 3.18 provides an approximate value of the angle between the weld longitudinal axis and the weld displacement direction.

$$\tan\alpha_d = \frac{\tan\theta}{4} \tag{3.18}$$

Kennedy and Kriviak (1985)

Kennedy and Kriviak (1985) discussed Butler and Kulak (1971) Equation 3.5, plotting it as an interaction curve, along with the available experimental data. This led to the surprising conclusion that the strength of a longitudinally loaded fillet weld increases when a transverse load is added as shown in Figure 3.7. The authors developed Equation 3.19, which provides a more conservative estimate of fillet weld strength compared to Equation 3.5. Equation 3.19 results in k_{ds} = 1.42 when θ = 90°.

$$1.2\left(\frac{V_T}{V_u}\right)^2 - \frac{V_T}{V_u} + \frac{V_L}{V_u} = 1.0 \tag{3.19}$$

where

V_L = longitudinal load, kips
V_T = transverse load, kips
V_u = weld strength at θ = 0°, kips

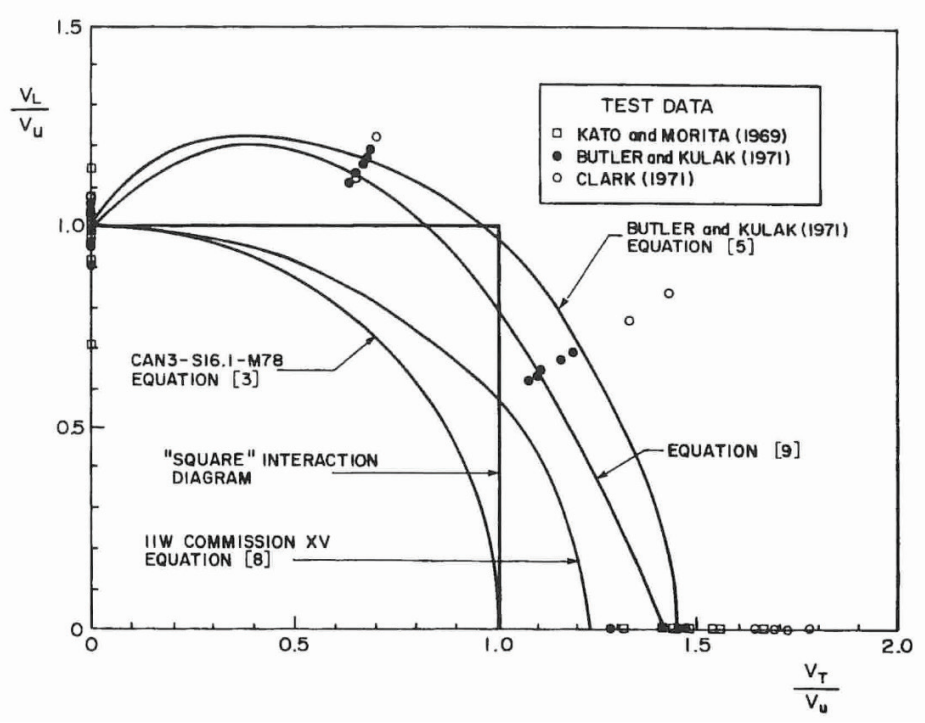

Fig. 3.7. Interaction of longitudinal and transverse fillet welds. (from Kennedy and Kriviak, 1985)

Faltus (1986)

Early attempts by International Institute of Welding (IIW) committees to develop an accurate design equation resulted in Equation 3.20, which was originally proposed by Van der Eb in 1952. This equation was later adopted by the International Organization for Standardization (ISO).

$$\sqrt{\sigma_T^2 + 1.8\left(\tau_T^2 + \tau_L^2\right)} = F_{EXX} \tag{3.20}$$

Equation 3.20 results in a shear rupture stress of $0.745F_{EXX}$ when $\theta = 0°$ and $k_{ds} = 1.13$ when $\theta = 90°$. In 1974, the 1.8 constant was changed to 3, which results in von Mises equation. Because this increased the conservative error compared to the experimental results, the stress was reduced by a correlation factor, β_w, which had values of 0.70 or 0.85 depending on the steel grade. Also, a limit was added to ensure that the normal stress was not greater than the weld metal tensile strength. This resulted in Equations 3.21 and 3.22, which is the basis for the equations in Eurocode 3.

$$\beta_w\sqrt{\sigma_T^2 + 3\left(\tau_T^2 + \tau_L^2\right)} \le F_{EXX} \tag{3.21}$$

$$\sigma_T \le F_{EXX} \tag{3.22}$$

Sanaei and Kametkar (1988)

Sanaei and Kametkar (1988) tested seven concentrically loaded double-lap specimens with either longitudinal, transverse or skewed fillet welds. The specimens were loaded by applying a compression force to the center plate, which was resisted by opposing compression forces in the lap plates. The skewed specimens were tested at load angles, θ, equal to 30° and 60°. The weld metal tensile strength, σ_w, from all-weld-metal coupons was 71.2 ksi. The specified fillet weld size was 8 mm and the actual weld sizes were recorded. All welds were 100 mm long.

McClellan (1989), NSRP (1989)

McClellan (1989) and NSRP (1989) tested 96 double-lap specimens with either longitudinal or transverse fillet welds. The joints were fabricated using the FCAW process with either CO_2 or 75% argon/25% CO_2 shielding gasses. The specified weld sizes were either ¼ or ⅜ in. and the specified electrode strengths were either 70 or 100 ksi. By evaluating the rupture surfaces and macro-etches, the author concluded that the penetration depth was similar to that of a weld deposited with the SMAW process. The rupture surface for the transverse welds was oriented at approximately 22.5° from the load direction. The transverse welds averaged 1.51 and 1.39 times stronger than longitudinal welds for 70 and 100 ksi electrodes, respectively.

Miazga and Kennedy (1986), Miazga and Kennedy (1989), Lesik and Kennedy (1990), Kennedy et al. (1990)

Miazga and Kennedy (1989) developed an analytical model to predict the fillet weld strength in double-lap joints as a function of the loading direction. The model includes a variable failure plane angle and restraining conditions at the weld root. They validated their model by testing 42 specimens with varying load angles from 0 to 90° in 15° increments. The fracture was ductile for the cases of longitudinal loading. For transverse loading, the fracture transitioned from brittle at the weld root where the crack initiated to ductile fracture at the crack termination. The area of the rupture surface is

$$A_\theta = \frac{wL\sin(45°)}{\sin(45° + \alpha)} \tag{3.23}$$

Where α is the angle between the loading direction and the rupture surface as shown in Figure 3.8. The normal stress on the rupture surface is

$$\sigma = \frac{P\sin\theta}{A_\theta}(\sin\alpha + a\cos\alpha) \tag{3.24}$$

The shear stress on the rupture surface is

$$\tau = \frac{P}{A_\theta}\sqrt{(\sin\theta\cos\alpha + a\sin\theta\sin\alpha) + \cos^2\theta} \tag{3.25}$$

Where *a* is a portion of *P* that defines the transverse force on the weld cross section that is required for equilibrium of the weld free body diagram as shown in Figure 3.8. Due to the nonlinear stresses at the weld cross section, the authors were unable to determine an accurate equation to define *a*; however, the experimental results showed that a constant value of 0.345 is applicable for θ between 45° and 90°. For smaller values of θ, *a* could not be determined due to the scattered test results.

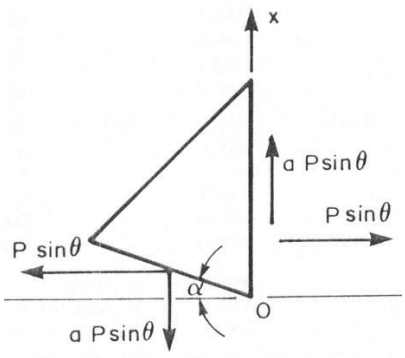

Fig. 3.8. Weld free body diagram.
(from Miazga and Kennedy, 1989)

Among the failure theories considered by Miazga and Kennedy (1986), which included von-Mises, maximum normal stress and maximum shear stress (Tresca), the Tresca theory was the most accurate in determining the ultimate weld strength and rupture plane orientation, α. Setting dτ/dα = 0, results in Equation 3.26.

$$\tan(45° + \alpha) = \frac{(\cos\alpha - a\sin\alpha)^2 + \cot^2\theta}{(\cos\alpha - a\sin\alpha)(\sin\alpha + a\cos\alpha)} \tag{3.26}$$

The weld strength, P_θ, at a loading angle θ is calculated by setting the maximum shear stress equal to the ultimate shear strength, τ_u. Combining Equations 3.23 and 3.25 results in Equation 3.27.

$$P_\theta = \frac{\tau_u w L \sin(45°)}{\sin(45° + \alpha)\sqrt{(\sin\theta\cos\alpha - a\sin\theta\sin\alpha)^2 + \cos^2\theta}} \tag{3.27}$$

Based on the six experimental specimens with longitudinal fillet welds, τ_u can be estimated as 0.764 of the electrode tensile strength. For a = 0.345, α = 13.0°, which results in k_{ds} = 1.32 when θ = 90°. The effect of constraint in the plane of the rupture surface was considered by multiplying Equation 3.27 by a semi-empirical constraint factor, k, which is calculated with Equation 3.28. This results in k_{ds} = 1.50 when θ = 90° and an experimental-to-calculated strength ratio of 1.004 with a standard deviation of 0.088. A plot of $k \times P_\theta$ and the experimental results are shown in Figure 3.9.

$$k = 1 + 0.141\sin\theta \tag{3.28}$$

The weld strength is determined by calculating the rupture angle with Equation 3.26, substituting this value into Equation 3.27 and multiplying by Equation 3.28. In an effort to simplify the design process, Lesik and Kennedy (1990) developed AISC *Specification* Equation J2-5 by fitting the curve in Figure 3.9. Based on the plotted data, Equation J2-5 is slightly conservative, with a maximum error of 1.5% at θ = 45°.

For lap-joints in compression, the transverse force is not available. Miazga and Kennedy (1989) noted that the welds for these joints can be designed with a = 0, which results in α = 22.5° and k_{ds} = 1.34 when θ = 90°. For this condition, the experimental-to-calculated strength ratio is 0.928 with a standard deviation of 0.065 when compared to the experimental results of Swannell and Skewes (1979). This approach was also recommended for T-joints in both tension and compression. To simplify the design process, Kennedy et al. (1990) developed Equation 3.29 by fitting a curve based on Equation 3.27 with a = 0.

$$k_{ds} = 1.0 + 0.34\sin^{1.5}\theta \tag{3.29}$$

For the E48014 electrodes in the Miazga and Kennedy (1989) research, the specified uniaxial tensile strength was 480 MPa and the measured strength was 538 MPa resulting in an overstrength factor of 1.12. Lesik and Kennedy (1988, 1990) summarized the electrode strength statistics for four previous projects found in the literature with a total of 672 weld metal tensile tests. For these tests, the average overstrength factor, σ_{uw}/F_{EXX}, was 1.12 with a coefficient of variation of 0.077.

Miazga and Kennedy (1986) measured the weld leg sizes with a digital micrometer with a minimum of 44 readings per specimen. For the 5 mm welds, the average measured-to-specified leg ratio, w_m/w, was 1.04 with a coefficient of variation of 0.026. For the 9 mm welds, the average measured-to-specified leg ratio, w_m/w, was 1.03 with a coefficient of variation of 0.027.

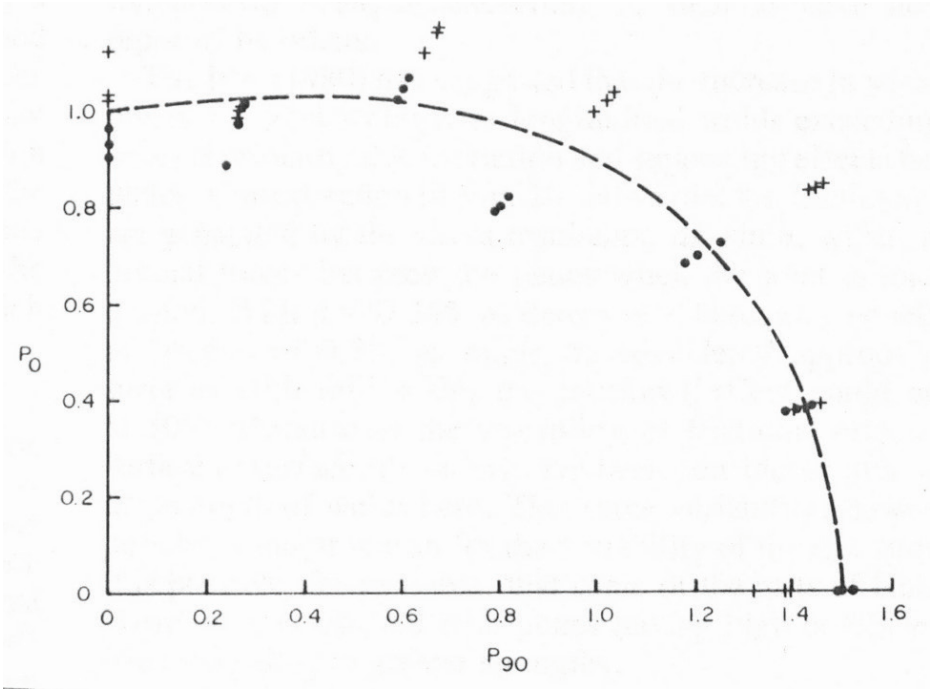

Fig. 3.9. Plot of $k \times P_\theta$ compared to the experimental results. (from Miazga and Kennedy, 1989)

Chan and Ogle (1992)

Chan and Ogle (1992) tested a 12.5 mm flat plate that was cut to the geometry of a large transversely loaded double-lap splice connection. The simulated fillet welds had 100 mm leg sizes. When loaded to 82% of the rupture load, strain gages showed that inelastic stress redistribution resulted in a near constant von Mises stress along planes oriented at both 0° and 22.5° from the load. After significant plastic flow approximately along the 22.5° plane, a crack formed at the root and grew to about 22 mm long in the direction of the plastic band.

Bowman and Quinn (1994)

Bowman and Quinn (1994) experimentally examined the strength and deformation of fillet welds in double-lap joints for three different weld leg sizes (¼, ⅜, and ½ in.), weld orientations (longitudinal and transverse), and three root gap sizes (0, 1⁄16, and ⅛ in.). Root gaps were fabricated by using spacer bars between the plates to represent distortions or inadequate fitup of plates. Eighteen specimens were prepared using 70 ksi SMAW welds with A572 Grade 50 plates.

The strength ratio between the transverse and longitudinal weld was between 1.3 and 1.7 for specimens with no gaps and 1.2 and 1.4 for gapped specimens. For the same specified weld size, the strength of the gapped specimens did not decrease significantly from non-gapped specimens because of the relatively higher weld penetration in the gapped specimens.

Wilcox (1995)

To study the effect of penetration, Wilcox (1995) tested 10 transversely loaded fillet weld specimens in cruciform T-joints. The specimens were welded with the FCAW process with 100%

CO_2 gas shielding. The penetration was increased by varying the arc voltage, current, wire feed speed and travel speed. As expected, the experimental rupture loads increased significantly with increased penetration.

Mellor et al. (1999)

Using experimental results from the literature and the results of finite element models, Mellor et al. (1999) simplified an empirical equation that predicts the strength of fillet welds, resulting in Equation 3.30.

$$R_n = K_{at} F_c E_p L \tag{3.30}$$

Where E_p is the actual weld throat defined as the penetration depth plus the effective throat according to AISC *Specification* Section J2.2a. L is the weld length. F_c is the rupture stress that considers the effect of base metal dilution. The authors developed Equation 3.31 as a simplified expression for F_c.

$$F_c = 0.6F_{EXX} + 0.4F_u \tag{3.31}$$

Where F_u is the tensile strength of the base metal. K_{at} is an empirical coefficient, which can be calculated with Equation 3.32 for transversely loaded double-lap fillet weld joints.

$$K_{at} = 0.079 + 1.931\frac{E}{E_p} - 1.084\left(\frac{E}{E_p}\right)^2 \tag{3.32}$$

The authors found that, for transversely loaded fillet welds, double-lap joints are stronger than T-joints. The higher loads were believed to be caused by friction at the faying surfaces in the lap joints, higher stress concentrations in the T-joint, and higher rigidity of the T-joint. Based on the experimental and theoretical results, the range of K_{at} was 0.93-1.04 and 0.82-0.98 for double-lap and T-joints, respectively.

Ng et al. (2002), Ng et al. (2004)

Ng et al. (2002) tested 102 transversely loaded fillet weld specimens in double-lap and cruciform T-joints. Both the SMAW and FCAW processes were used in the fabrication. The specified weld size for the cruciform specimens was ¼ in. For the lapped specimens, two weld sizes were considered: ¼ in. and ½ in.

The mean calculated strength, using the measured rupture surface area, was approximately the same for both welding processes. However, the penetration for the FCAW specimens was much higher than for the SMAW specimens, resulting in higher rupture strengths for the FCAW specimens. The measured rupture surface width for the SMAW welds was similar to the theoretical effective throat dimension. The measured rupture surface width of the FCAW welds was about 1.5 to 2 times the theoretical effective throat dimension.

The tests showed that the rupture stress decreased nonlinearly with an increase in weld size. The average rupture stress for the lapped specimens was 13% higher than that of the cruciform

specimens. Also, the lapped specimens were approximately 3.8 times as ductile as the cruciform specimens. Most of the specimens failed by ductile shear rupture at, or near, the weld shear leg (α = 0°). The test-to-predicted strength ratio ranged from 1.28 to 2.57 compared to the AISC *Specification* equations.

Deng et al. (2003)

Deng et al. (2003) investigated the strength of fillet welds in double-lap joints fabricated with both the SMAW and FCAW processes. The welds were subjected to three loading angles: θ = 0°, 45° and 90°. A reliability analysis showed that the AISC *Specification* equations are applicable to welds fabricated with both SMAW and FCAW processes. The FCAW process resulted in higher root penetration than the SMAW process; therefore, the calculations are more conservative for FCAW welds. The average experimental strength for the FCAW specimens was approximately 50% higher than that of SMAW specimens. However, the mean rupture stress calculated with the measured rupture surface area was approximately the same for both welding processes. Based on the shear stress at the measured rupture surface of the longitudinal welds, the mean shear-to-tensile strength ratio was 0.778 with a coefficient of variation of 0.075.

Yasui et al. (2004)

Yasui et al. (2004) tested eight fillet welded T-joints that were fabricated with the GMAW process (Group W specimens). Also tested were seven similar specimens with the fillet weld joints machined from plates (Group C specimens). Both specimen groups were tested at various load angles: θ = 0°, 15°, 30°, 45°, 60°, 75° and 90°. The weld metal strengths were measured with coupons extracted from the fillet welds, resulting in σ_{EXX} = 651 MPa (94.4 ksi). The measured base metal tensile strengths were F_u = 534 MPa (77.4 ksi) for Group W specimens and F_u = 527 MPa (76.4 ksi) for Group C specimens. Effective throat dimensions measured from etched sections showed penetrations between 1 and 1.2 mm. Using a slip line analysis, the authors derived Equation 3.33 for the directional strength increase, which results in k_{ds} = 1.26 at θ = 90°.

$$k_{ds} = \sqrt{\frac{2\left(1+3\sin^2\theta\right)}{2+3\sin^2\theta}} \tag{3.33}$$

Callele et al. (2005, 2009)

Callele et al. (2005, 2009) tested 34 double-lap fillet weld specimens, including nine specimens with longitudinally loaded welds, three transversely loaded specimens and 22 multi-orientation specimens. Of the multi-orientation joints, 14 specimens had both longitudinal and transverse fillet welds and eight specimens combined skewed (θ = 45°) and transverse (θ = 90°) welds.

The specimens were fabricated using the FCAW-S process with E70T-7 electrodes and A572 grade 50 steel plates. The weld metal tensile strengths, σ_w, from all-weld-metal coupons were 83.4 ksi and 82.7 ksi for Heats 1 and 2, respectively.

The results showed that it is not required to consider base metal rupture at the fusion zone for fillet welds. The authors noted that the tensile strength at the fusion zone is affected by

intermixing/dilution and tempering/heat treatment which is not considered in the design equations. The research also indicated that the weld strength is independent of the number of weld passes.

Li et al. (2007)

Li et al. (2007) tested 12 transversely loaded fillet weld specimens in cruciform T-joints. The specimens were welded with the FCAW process. The tests showed that lap-joints are between 0 and 30% stronger than T-joints. A reliability analysis was performed on transversely loaded fillet welds using 1160 experimental data points from previous and current research. This indicated that, for lap-joints, the safety index is 4.5 and for T-joints, the safety index is 4.3. The authors analyzed 1,706 measurements on weld leg or throat dimensions from 12 research projects and determined that the average measured-to-specified ratio, ρ_G, is 1.08 with a coefficient of variation of 0.142. For the weld uniaxial metal tensile strength, 716 specimens from eight research projects showed that the average measured-to-specified ratio, ρ_{M1}, is 1.13 with a coefficient of variation of 0.080.

Based on the results of 304 specimens from eight research projects, the shear-to-tensile strength ratio of 0.60 in the AISC *Specification* equations is conservative. The average measured-to-specified ratio, ρ_{M2}, is 1.29 with a coefficient of variation of 0.130. This is identical to an average $\tau_u/\sigma_{uw} = 0.774$.

Gomez et al. (2008) and Kanvinde et al. (2009a)

The strength in fillet-welded cruciform T-joints was determined theoretically and experimentally, while changing different parameters. The FCAW process was used with two electrodes: E70T7 (non-toughness rated) and E70T7-K2 (toughness rated), two root notch lengths (plate thickness): 1.25 and 2.5 in., and two weld sizes: ½ and 5⁄16 in. The experimental program consisted of eight combinations with three specimens each. The CVN energy at 21° C for all-weld-metal tests were 25.1 J for the E70T7 specimens and 80.0 J for E70T7-K2 specimens.

The root notch length had an insignificant effect on the weld strength and ductility. The rupture strengths were proportional to the weld size, indicating that the weld size had an insignificant effect on the rupture stress. Generally, the calculated strength according to the AISC *Specification* was accurate compared to the experimental results. The weld metal toughness had a significant effect, with the specimens fabricated with the E70T7-K2 electrodes 12% stronger than the E70T7 specimens. The ductility of the specimens with E70T7-K2 electrodes was almost twice that of the specimens with E70T7 electrodes. From the experimental results, the rupture angle of the weld, measured from the tension face, ranged from 20° to 80°. A photomicrograph of the fracture surface showed that the crack initiated at the weld root for about 0.06 in. (1.5 mm) as a ductile tension fracture (crack opening fracture mode) and then transitioned to the measured fracture angle as a brittle shear fracture.

The authors were able to predict the weld strength using fracture mechanics and finite element models. From the experimental results, a 2D plain-strain model was created to simulate the test specimens. The weld root was modeled as a half circle of 0.004 in. radius, which is acceptable because the anticipated crack tip blunting in the weld root at fracture is about 0.01 in. The size of the elements around the notch tip was 0.002 in. The FEA model was validated and calibrated by comparing the load-deformation curve of the weld with the curves obtained from testing. The critical fracture toughness of the weld root was calculated by integrating the stresses and strains

within the 20 mesh contours around the crack tip. This value was used to determine the fracture load of other specimens of the same weld size, yet with different root notch lengths. The specimens were loaded gradually until the fracture toughness of the zone around the crack tip reached the previously calculated critical fracture toughness. This was considered the weld rupture strength. It was found that the strength and fracture ductility of pre-cracked welds are not dependent on the crack length, if it is above 1 in. This can be supported by the fact that the weld yields and exceeds its plastic limit prior to failure. Smaller root notch lengths (less than 1 in.) were claimed to have higher ductility, but same strength.

Sugitani and Mochizuki (2013)

Sugitani and Mochizuki (2013) tested 112 transverse fillet welds in cruciform T-joints. The specimens were fabricated using either the SMAW or GMAW process with varying welding parameters (current, voltage, travel speed). Other variables included plate thickness (12.5 mm, 25 mm), root gap (0, 3 mm, 5 mm) weld size (6 mm, 9 mm) and welding position (flat, vertical upward). The measured base material yield and tensile strengths were 372 N/mm^2 and 489 N/mm^2, respectively. The measured weld metal uniaxial tensile strength was 570 N/mm^2. Before testing, the weld dimensions were measured using a cross section of each weld.

The first group of 64 specimens had no root gap. This group was fabricated with eight different welding conditions with eight duplicate specimens each. The second group, which was intended to study the effect of root gap size, consisted of three duplicate specimens for each of 16 joint geometries for a total of 48 tests.

The authors concluded that penetration can significantly increase the weld strength. As a result of deeper penetration, the GMAW welds were stronger than the SMAW welds. Because the joints with root gaps had deeper penetration and higher strengths, the authors recommended that welds can be designed without consideration of the root gap.

Lu et al. (2015)

Both transverse and longitudinal fillet welds were studied by Lu et al. (2015). The objective was to develop a unified shear strength definition for fillet welds that account for the actual stress distribution and rupture plane. Finite element results and the traction stress approach were used to determine the critical fracture plane and the stress concentrations along the weld line of longitudinal fillet welds. The results were verified with 128 experimental tests.

The authors found that the weld strength can be determined from the membrane term and that the bending term can be neglected. Accordingly, the shear stress on the rupture plane of a transverse fillet weld is calculated with Equation 3.34.

$$\tau_T = \frac{P}{EL}\frac{\sqrt{2}}{4}\left[1+\sin\left(2\alpha\right)+\cos\left(2\alpha\right)\right] \tag{3.34}$$

Where α is the angle between the loading direction and the rupture plane. Setting $d\tau_T/d\alpha = 0$, results in $\alpha = 22.5°$. Substituting $\alpha = 22.5°$ into Equation 3.34 results in Equation 3.35. According to Equation 3.35, $k_{ds} = 1.48$.

$$\tau_T = \frac{P}{EL}\frac{2+\sqrt{2}}{4} = 0.854\frac{P}{EL} \tag{3.35}$$

Grismo et al. (2017)

To determine the strength of fillet welds subjected to impact loading, Grismo et al. (2017) tested both longitudinal and transverse fillet weld specimens. The specimens were fabricated by welding S355 plates with a tensile strength of 68.2 ksi (470 MPa) using E70XX SMAW electrodes. The authors concluded that "the resistance to fillet welds was practically unaffected by the applied displacement rate."

In addition to the impact tests, longitudinal and transverse fillet welds were tested with quasi-static loading (strain rate ≈ 300 s^{-1}). The experimental rupture loads for these specimens are compared to the strengths calculated with the AISC *Specification* equations in Table 3.2. The calculated strengths are based on the measured weld metal tensile strength from the quasi-static groove weld coupons (σ_{uw} = 80.0 ksi).

Table 3.2. Experimental results of Grismo et al. (2017).

Loading Direction	P_e kips	P_c kips	P_e/P_c
Longitudinal	47.2	35.6	1.33
Transverse	79.1	57.4	1.38

The weld metal tensile properties were measured with uniaxial tension tests with two different all-weld-metal coupons: 1. Standard all-weld-metal coupons machined from groove-welded plates according to AWS B4.0 (AWS, 2016), 2. All-weld-metal coupons machined from fillet welds. These specimens were tested at a quasi-static strain rate of 10^{-3} s^{-1}. The mean tensile strengths of the fillet and groove weld specimens was 94 ksi (650 MPa) and 80 ksi (550 MPa), respectively. The difference was attributed to the cooling rate during and after welding "the butt weld was manufactured with several weld passes, which induced a comparatively low cooling rate. Thus, a coarser ferritic microstructure would develop, and a weaker weld metal was obtained."

For the base metal and the all-weld-metal coupons machined from groove-welded plates, three different strain rates were used to determine the uniaxial properties: 10^{-3} s^{-1}, 10^{-1} s^{-1} and 300 s^{-1}. Although the base metal was more strain-rate sensitive than the weld metal, the strain rate increase from 10^{-3} s^{-1} to 10^{-1} s^{-1} resulted in a weld metal tensile strength increase of 4% and the strain rate increase from 10^{-3} s^{-1} to 300 s^{-1} resulted in a 22% increase.

Shi and Chen (2018)

Shi and Chen (2018) tested five transverse fillet welds in double-lap joints. The specimens were fabricated from 460 MPa (F_y = 66.7 ksi) plates using the GMAW process with CO_2 shielding gas. The specified tensile strength of the weld metal was 550 MPa (80 ksi) and the tensile strength measured with all-weld-metal coupons was 669 MPa (97.0 ksi). The rupture surface angles, measured from the loading plane, varied from 16.5 to 19.0°.

Lu and Dong (2020)
Based on the shear stresses on the rupture plane, Lu and Dong (2020) derived Equation 3.36.

$$P_\theta = \frac{\tau_u wL}{(\sin\alpha + \cos\alpha)\sqrt{(\sin\theta\cos\alpha)^2 + \cos^2\theta}} \tag{3.36}$$

For transversely loaded welds, the transverse compression force, a, that was originally included in the Miazga and Kennedy (1989) derivations, was used to develop Equation 3.37.

$$P_\theta = \frac{\tau_u wL}{(\sin\alpha + \cos\alpha)(\cos\alpha + a\sin\alpha)} \tag{3.37}$$

Setting $d\tau_u/d\alpha = 0$, results the critical angle between the loading direction and the rupture surface according to Equation 3.38.

$$\tan 2\theta = \frac{1-a}{1+a} \tag{3.38}$$

The authors showed that the theoretical value for a is approximately 0.3, which results in $\alpha = 14.2°$ and $k_{ds} = 1.30$. For $a = 0$, the directional strength increase factor is calculated using Equation 3.39 with $\alpha = 22.5°$, which results in $k_{ds} = 1.17$.

$$k_{ds} = \frac{4}{\sqrt{2}(1 + \sin 2\alpha + \cos 2\alpha)} \tag{3.39}$$

Luo et al. (2020a)
Luo et al. (2020a) evaluated the limit loads of welded T-joints using both slip-line theory and finite element models. Three different weld types were evaluated: 1. Double fillet welds, 2. PJP double-bevel groove welds with 45° groove angles, 3. Combined fillet/PJP welds. The calculations showed that transverse fillet welds are 41% stronger than longitudinal fillet welds. For longitudinal welds, the theoretical rupture surface angles coincided with the orientation of the effective throat as defined in AISC *Specification* Section J2.2a. According to their theory, the rupture surface angle for transverse fillet welds is 0° from the loading direction.

Luo et al. (2020b)
Luo et al. (2020b) studied the effect of loading angle on both fillet and PJP welds using 17 experimental specimens and 21 finite element models. T-joints were used for the fillet welds and both T- and butt-joints were studied for the PJP welds. The specimens were fabricated with a 5 mm specified effective throat using the GMAW process with CO_2 shielding.

The research showed that the directional strength increase for fillet welds in *Specification* Equation J2-5 is non-conservative. The strength of fillet welds can be calculated with Equation 3.29, which has a mean test-to-predicted ratio of 1.00 and a standard deviation of 0.036.

Dowswell et al. (2021)

Dowswell et al. (2021) tested experimental specimens with both fillet and PJP welds. Three different base metal strengths and three different weld metal strengths were specified. A total of 71 specimens were tested, including 18 transverse fillet weld specimens and 15 longitudinal fillet weld specimens. The transverse specimens were fabricated with T-joints and the longitudinal specimens used double-lap joints. All specimens were shop welded using the FCAW process with CO_2 gas shielding.

All-weld-metal tension tests, according to ASTM A370 (ASTM, 2020), were used to measure the weld metal strength. Tension coupons were machined from standard groove-welded test plates. Three test plates for each weld classification were manufactured according to AWS A5.20 (AWS, 2015). Tension coupons were prepared according to AWS B4.0 (AWS, 2016). The mean measured tensile strengths, σ_{uw}, are listed in Table 3.3 along with the tensile strengths reported in the certificates of conformance.

Table 3.3. Weld metal tensile strength (Dowswell et al., 2021).

Classification	σ_{uc} ksi	σ_{uw} ksi
E71T-1, E70T-1	71	75.8
E80T-1	82	80.8
E100T-1	107	100

σ_{uw} = experimental uniaxial tensile rupture stress, ksi
σ_{uc} = tensile stress reported in the certificate of conformance, ksi

Generally, the specimens ruptured in the weld metal. Table 3.4 shows the average P_e/P_n, P_e/P_c and f_r/σ_{uw} ratios for the longitudinal fillet weld specimens, where P_e is the experimental rupture load, P_n is the nominal strength calculated with the AISC *Specification* equations, P_c is the strength calculated with the measured weld size and the measured weld metal tensile strength, f_r is the rupture stress calculated with the measured rupture surface area and σ_{uw} is the experimental uniaxial tensile rupture stress based on all-weld-metal specimens. Table 3.5 shows the average values for the P_e/P_n, P_e/P_c and f_r/σ_{uw} ratios for the transverse fillet weld specimens.

Table 3.4. Strength ratios for longitudinal fillet welds.

F_{EXX} ksi	P_e / P_n		P_e / P_c		f_r / σ_{uw}	
	Average	Standard Deviation	Average	Standard Deviation	Average	Standard Deviation
70	2.09	0.266	1.66	0.160	0.857	0.0448
80	1.95	0.0988	1.83	0.112	0.978	0.0610
100	1.44	0.153	1.24	0.0906	0.769	0.119
All Specimens	1.85	0.366	1.54	0.260	0.844	0.103

Table 3.5. Strength ratios for transverse fillet welds.						
F_{EXX} ksi	P_e / P_n		P_e / P_c		f_r / σ_{uw}	
	Average	Standard Deviation	Average	Standard Deviation	Average	Standard Deviation
70	1.84	0.306	1.51	0.175	0.888	0.100
80	1.53	0.189	1.42	0.103	0.980	0.0418
100	1.24	0.102	1.06	0.0730	0.857	0.0770
All Specimens	1.59	0.360	1.34	0.245	0.893	0.0946

Table 3.6 lists the average shear-to-tensile strength ratios, τ_u/σ_{uw}, based on weld metal strength. These values include the results for all longitudinally loaded fillet and PJP weld specimens. Generally, these values are in agreement with the equations developed by Krumpen and Jordan (1984). The data also agrees reasonably-well with the statistical analysis by Lesik and Kennedy (1988) and Lesik and Kennedy (1990), who calculated an average shear-to-tensile strength ratio, τ_u/σ_{uw}, of 0.749 with a coefficient of variation of 0.121.

Table 3.6. Shear-to-tensile strength ratios.		
F_{EXX} ksi	τ_u/σ_{uw}	
	Average	Standard Deviation
70	0.820	0.0725
80	0.843	0.134
100	0.752	0.0996
All Specimens	0.803	0.104

Based on their test results, Equation 3.40 was proposed for calculating the nominal weld metal stress for fillet welds, F_{nw}. This results in $k_{ds} = 1.30$ when $\theta = 90°$.

$$F_{nw} = 0.7F_{EXX}(1.0 + 0.30\sin^{1.5}\theta) \tag{3.40}$$

The results showed that, for fillet and PJP joints with matching electrodes, calculation of the fusion zone strength is not required. For fillet and PJP joints with overmatching electrodes, the fusion zone strength can be calculated by replacing F_{EXX} with the average of the base metal strength, F_u, and the weld metal strength, F_{EXX}.

Chen and Chen (2022)

To determine the effect of exposure to elevated temperatures, Chen and Chen (2022) tested 120 double-lap joints subjected to compression. The test variables were exposure temperature, cooling method, fillet weld leg size (2, 4, 6, 8 mm) and weld orientation (transverse, longitudinal). Eight control specimens (four transverse, four longitudinal) were tested without exposure to elevated temperature. The weld metal tensile strength was not reported; however, the control specimens can be used to show the strength difference between tension and compression loading in double-lap joints with transverse fillet welds. The transverse-to-longitudinal load ratios per unit length of the specimens with 2, 4, 6, and 8 mm leg sizes are 0.869, 0.899, 0.875 and 1.02, respectively. The average load ratio is 0.940. As shown in Table 4.8, the expected load ratio (k_{ds}) for transverse fillet welds in double-lap joints is significantly greater than 1.00. This difference is likely caused by the perpendicular constraining force, $F = a \times P$ (Gallow, 2019), which is present only in the tension specimens.

Waite et al. (2022)
As part of a group of specimens tested to determine the strength of joints with both bolts and welds, eight double-lap specimens with longitudinal welds were tested by Waite et al. (2022). The specimens had 5⁄16 in. equal-leg fillet welds, welded with the SMAW process using E7018-H4R electrodes. Three weld lengths were used: 2, 3 and 4 in. Due to the weld penetration and reinforcement, the mean rupture surface width (based on post-test measurements) was 28% larger than the effective throat calculated with the measured leg dimensions (based on pre-test measurements). The uniaxial tensile strength of the weld metal, based on all-weld-metal coupons, was 83 ksi.

MULTI-ORIENTATION FILLET WELD GROUPS

Multi-orientation fillet weld groups are the result of combining fillet welds that are loaded at different angles in the same joint. The most common combination is for joints with both longitudinal ($\theta = 0°$) and transverse ($\theta = 90°$) fillet welds. For many of the research projects already discussed, multi-orientation fillet welds were tested as part of a larger project. Because the details of these specimens are provided in the section on Fillet Welds, only a summary of those tests will be provided in this section.

ABW (1931)
The ABW (1931) report included 34 experimental tests on multi-orientation joints with both longitudinal and transverse fillet welds. These tests showed that failure of the transverse welds always precludes failure of the longitudinal welds at loads that are less than the sum of the independent strengths.

Spraragen and Claussen (1942)
Spraragen and Claussen (1942) discussed several projects from the 1930s, where multi-orientation fillet weld joints were tested. The various research projects resulted in similar behavior, with rupture initiating in the transverse welds. Depending on the longitudinal-to-transverse length ratio, the strength of the longitudinal welds may be only partially utilized when the transverse welds ruptured.

Lord and Schutz (1963)
Lord and Schutz (1963) tested several specimens with both longitudinal and transverse fillet welds. The transverse welds always ruptured before the longitudinal welds, and the authors concluded that the behavior was dependent on the transverse-to-longitudinal weld area ratio. Relatively larger transverse welds resulted in higher deformation capacity, allowing an increase in the load transferred through the longitudinal welds. The specimen geometries and material strengths were omitted from the report; therefore, the tests were excluded from the data set in this report.

Ligtenburg (1968)
Ligtenburg (1968) reported the results of 224 experimental tests on multi-orientation joints with both longitudinal and transverse fillet welds.

Strating (1971)
Strating (1971) reported the results of 23 experimental tests on multi-orientation joints with both longitudinal and transverse fillet welds.

Swannell (1974)
Swannell (1974) tested seven multi-orientation joints with both longitudinal and transverse fillet welds.

Gresnigt (1992)
Gresnigt (1992) documented tests on four double lap multi-orientation fillet weld joints. As with single orientation joints, the longitudinal and transverse welds ruptured at angles of approximately 45° and 25°, respectively. The weld metal tensile strengths were measured with coupons extracted from conventional groove welded plate specimens and coupons extracted from fillet welds. The strength ratios, which are listed in Table 3.7, show that the fillet weld coupons are 9% stronger on average than the groove weld coupons.

Table 3.7. Weld metal strengths from Gresnigt (1992).

Consumable	F_{EXX} MPa	σ_{uw} MPa	σ_{uf} MPa	σ_{uw}/F_{EXX}	σ_{uf}/σ_{uw}
Conarc 60 G	620	656	753	1.06	1.15
Kardo	470	478	511	1.02	1.07
PZ 6030	520	540	633	1.04	1.17

σ_{uf} = tensile stress from small-scale coupon extracted from fillet weld
σ_{uw} = tensile stress from conventional coupon extracted from groove weld

Dowswell (2003)
Using the equations in AWS D1.1 Section 4.6.4.3, Dowswell (2003) developed a simple design method to combine the strengths in multi-orientation fillet welds. The design method is based on deformation compatibility where the welds meet: the strength of the most ductile weld is calculated at the rupture deformation of the least ductile weld.

For joints with both longitudinal and transverse welds, the rupture deformation, Δ_u, of the transverse weld is $0.056w$ and the deformation of the longitudinal weld at maximum strength, Δ_m, is $0.167w$. At $\Delta_i = 0.056w$, the strength of the longitudinal weld is 82.5% of the strength at Δ_m. Based on this, comparisons with experimental results and the equations proposed by Butler and Kulak (1971), Dowswell (2003) recommended combining 85% of the longitudinal weld strength with 100% (using $k_{ds} = 1.50$) of the transverse weld strength. This is identical to AISC *Specification* Equation J2-6b, which was added to the *Specification* based in an independent analysis. Dowswell (2003) noted that these reductions are likely conservative because only the welds were assumed to deform. In real joints, the connected elements will also deform, allowing the longitudinal welds to attract more load.

Callele et al. (2005, 2009)
Callele et al. (2005, 2009) tested 22 multi-orientation joints, including 14 specimens with both longitudinal and transverse fillet welds and eight specimens that combined skewed ($\theta = 45°$) and transverse ($\theta = 90°$) welds.

SKEWED DIHEDRAL ANGLES

When two elements are connected at an angle other that 90° (± 10°), welds can be located on either the acute or obtuse side of the joint, as shown in Figure 3.10a and 3.10b, respectively. In many cases, the joint is welded on both sides. The dihedral angle, ψ, is the angle between the welded elements. On the acute side of the joint, the potential area of incomplete fusion near the weld root is addresses with the Z loss factor (Figure 3.10a). On the obtuse side of the joint, root openings, R_n, can be large when square-cut elements are used (Figure 3.10b); however, this can be prevented by beveling the edge. Welds with skewed dihedral angles are designed according to the requirements of AWS D1.1 Subclause 4.4.3.

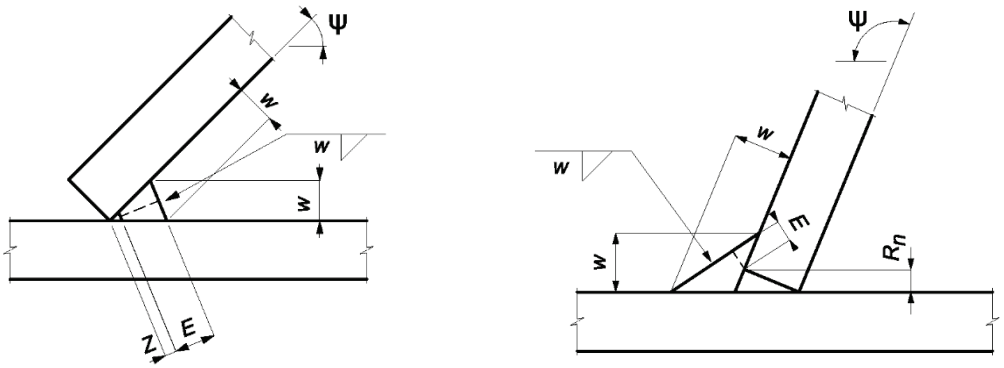

a. Acute *b. Obtuse*

Fig. 3.10. Welds with skewed dihedral angles.

Gallow (2019)

To determine the strength of welds in skewed joints, Gallow (2019) tested 35 experimental double-lap specimens, including 17 specimens loaded longitudinally and 18 loaded transversely. The specimens were fabricated from A572 Grade 50 plates, with welds using the FCAW-G process and E71T-1 electrodes. The plate edges were beveled at various angles from 30° to 150°.

Based on three all-weld-metal tests according to AWS A5.20, the mean measured tensile strength was σ_{uw} = 83.4 ksi. For the 17 longitudinal specimens, the mean shear-to-tensile strength ratio was τ_u/σ_{uw} = 0.948, where τ_u is the maximum test load divided by the weld rupture surface area measured after testing. In addition to the all-weld-metal tensile tests documented by Gallow (2019), three coupons were extracted from the same AWS A5.20 test plates for all-weld-metal torsion tests. The unpublished results from these specimens were used to verify the weld metal shear strength. The plastic torsional rupture moment is calculated with Equation 3.41, which was derived using plastic torsion theory.

$$T_u = \tau_u \frac{2\pi r^3}{3} \tag{3.41}$$

Solving Equation 3.41 for τ_u, substituting $r = d/2$ and dividing by σ_{uw} results in the shear-to-tensile strength ratio

$$\frac{\tau_u}{\sigma_{uw}} = \frac{12T_u}{\pi\sigma_{uw}d^3} \tag{3.42}$$

The test results, which are shown in Table 3.8, have a mean shear-to-tensile strength ratio of 0.837. This value is 13% lower than the 0.948 mean ratio from the longitudinal specimens.

Table 3.8. Torsion test results.

Specimen	d_m In.	T_e kip-in.	τ_u/σ_{uw}
1	0.496	2.21	0.829
2	0.506	2.42	0.856
3	0.500	2.25	0.825
mean			0.837

d_m = mean diameter of the specimen, in.
T_e = experimental rupture torsion, kip-in.

Barry et al. (2023)

To determine the effect of root gaps on the strength of skewed welds, Barry et al. (2023) tested 27 double-lap specimens that were similar to those tested by Gallow (2019). While Gallow's specimens were fabricated without a root gap, three different root gaps (3⁄16, ⅛, and ¼ in.) were used in the specimens tested by Barry et al. (2023). The plate edges were beveled at various angles from 90° to 150°. The experimental program consisted of 12 longitudinally loaded specimens and 15 transversely loaded specimens. As with the Gallow (2019) research, the specimens were fabricated from A572 Grade 50 plates, with welds using the FCAW-G process and E71T-1 electrodes. Based on three all-weld-metal tests according to AWS A5.20, the mean measured tensile strength was σ_{uw} = 83.4 ksi.

SINGLE-SIDED FILLET WELDS

Single-sided fillet welds are typically used when access to one side of the joint is restricted, allowing welding on only one side. For single-sided fillet welds, the transverse force, *a*, that was discussed by Miazga and Kennedy (1989) and Gallow (2019) is not present. This affects the weld strength only when $\theta > 0°$.

Transverse fillet welds in single-lap joints are addressed in AWS D1.1 Section 4.9.1.1, which requires either an out-of-plane restraining force or welds along the ends of both plates. Unrestrained single-lap joints with single transverse fillet welds are prohibited to prevent opening of the joint, which causes flexural tension stresses at the weld root.

For many of the research projects already discussed, single-sided fillet welds were tested as part of a larger project. Because the details of these specimens are provided in the section on Fillet Welds, only a summary of those tests will be provided in this section.

ABW (1931)

The ABW (1931) tests included specimens with transverse welds in both single-lap and double-lap joints, as shown in Figure 3.11. Upon inspection, several of the welds were determined to be defective. Additionally, several specimens failed by rupture at the gross section of the connected plate. For the non-defective welds that ruptured in the weld, the single-lap specimens included 54 with a single transverse fillet weld (Figure 3.11a) and 110 with transverse welds along the ends of both plates (Figure 3.11b).

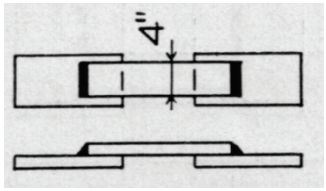

a. Single-lap single-weld specimens

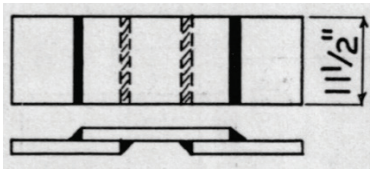

b. Single-lap double-weld specimens

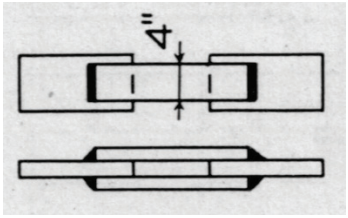

c. Double-lap specimens

Fig. 3.11. Lap specimens reported by ABW (1931).

For the single-lap single-weld specimens, the joints rotated and opened as shown in Figure 3.12. Using k_{ds} = 1.5 results in a mean test-to-calculated strength ratio, ρ_P, of 0.773. Using k_{ds} = 1.0, ρ_P = 1.16 with a coefficient of variation, V_P, of 0.193. In both cases, the reliability index, β, with ϕ = 0.75 is less than the target reliability index, β_T, of 4.0. Therefore, the prohibition of unrestrained single-lap joints with single transverse fillet welds in AWS D1.1 Subclause 4.9.1.1 is justified by these results.

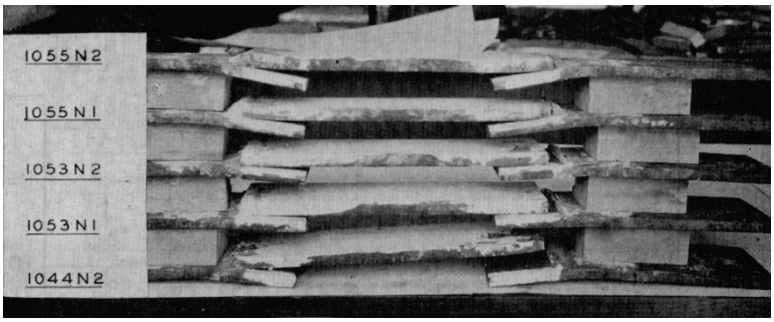

Fig. 3.12. Deformation of single-lap single-weld specimens (ABW, 1931).

For the single-lap double-weld specimens, the mean rupture stress equal to 0.903 times that of double-lap specimens. Using k_{ds} = 1.5 results in ρ_P = 0.933 and $\beta < \beta_T$. Using k_{ds} = 1.0, ρ_P = 1.40 and V_P = 0.148. As shown in Figure 3.13, the joints rotated; however, the opening that was observed in the single-lap single-weld specimens was prevented.

Fig. 3.13. Deformation of single-lap double-weld specimens (ABW, 1931).

Zhao and Hancock (1995)

Zhao and Hancock (1995) tested 18 axially loaded rectangular HSS members that were fillet welded to perpendicular end plates as shown in Figure 3.14. Nine of the specimens were welded completely around the perimeter and nine were welded only over a portion of each side. Due to the thin HSS walls, which were less than 3 mm thick, only eight of the specimens ruptured at the weld throat. Only these specimens, which were in the partially welded group, were considered in this report. Using k_{ds} = 1.0, ρ_P = 1.15 and V_P = 0.0441.

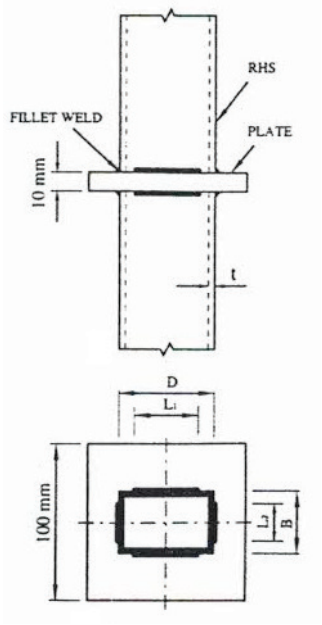

Fig. 3.14. HSS specimens tested by Zhao and Hancock (1995).

Chen et al. (2001)
Chen et al. (2001) tested both longitudinal and transverse T-joints with single-sided welds. The specimens were welded with the SAW process by three different fabricators and welding procedures.

The throat sizes were significantly increased by penetration and reinforcement, with a mean increase of 0.080 in. Therefore, the calculations are based on the measured throat sizes, which include the penetration and reinforcement. Because the weld metal tensile strength was not measured, the calculated strengths are based on the measured base metal tensile strength.

Most of the longitudinal specimens ruptured at the gross section of the web plate (not the fusion zone), and only eight specimens ruptured in the weld. Based in the experimental rupture load and the measured rupture surface for these eight specimens, the mean shear-to-tensile strength ratio, σ_r/σ_{uw}, is 0.820. The mean test-to-calculated ratio is similar to that of double-sided specimens, with $\rho_P = 1.37$ and $V_P = 0.132$.

20 cruciform T-joints with transverse welds were tested using the setup in Figure 3.15. The specimens were fabricated with double-fillet welds on the non-test side and single-sided fillet welds on test side. All specimens ruptured in the single-sided weld with a rupture deformation of approximately 10% of the leg size. Generally, the rupture surface was approximately 45° from the plates. Although the testing machine grips clamped the tee stems, "considerable flexural stress occurred not only in the weld itself, but in the web plate due to the eccentricity." This caused flexural tension stresses at the weld root, resulting in a mean rupture stress ratio, σ_r/σ_{uw}, of only 0.747, which is lower than that of similar double-sided specimens. Using $k_{ds} = 1.0$, $\rho_P = 1.24$ and $V_P = 0.185$.

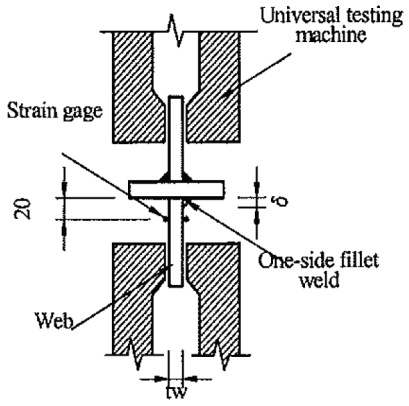

Fig. 3.15. Test setup for the Chen et al. (2001) transverse specimen.

Packer et al. (2016)

To determine the strength of fillet welds around the perimeter of HSS members, Packer et al. (2016) tested 33 axially loaded rectangular and round HSS shapes that were fillet welded to end plates as shown in Figure 3.16. Ten of the specimens had skewed end plates that were oriented 60° from the member axis. Only the 23 specimens (17 rectangular HSS and six round HSS) with perpendicular end plates were considered in this report.

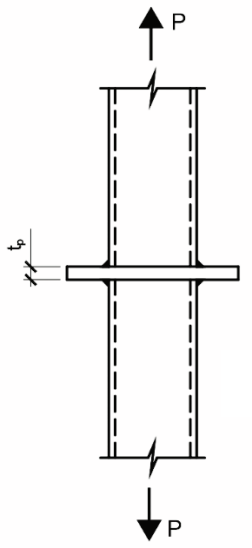

Fig. 3.16. HSS specimens tested by Packer et al. (2016).

The specimens were fabricated using the FCAW process with E71T-1c electrodes. The test welds were formed into a triangular shape by grinding and both leg sizes were measured before testing. After testing, saw-cut weld sections were scanned, and the rupture surface was measured from the scanned image.

The authors concluded that calculations for using the AISC *Specification* with k_{ds} = 1.5 result in an insufficient safety margin. However, they noted that a more rigorous reliability analysis may indicate that a higher safety margin. Using k_{ds} = 1.0 for the 17 rectangular specimens, ρ_P = 1.21 and V_P = 0.188. Using k_{ds} = 1.5 for the six round specimens, ρ_P = 1.15 and V_P = 0.121.

Tuominen et al. (2018)

Tuominen et al. (2018) tested single-sided transverse fillet and PJP welds in T-joints with various specimen geometries and loading conditions. Two specimens were subjected to tension, eight were subjected to flexure and three were subjected to combined tension and flexure. The welds were subjected to either tension or compression at the root and the authors concluded that "tensile stresses on the root side of the weld due to bending and tension loads is the most critical combination."

Specimens RC03 and RC04T were the only transverse fillet weld specimens tested in tension with an eccentricity equal to the distance between the loading plate and the weld. Therefore, the remaining specimens are not considered in this study. These specimens were fabricated from high strength steel using the GMAW process. The measured tensile strengths of the base and weld metal are 1,210 MPA (175 ksi) and 980 MPa (142 ksi), respectively. Using k_{ds} = 1.0 results in experimental-to-calculated ratios of 1.14 and 1.43 for Specimens RC03 and RC04T, respectively.

Torabian et al. (2018)

Torabian et al. (2018) tested 28 single-lap double fillet weld joints with transverse welds along the ends of both plates (Figure 3.17). The specimens were fabricated from plates with nominal thicknesses between 2.26 and 4.06 mm with specified weld sizes equal to nominal plate thickness. The plate material was ASTM A1011 Grade 50 high strength low alloy steel. The GMAW process was used with ER70S-3 electrodes and 80% Argon and 20% CO_2 shielding gas. The electrode strength was not measured; however, the uniaxial tensile strength was assumed to be 527 MPa (76.4 ksi) based on the manufacturers certificate of conformance.

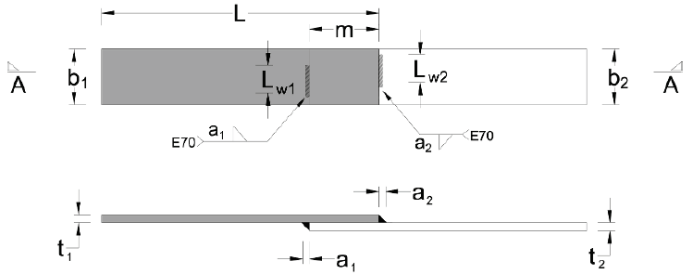

Fig. 3.17. Single-lap specimens tested by Torabian et al. (2018).

Only three of the specimens failed solely at the weld throat of both welds. Many of remaining specimens ruptured either at the HAZ or the shear leg, and some specimens had multiple failure modes. The authors noted that the failure modes were not correlated with the plate thickness. Using k_{ds} = 1.0 results in experimental-to-calculated ratios of 1.64, 1.89 and 1.47 for Specimens S-89-5, S-89-6 and S-160-1, respectively.

Thomas (2021)

Thomas (2021) tested 40 cruciform T-joints with transversely loaded single-sided fillet welds on one side of the transverse plate and double fillet welds on the opposite side. The test setup is shown in Figure 3.18. The specimens were fabricated using the FCAW process with matching E491T electrodes (F_{EXX} = 71 ksi), which have a measured weld metal tensile strength of 561 MPa (81.4 ksi). The plate material is CSA Grade 350W steel, which has F_y = 350 MPa (51 ksi) and F_u = 450 MPa (65 ksi). Both leg sizes of the test welds were measured before testing. After testing, saw-cut weld sections were scanned and the minimum throat dimension (shortest distance from the root to the face) was measured from the scanned image. Although the testing machine grips clamped the tee stems, strain measurements near the test welds indicated flexural stress transfer through the weld.

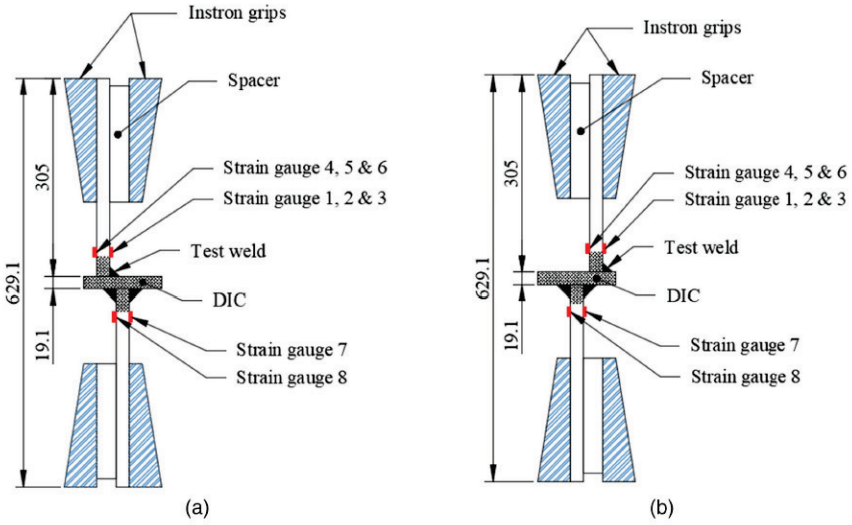

Fig. 3.18. Test setup for the Thomas (2021) specimen.

18 of the specimens had no specified eccentricity. For these specimens, the actual (measured) offset between the branch plates was equal to or less than 18% of the branch plate thickness. Using k_{ds} = 1.0 for the 18 specimens with no specified eccentricity, ρ_P = 1.34 and V_P = 0.119. The remaining specimens had eccentricities of 15 mm or 30 mm that induced either tension or compression at the weld root. The test results from these specimens clearly showed that flexural tension stress at the root causes a significant strength reduction.

Ltaief and Mensinger (2023)

Ltaief and Mensinger (2023) Tested three single-sided fillet welds that were subjected to flexure with tension at the root. The specified leg sizes were 5 mm and the weld lengths, L, were 150 mm. The filler metal was T46 3M, which has $F_{EXX} \approx 70$ ksi. The maximum moments were consistently reached at approximately 2° rotations. Rupture rotations varied significantly, with rupture at the root occurring approximately between 3° and 7°. The experimental strengths were significantly higher than the nominal plastic strength. $M_p = F_{EXX} LE^2/4$.

PARTIAL JOINT PENETRATION (PJP) WELDS

Satoh et al. (1974)

Satoh et al. (1974) tested T-joints with PJP double-bevel groove welds with several variables including groove angle, preparation depth and size of the reinforcing fillet weld. Matching weld metal was used for all specimens. For the case without reinforcing fillet welds, the nominal stress on the effective throat as defined in AISC *Specification* Section J2.2a can be calculated with Equation 3.43.

$$F_{pjp} = F_{EXX}\sqrt{\frac{1}{3} + \sin^2 \theta_p} \tag{3.43}$$

Where θ_p is the groove angle measured from the load direction. The specimens ruptured either in the weld metal, in the fusion zone perpendicular to the load, or a combined path forming a bilinear crack through the PJP fusion zone and the fillet weld metal. Based on these ruptures in the fusion zone, the authors recommended that the tensile stress on the fusion zone perpendicular to the load should not exceed the base metal tensile strength.

The specimens were fabricated using the SMAW process with F_{EXX} = 78.2 ksi electrodes; however, the weld metal tensile strength was not measured. The expected tensile strength of the weld metal can be calculated with the values from Table 4.1, which results in $\sigma_{uw} \approx$ (1.09)(78.2 ksi) = 85.3 ksi.

Lawrence and Cox (1976)

Lawrence and Cox (1976) tested CJP butt-welded plates of A514 steel with matching electrodes and intentional defects of varying length at the center of the weld thickness. Based on a limit analysis of a cracked plate, they determined that reasonable upper- and lower-bound predictions could be based on the von Mises and Tresca criteria, respectively. This results in weld rupture stresses on the net weld cross section between 1.00 and $2/\sqrt{3}$ = 1.15 times F_{EXX}.

Popov and Stephen (1977)

Popov and Stephen (1977) tested column splice details with butt-welded flanges subjected to static tension and reversible cyclic loading. The specimens were fabricated using W14x320 (t_f = 2.09) shapes of A572 Grade 50 material with matching (70 ksi) filler metal. The welds "were made using NR311 Inner-Shield welding." Although the weld metal tensile strength was not measured, the expected tensile strength can be calculated with the value from Table 3.1: $\sigma_{EXX} \approx$ (1.04)(70 ksi) = 72.8 ksi. For one specimen, the flanges had CJP welds. The six remaining specimens were fabricated with PJP single-bevel groove welds with a 45° groove angle and specified weld sizes of ⅜, ¾ and 1 in.

The weld rupture stresses increased with decreasing weld sizes, resulting in strength increases of 6% for a 49% penetration ratio, 28% for a 38% penetration ratio and 40% for a 23% penetration ratio. The authors noted that the specimens with PJP welds exhibited "very little ductility." Similar column splice specimens with penetration ratios between ¼ and ¾ were subjected to cyclic axial and flexural loads by Yabe et al. (1994). The results showed that the deformation capacity increases with the penetration ratio.

Gagnon and Kennedy (1987, 1989)

Gagnon and Kennedy (1987, 1989) tested 75 PJP groove weld specimens with butt joints subjected to tension. The specimens were fabricated with SMAW electrodes using single-bevel preparations and 45° groove angles. Five penetration (groove depth-to-plate thickness) ratios, p (20, 40, 60, 80 and 100%), and two steel strengths were tested.

Because the welds were offset from the plate centerlines, they were subjected to a moment in addition to the tension force. The effect of eccentricity was studied by using both single specimens and paired specimens oriented back-to-back. Both a theoretical analysis and strain gage readings on the plates confirmed that flexural stresses were transferred through the welds. With increasing load, second-order self-limiting deformations caused a reduction in eccentricity. The rotational ductility of the yielded welds allowed the welds to align with the line of force, causing the moment in the weld to approach zero at the ultimate load. Therefore, for self-limiting conditions where the weld has adequate ductility, the effect of eccentricity is negligible. The tests showed similar strengths for both the single and back-to-back specimens and Gagnon and Kennedy (1987, 1989) concluded that "the strength of a properly made weld exhibiting ductile behavior can be based on its tensile capacity."

The specimens ruptured at or near the fusion zone of the plate with the square preparation. The rupture stresses for all specimens were similar to or greater than the measured uniaxial tensile stress of the weld metal. Table 3.9 shows the effect of the penetration ratio on the rupture stress, where the rupture stress decreases with increasing penetration. This effect, which is caused by the transverse constraint of the weld metal by the base metal, can be calculated with Equation 3.44.

$$F_c = F_{EXX}\,(1.55 - 1.16p + 0.61p^2) \tag{3.44}$$

where

F_c = nominal tension rupture stress considering constraint, ksi
p = penetration ratio

Table 3.9. Mean experimental rupture stress ratio for each penetration ratio.

p	20%	40%	60%	80%	100%
$(\sigma_e/\sigma_{uw})_{mean}$	1.33	1.18	1.13	1.08	1.00

σ_e = experimental rupture stress, ksi
σ_{uw} = measured weld metal uniaxial tensile stress, ksi

Rasmussen et al. (1999)

Rasmussen et al. (1999) tested nine PJP welds in offset T-joints with single-bevel 45° groove angles and 10 mm bevel sizes. Rupture was prevented at the bottom plate by welding on both sides. The tested weld at the top plate was single-sided. By varying the distance between the center of the top and bottom plates from –29.9 mm to +30.1 mm, the eccentricity about the weld longitudinal axis was varied. Negative eccentricities caused tension at the weld root. The specimens were fabricated from 20 mm hot-rolled plates with F_y = 350 MPa (50 ksi) and F_u = 450 MPa (65 ksi) using the GMAW process with F_{EXX} = 500 MPa (70 ksi). Although the weld metal tensile strength

was not measured, the expected tensile strength can be calculated with the value from Table 4.7: $\sigma_{uw} \approx (1.14)(70 \text{ ksi}) = 79.8 \text{ ksi}$.

The mean measured weld size was 9.1 mm, indicating a mean 0.9 mm distance at the root due to lack of fusion. In all specimens, rupture occurred in the weld metal at an approximate angle of 75° from the load direction. Although both positive and negative eccentricities equal to one-half of the weld size reduced the strength by about 20%, the authors concluded that the weld strength can be calculated as the product of the effective area and F_{EXX} for small eccentricities.

Khurshid et al. (2015)
Khurshid et al. (2015) tested CJP and PJP butt welded joints in high-strength steel plates with specified tensile strengths of 750 and 980 MPa. Both matching and undermatching filler metals were used, and specimens with overmatching filler metal were tested for the lower-strength base metal. The CJP preparations were double-V grooves and the PJP welds had single-V grooves. The PJP welds had a 67% penetration ratio and both weld types had 90° groove angles. All CJP specimens ruptured in the base metal. Rupture in the PJP specimens started at the root and propagated along the fusion zone. The deformation capacity of the CJP specimens was several times that of the PJP specimens. The ductility of overmatching PJP welds was slightly lower than for matching welds, and the deformation capacity of the undermatching welds was significantly higher (25% to 53%). The available design strengths were compared to the experimental rupture loads, showing actual safety factors between 2.1 and 3.0 for the AWS D1.1 allowable strength equations.

Ran et al. (2019)
Ran et al. (2019) tested 108 butt-welded high-strength CJP specimens with mismatched tensile strength ratios between 0.696 and 1.27. The results indicated a slight increase in the rupture load (between 4 and 10%) for undermatching welds when the weld length increased from 25 mm to 100 mm. This behavior is caused by the transverse restraint in the width and thickness directions provided by the adjacent plates. The authors noted that the weld metal yields at a load equal to $(2/\sqrt{3})^{n+1}$ times the yield stress, where n is the strain-hardening exponent. This results in a yield load of 1.18 times the uniaxial yield load. Similar behavior can be expected in both matched and mismatched PJP joints.

Luo et al. (2020a)
Luo et al. (2020a) evaluated the limit loads of welded T-joints using both slip-line theory and finite element models. Three different weld types were evaluated: 1. Double fillet welds, 2. PJP double-bevel groove welds with a 45° groove angle, 3. Combined fillet/PJP welds. The calculations showed that transverse PJP welds are 83% stronger than longitudinal PJP welds. For longitudinal welds, the theoretical rupture surface angles coincided with the orientation of the effective throat as defined in AISC *Specification* Section J2.2a. According to the theory, the rupture surface angle for transverse PJP welds is 36° from the loading direction.

Luo et al. (2020b)
Luo et al. (2020b) studied the effect of loading angle on both fillet and PJP welds using 17 experimental specimens and 21 finite element models. T-joints were used for the fillet welds and both T- and butt-joints were studied for the PJP welds. The PJP welds had double-bevel grooves

with a 45% penetration ratio and 45° groove angles. The specimens were fabricated with a 5 mm specified effective throat using the GMAW process with CO_2 shielding.

The research showed that the AISC *Specification* equations for PJP welds are over-conservative for $\theta > 0$. Due to the effects of transverse constraint and weld reinforcement (measured dimensions were not reported), the strength of the PJP T-joints were 1.23 times the strength of the butt-joints. The authors proposed Equation 3.45 for PJP T-joints, which has a mean test-to-calculated ratio of 1.00 and a standard deviation of 0.014.

$$k_{ds} = 1.0 + 0.629\theta + 0.068\theta^2 \tag{3.45}$$

They also proposed Equation 3.46 for PJP Butt-joints, which has a mean test-to-calculated ratio of 0.995 and a standard deviation of 0.038.

$$k_{ds} = 1.0 + 0.035\theta + 0.295\theta^2 \tag{3.46}$$

Reynolds et al. (2020)

Reynolds et al. (2020) tested six PJP welds in T-joints with single-bevel 45° groove angles and specified effective throats of ⅞ and 1¾ in. 1- and 2-in. thick A572 Grade 50 plates were welded in the flat position with FCAW-G 70 ksi matching electrodes. Three specimens were loaded longitudinally and three were loaded transversely. Additionally, 15 PJP specimens with reinforcing fillet welds were loaded transversely.

All strength calculations used the measured weld geometries and material properties. The longitudinally loaded specimens ruptured in the weld metal at loads that were accurately predicted with the AISC *Specification* equations. The mean rupture load for the transversely loaded PJP specimens was 30% higher than the strength calculated with the AISC *Specification* equations. The authors noted that the rupture strength is most accurately predicted using the base metal tensile strength and the fusion zone area at the transverse plate (which is identical to the effective weld area) according to Equation 3.47.

$$R_n = F_u A_{we} \tag{3.47}$$

The mean rupture load for the combined PJP/fillet specimens was 21% higher than the strength calculated with the AISC *Specification* equations. These specimens ruptured along a roughly bilinear path forming a crack near the PJP fusion zone at the transverse plate and projecting diagonally through the weld metal. This rupture pattern, which is similar to that described by Satoh et al. (1974), is shown in Figure 3.19. The authors noted that the reinforcing fillet welds provided no significant increase in strength for the geometries tested and they recommended that the strength is best calculated by neglecting the reinforcing fillet. However, they noted that this may not be the case where overmatching electrodes are used.

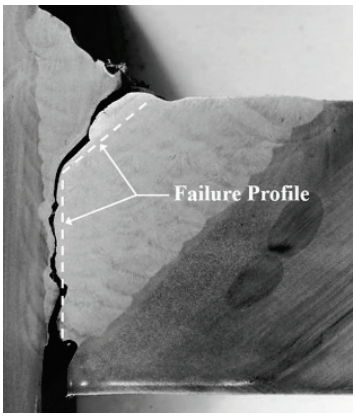

Fig. 3.19. Rupture plane from Reynolds et al. (2020).

Dowswell et al. (2021)

Dowswell et al. (2021) tested experimental specimens with both fillet and PJP welds. Three different base metal strengths and three different weld metal strengths were specified. A total of 71 specimens were tested, including 17 transverse PJP weld specimens, 15 longitudinal PJP weld specimens and 6 skewed PJP weld specimens. The transverse and skewed specimens were fabricated with butt joints and the longitudinal specimens used double-lap joints. Weld preparations were double-bevel with 45° groove angles and all specimens were shop welded using the FCAW process with CO_2 gas shielding.

All-weld-metal tension tests, according to ASTM A370 (ASTM, 2020), were used to measure the weld metal strength. Tension coupons were machined from standard groove-welded test plates. Three test plates for each weld classification were manufactured according to AWS A5.20 (AWS, 2015). Tension coupons were prepared according to AWS B4.0 (AWS, 2016). The mean measured tensile strengths, σ_{uw}, are listed in Table 3.3 along with the tensile strengths reported in the Certificates of Conformance.

Generally, the specimens ruptured in the weld metal. Table 3.10 shows the average P_e/P_n, P_e/P_c and f_r/σ_{uw} ratios for the longitudinal PJP specimens, where P_e is the experimental rupture load, P_n is the nominal strength calculated with the AISC *Specification* equations, P_c is the strength calculated with the measured weld size and the measured weld metal tensile strength, f_r is the rupture stress calculated with the measured rupture surface area and σ_{uw} is the experimental uniaxial tensile rupture stress based on all-weld-metal specimens. Tables 3.11 and 3.12 show the average values for the P_e/P_n, P_e/P_c and f_r/σ_{uw} ratios for the transverse and skewed PJP specimens, respectively. P_c was calculated with an effective throat equal to the groove depth with no consideration of the reinforcement.

Table 3.10. Strength ratios for longitudinal PJP welds.						
F_{EXX} ksi	P_e / P_n		P_e / P_c		f_r / σ_{uw}	
	Average	Standard Deviation	Average	Standard Deviation	Average	Standard Deviation
70	1.48	0.153	1.36	0.142	0.762	0.0704
80	1.18	0.277	1.17	0.274	0.776	0.106
100	1.23	0.122	1.23	0.122	0.730	0.0620
All Specimens	1.31	0.234	1.26	0.205	0.756	0.0831

Table 3.11. Strength ratios for transverse PJP welds.						
F_{EXX} ksi	P_e / P_n		P_e / P_c		f_r / σ_{uw}	
	Average	Standard Deviation	Average	Standard Deviation	Average	Standard Deviation
70	2.33	0.362	2.15	0.334	1.28	0.156
80	1.71	0.225	1.69	0.223	1.56	0.182
100	1.56	0.123	1.56	0.123	1.17	0.130
All Specimens	1.97	0.446	1.88	0.372	1.34	0.219

Table 3.12. Strength ratios for skewed PJP welds.						
F_{EXX} ksi	P_e / P_n		P_e / P_c		f_r / σ_{uw}	
	Average	Standard Deviation	Average	Standard Deviation	Average	Standard Deviation
70	1.62	0.149	1.50	0.138	1.02	0.0723
100	1.16	0.0112	1.16	0.0112	0.94	0.0236
All Specimens	1.39	0.255	1.33	0.196	0.98	0.0689

Similar to the proposals by Van der Eb (Faltus, 1986) and Collin and Johansson (2005), a design equation for skewed PJP welds was developed by modifying von Mises criterion according to Equation 3.48. Equation 3.48 is conservative compared to the experimental rupture stresses of the skewed PJP specimens, with an average experimental-to-calculated ratio of 1.31 and a standard deviation of 0.0728.

$$\sqrt{\sigma_T^2 + 2\tau_L^2} \le F_c \tag{3.48}$$

where

F_c = F_{EXX} for joints with matching and undermatching weld metal, ksi
= (F_{EXX} + F_u)/2 for joints with overmatching weld metal, ksi

The authors noted that all PJP welds can be designed using Equation 3.48. Compared to AISC *Specification* Equation J2-3 with $F_{nw} = 0.60F_{EXX}$, Equation 3.48 results in a 67% strength increase for transversely loaded welds and a 18% increase for longitudinally loaded welds.

The results showed that, for fillet and PJP joints with matching electrodes, calculation of the fusion zone strength is not required. For fillet and PJP joints with overmatching electrodes, the fusion zone strength can be calculated by replacing F_{EXX} with the average of the base metal strength, F_u, and the weld metal strength, F_{EXX}.

Chen et al. (2023)
Chen et al. (2023) tested PJP welds subjected to both quasi-static and intermediate strain rates. All specimens were welded using the GMAW process with a filler metal classification strength, F_{EXX} = 500 MPa (72.5 ksi). Both Q345 (F_u = 470 MPa) and Q235 (F_u = 370 MPa) base metals were used, creating specimens with matching and overmatching electrodes, respectively.

Five quasi-static specimens were loaded with normal stress perpendicular to the plane of the throat. These specimens were fabricated using butt joints with 90° double-vee grooves. The two specimens with matching welds ruptured at the weld throat with a mean tensile rupture stress of 560 MPa, which is 12% higher than the filler metal classification strength. The three specimens with overmatching welds ruptured along the fusion zone with a mean tensile stress along the throat of 488 MPa, which is 98% of the filler metal classification strength.

Six quasi-static specimens were loaded with shear stress in the plane of the throat, perpendicular to the weld axis. These specimens were fabricated using double-lap joints with 90° double-vee grooves. These specimens ruptured along the weld throat, with shear rupture stresses of 452 and 357 MPa for the matching and overmatching welds, respectively. The data for matching welds results in a shear-to-tensile strength ratio of 0.807.

HIGH STRENGTH WELDS

Li and Wang (2021) define high strength steel used in the construction industry as a family of steels with a minimum yield strength of 460 MPa (66.7 ksi). Approved high strength steels listed in AISC *Specification* Section A3.1a include:

- A913 Grade 70 high-strength low-alloy shapes with F_y = 70 ksi and F_u = 90 ksi
- A1066 Grade 80 high-strength low-alloy plates with F_y = 80 ksi and F_u = 90 ksi
- A514 quenched and tempered alloy plates with F_y = 100 ksi and F_u = 110 ksi

AWS D1.1 Table 5.4 lists filler metals with F_{EXX} = 70, 80 and 90 ksi for matching strength of base metals in Table 5.3. A913 Grade 70 is the material with the highest F_u in AWS D1.1 Table 5.3, which lists the approved base metals for prequalified welds. With qualification, AWS D1.1 Table 6.9 allows filler metals with F_{EXX} = 100 and 110 ksi. In this report, high strength welds are defined as those with either F_{EXX} > 110 ksi or F_u > 110 ksi.

Collin and Johansson (2005)
Collin and Johansson (2005) tested 27 longitudinally- and transversely loaded fillet welds in high-strength steel joints. The measured uniaxial weld metal tensile strengths were 548 and 758 MPa. The authors noted that the Eurocode 3 (CEN, 2005) directional method is over-conservative for transverse fillet welds. They recommended Equation 3.49, which compared well with the experimental rupture loads and results in k_{ds} = 1.41 when θ = 90°.

$$\sqrt{\sigma_T^2 + 2\tau_T^2 + 3\tau_L^2} \leq F_{EXX} \tag{3.49}$$

The authors noted that the calculation accuracy can be improved by using the higher of the base metal and weld metal tensile strengths. They concluded that the mean value, which was originally recommended by Lightenburg (1968) was conservative but appropriate.

Kuhlmann et al. (2008)
Kuhlmann et al. (2008) tested both longitudinally and transversely loaded fillet welds as well as PJP welds in high-strength steel joints. Compared to the Eurocode 3 (CEN, 2005) directional method, the authors proposed a less conservative value of β_w = 0.85 for S460 steel. For the longitudinally loaded fillet welds, the shear rupture stress was accurately calculated with Equation 2.13.

Rasche and Kuhlmann (2009)
Rasche and Kuhlmann (2009) studied both the strength and ductility of fillet-welded connections in high strength steel using experimental and numerical analyses. The weld electrode was selected to match the base metal in the first part of the study. The objective was to determine a more accurate correlation factor, β_w, for use in Eurocode 3 (CEN, 2005). The authors recommended β_w = 0.79 for longitudinal fillet welds connecting S460M steel, instead of 1.0 as specified in Eurocode 3.

In investigating different filler metals, overmatching electrodes increased the strength. For tests with S690Q base metals, changing the filler metal from 690 MPa specified strength to 890 MPa increased the weld resistance by 9%; however, the ductility was reduced by almost 50%. Consequently, they concluded that the strength is controlled by the filler metal rather than the base metal.

Bjork et al. (2012)
Bjork et al. (2012) tested 34 fillet welded high-strength steel joints. The project included 12 longitudinal specimens, seven transverse double-lap joints, nine transverse cruciform T-joints and six multi-orientation joints that combined longitudinal and transverse welds. The specified minimum yield and tensile strengths of the base metal were 960 MPa (139 ksi) and 1000 MPa (145 ksi), respectively. The measured yield and tensile strengths of the base metal were 1014 MPa (147 ksi) and 1,076 MPa (156 ksi), respectively. The GMAW process was used, and the measured uniaxial weld metal tensile strengths were 690 MPa (100 ksi), 915 MPa (133 ksi) and 1,245 MPa (181 ksi).

Most of the specimens with transversely loaded T-joints ruptured along the HAZ or fusion zone and generally, the remaining specimens ruptured in the weld metal. The longitudinally loaded welds ruptured approximately along the theoretical effective throat, which is defined with a rupture angle of 45°. For the transversely loaded specimens that ruptured in the weld metal, the rupture angles were approximately 20° from the load direction.

The strength of the longitudinally loaded specimens with $l/E \leq 50$ was accurately predicted with the Eurocode equations. For the specimens with $50 < l/E \leq 150$ the strength was approximately 15% less than for the shorter welds.

Sun et al. (2019)
Sun et al. (2019) tested 44 transversely loaded fillet welds in high-strength double-lap joints and T-joints. The GMAW process was used, and the measured uniaxial weld metal tensile strengths were 627, 727, 771 and 956 MPa (90.9, 105, 112 and 139 ksi). The rupture angles were approximately 20° (13° to 24°) from the load direction for all weld sizes and electrode grades. The average ductility of double-lap joints was similar to that of T-joints. The test-to-predicted ratios were between 1.68 and 2.52 with an average of 2.01 for the Eurocode equations. For the AISC equations, the test-to-predicted ratios were between 1.08 and 1.61 with an average of 1.29.

Of the two joint types, the measured rupture surface area was larger for the T-joints. Due to the penetration and the low rupture surface angle, much of the rupture area for the T-joints was in the HAZ rather than the weld metal. In high-strength welds, metallurgical softening causes the HAZ to be weaker than the base metal. This may explain why, although the measured rupture surface was larger at the T-joints, the rupture load for both joint types was approximately the same. Another factor that was discussed by the authors is the presence of friction at the faying surfaces of the lap-joints which cannot exist in the T-joints.

Ran et al. (2021)
Ran et al. (2021) tested 48 fillet welded specimens in high-strength double-lap joints with various loading angles. The loading angles varied from 0° to 90° in 15° increments. After welding, the welds were machined to obtain a perfect triangular shape with the specified weld size of $w = 5$ mm at each leg. The GMAW process was used, and the mean measured uniaxial weld metal tensile strength was 1,052 MPa (153 ksi). For all specimens, the rupture location was in the weld metal. The test-to-predicted ratios were between 1.75 and 2.42 with an average of 2.15 for the Eurocode equations. For the AISC equations, the test-to-predicted ratios were between 1.50 and 2.31 with an average of 1.80.

Ghimire and Wald (2023)
Ghimire and Wald (2023) tested six transversely loaded fillet welds in high-strength double-lap joints. The GMAW process was used, and the measured uniaxial weld metal tensile strength was 779 MPa (113 ksi). The test-to-predicted ratios were between 1.06 and 1.29 with an average of 1.21 for the AISC equations.

ECCENTRICALLY LOADED FILLET WELD JOINTS

Several projects tested eccentrically loaded T-joints, where the eccentricity is perpendicular to the plane of the weld group (Schreiner, 1935; Jensen and Crispen, 1938; Archer et al., 1959; Dawe and Kulak, 1974; Beaulieu and Picard, 1985; Kanvinde et al., 2009b). However, for these specimens, the weld strength cannot be properly isolated from the other variables. This difficulty is caused by the interaction between the weld on the tension side of the neutral axis and the bearing strength of the connecting elements on the compression side of the neutral axis. Therefore, these tests were omitted from the data set in this report and only the data from the lap-joint specimens were included in the analysis.

Schreiner (1935)
In addition to testing two eccentrically loaded T-joints, Schreiner (1935) tested 25 double-lap fillet welded specimens that were subjected to flexural loads. Sixteen specimens were subjected only to flexure and nine specimens were tested with eccentric shear loads oriented parallel to the axis of the welds. The variables were weld size (⅜ and ½-in.), weld length (1.5, 3, 6 and 10 in.), electrode type (lightly and heavily coated) and eccentricity. The weld metal strength was measured from specimens that were machined from fillet welds. The heavily coated electrodes had a measured weld metal tensile strength of 67.0 ksi with 26.5% elongation and 60.5% reduction in area. The lightly coated electrodes had lower strength and ductility, with a measured weld metal tensile strength of 54.5 ksi and only 5.8% elongation and 13.3% reduction in area. The measured weld sizes were between 0 and ⅛ in. larger than the specified weld sizes.

The rupture surface orientations were dependent on the electrode type. For the specimens that were welded with the lightly coated electrodes, the welds ruptured along the 45° theoretical throat. The specimens that were fabricated with the heavily coated electrodes had rupture planes in the weld that were oriented at "a very flat angle to the main plate."

Although the welds made with the lightly coated electrodes had low ductility, the tests showed that the plastic stress distribution was reached for all specimens. Schreiner (1935) concluded that the plastic distribution is more accurate than the elastic distribution for predicting the experimental rupture loads.

Koenigsberger (1951)
Koenigsberger (1951) tested five eccentrically loaded single-lap fillet welded specimens. The weld group geometries included a C-shaped group and four groups with two parallel welds. The variables were the weld group dimensions (2, 3 and 6 in.), eccentricity (2.50, 3.00 and 5.75 in.) and load orientation relative to the weld axis (parallel and perpendicular). The weld metal tensile strength, σ_{uw}, from all-weld-metal coupons was 74 ksi and the elongation was approximately 28%.

Equations were derived to determine the plastic strength of the tested weld groups, and these equations were used to plot design graphs. Comparisons between the calculated and experimental strengths revealed that the weld rupture strength can be predicted accurately with the plastic design graphs.

Butler et al. (1972)
Butler et al. (1972) tested 13 eccentrically loaded double-lap fillet weld specimens. The program included five specimens with C-shaped weld groups and eight specimens with linear weld groups. The variables were the weld group dimensions (3, 4, 6, 8, 10, 12 and 16 in.) and eccentricity (5, 6, 8, 10, 12, 14, 15 and 16 in.). The specified fillet weld size was ¼ in. The weld sizes were measured, and the experimental loads were adjusted by multiplying by the measured-to-specified weld sizes. The specimens were fabricated with the SMAW process using E60 electrodes. The actual weld metal tensile strength was not measured.

Swannell and Skewes (1979), Swanell (1981)
Swannell and Skewes (1979) and Swanell (1981) documented 21 experimental tests on eccentrically loaded single-lap fillet weld specimens. Various weld group shapes were used,

including rectangular box-shaped, C-shaped and groups with two parallel welds. The variables were the weld group dimensions (30, 60, 90 and 150 mm), eccentricity (105, 120, 135 and 150 mm) and load orientation relative to the weld axis (parallel and perpendicular). The specified fillet weld size was ¼-in. and the actual weld sizes were measured. The specimens were fabricated with the SMAW process using E6013 electrodes. The weld metal tensile strength, σ_{uw}, from all-weld-metal coupons was 78.1 ksi.

Kulak and Timler (1984)
Kulak and Timler (1984) documented three experimental tests on eccentrically loaded single-lap fillet weld specimens. The weld groups had two parallel welds with eccentric shear loads oriented perpendicular to the axis of the welds. The variables were the distance between the parallel welds (200, 300 and 400 mm) and the eccentricity (140, 300 and 400 mm). The specified fillet weld size was ¼-in. and the actual weld sizes were measured. The specimens were fabricated with the SMAW process using E70 electrodes. The actual weld metal tensile strength was not measured.

Sanaei and Kametkar (1988)
In addition to the concentrically loaded joints that were tested by Sanaei and Kametkar (1988), nine eccentrically loaded double-lap specimens were tested. The specimens were loaded by applying a compression force to the center plate, which was resisted by opposing compression forces in the lap plates. The loading direction varied, with load angles, θ, equal to 0°, 30°, 60° and 90°. The weld metal tensile strength, σ_{uw}, from all-weld-metal coupons was 71.2 ksi. The specified fillet weld size was 8 mm and the actual weld sizes were recorded. All welds were 100 mm long.

Bjork et al. (2014)
Bjork et al. (2014) tested three high-strength linear fillet welds subjected only to in-plane moments. Two electrodes were specified with the same 980 MPa (140 ksi) strength but different elongation values: 14% and 19%. The specimen with 19% elongation reached the plastic strength according to AISC *Specification* Equation J2-5, including the directional strength factor ($M_n = 0.90F_{EXX}EL^2/4$). However, both specimens with 14% elongation reached only the elastic strength according to AISC *Specification* Equation J2-5, including the directional strength factor ($M_n = 0.90F_{EXX}EL^2/6$).

Soliman et al. (2021)
Soliman et al. (2021) tested two different specimens with duplicate specimens for a total of five eccentrically loaded double-lap fillet welded tests. The specimens were tested with eccentric shear loads oriented parallel to the axis of the weld group. A 3-in. eccentricity and a specified fillet weld size of 5⁄16 in. were used for all tests. The only variable was the weld length, with three tests for specimens with 4.5 in. long welds and two tests for specimens with 9.75 in. long welds. The specimens were fabricated with the SMAW process using E7018 electrodes. The weld metal tensile strength, σ_{uw}, from all-weld-metal coupons was 83 ksi. The actual weld sizes were not measured. Based on comparisons with the strengths calculated with the instantaneous center of rotation method, Soliman et al. (2021) concluded that "the AISC model is highly conservative in quantifying the capacity of these eccentric connections."

CHAPTER 4
STATISTICAL PARAMETERS

An accurate reliability analysis must consider the actual, measured, weld geometries and material strengths. The bias and variation between actual and specified properties are discussed in this chapter. The bias coefficient is

$$\rho_R = \rho_M \rho_G \rho_P \tag{4.1}$$

where

ρ_G = bias coefficient for the geometric properties, addressing the difference between the nominal throat area based on the specified weld size and the actual throat area. ρ_G is the mean value of E_m/E.

ρ_M = bias coefficient for the material properties, addressing the difference between the specified and actual weld metal tensile strengths. ρ_M is the mean value of σ_{uw}/F_{EXX}.

ρ_P = bias coefficient for the test-to-predicted strength ratios. Mean value of the professional factor calculated with the measured geometric and material properties

The coefficient of variation is

$$V_R = \sqrt{V_M^2 + V_G^2 + V_P^2} \tag{4.2}$$

where

V_G = coefficient of variation for the geometric properties, addressing the difference between the nominal throat area based on the specified weld size and the actual throat area

V_M = coefficient of variation for the material properties, addressing the difference between specified and actual weld metal tensile strengths

V_P = coefficient of variation for the test-to-predicted strength ratios

TENSILE STRENGTH

The bias coefficient and coefficient of variation for the material properties, ρ_M and V_M are discussed in this section of the report. ρ_M and V_M address the difference between the specified and actual weld metal tensile strengths.

Existing Literature

The statistical parameters for SMAW welds in Table 3.1 were published in a paper by Fisher et al. (1978), who based their reliability analysis on $\rho_M = 1.05$ and $V_M = 0.04$. The values in Table 4.1 were compiled by Omer Blodgett using the data from Certificates of Conformance (CC) from The Lincoln Electric Company (Miller, 2022).

Table 4.1. Statistical parameters for tensile strength for SMAW welds (Fisher et al., 1978).			
Electrode Classification	***n***	**ρ_M**	**V_M**
E60XX	127	1.06	0.039
E70XX	138	1.04	0.036
E80XX	136	1.10	0.049
E90XX	16	1.11	0.043
E110XX	72	1.06	0.040
n = sample size			

The reliability analysis by Fisher et al. (1978) was the basis for the weld provisions in the 1986 AISC LRFD *Specification* (AISC, 1986). The available research-oriented results are listed in Table 4.2. The ρ_M values for the welding processes currently used for most shop and field welds indicate that $\rho_M > 1.05$ may be appropriate. For the 70 ksi welds tested since 2000, $\rho_M = 1.20$.

Table 4.2. Research-oriented statistical parameters for tensile strength.				
Reference	**Electrode Classification**	**Welding Process**	***n***	**ρ_M**
Swannell (1974)	E6013	SMAW	1	1.15
Swannell and Skewes (1979)	E60XX	SMAW	2	1.31
Miazga and Kennedy (1986)	E7014	SMAW	3	1.11
Gagnon and Kennedy (1989)	E7018	SMAW	10	1.20
Gresnight (1992)	E9018	SMAW	3	1.06
Gresnight (1992)	68 ksi	SMAW	3	1.02
Gresnight (1992)	ER70S-6	GMAW	3	1.12
Bowman and Quinn (1994)	E7018	SMAW	3	0.986
Callele et al. (2005, 2009)	E70T-7	FCAW-S	6	1.19
Grismo et al. (2017)	E70XX	SMAW	3	1.14
Gallow (2019)	E71T-1	FCAW-G	3	1.19
Luo et al. (2020b)	ER70S-3	GMAW	3	1.36
Reynolds et al. (2020)	E71T-1	FCAW-G	2	1.30
Dowswell et al. (2021)	E70T-1	FCAW-G	3	1.08
Dowswell et al. (2021)	E80T-1	FCAW-G	3	1.01
Dowswell et al. (2021)	E100T-1	FCAW-G	3	1.00
Waite et al. (2022)	E7018	SMAW	2	1.19
n = sample size				

Lesik and Kennedy (1988, 1990) compiled the available data from several sources, including Fisher et al. (1978) and several of the references in Table 4.2. The resulting values from 672 specimens are $\rho_M = 1.12$ and $V_M = 0.077$. A later analysis by Li et al. (2007) included 716 specimens, resulting in $\rho_M = 1.13$ and $V_M = 0.080$. For their data set, Li et al. (2007) noted that "there seems to be no correlation between ρ_M and the nominal filler metal tensile strength." Background documentation to Eurocode 3 (CEN, 2005) indicates that the provisions in Section 4 were based on $\rho_M = 1.14$ and $V_M = 0.07$. Teh and Rasmussen (2002) used $\rho_M = 1.1$ and $V_M = 0.1$ in their analysis.

Current Welding Processes

Because the measured weld metal tensile strength varies with the welding process, information on current welding practices is required. Welding data was collected from eleven companies that

fabricate and/or erect structural steel for buildings and industrial structures. Various company sizes and capabilities make up the group, including a metal building manufacturer. Information from previous research, design and consulting projects by the authors were reviewed, and new data was collected.

The data, which is summarized in Table 4.3, follows the general trends discussed in AISC Design Guide 21 (Miller, 2017). For shop welds, FCAW-G is the primary process used by most fabricators; however, GMAW also has significant use. For field welds, the primary process is FCAW-S, with limited use of SMAW. SAW is used by metal building fabricators and has limited use with large structural steel fabricators for the fabrication of plate girders and other built-up members.

Table 4.3. Current welding practices.

Welding Process	Electrode Classification	Gas Shielding	Number of Companies	Notes
FCAW-G	E71T-1	100% CO_2	5	
FCAW-G	E71T-1	75% (+) Ar 25% (-) CO_2	4	
FCAW-G	E81T-1	100% CO_2	1	Dowswell et al. (2021)
FCAW-G	E101T-1	100% CO_2	1	Dowswell et al. (2021)
FCAW-S	E70T		2	
FCAW-S	E71T		2	
GMAW	E70C-6M-H4	75% (+) Ar 25% (-) CO2	2	
GMAW	ER70S-3	100% CO2	1	
GMAW	ER70S-6	85% Ar 15% CO2	1	
GMAW	E80C-Ni1	75% (+) Ar 25% (-) CO2	2	
SAW	F7A6-EM12K-H8		1	
SAW	F7A2-EM13K-H8		1	
SAW	F7A2-EM12K		1	
SMAW	E7018		2	
SMAW	E7014		1	

The information collected in the survey was considered in assigning weights for each welding process to determine weighted averages and standard deviations for the weld metal tensile strength. Because electrodes for some welding processes have a limited strength range, the weights assigned to each process were different for each strength level. Due to the approximate nature of the weighted average approach, the assigned weights were often based on conservative estimates. For example, although used primarily for tack welding in the shop and for minor field welds, E70XX SMAW electrodes were weighted at 5%. This is considered conservative because E70XX SMAW electrodes are used on less than 5% of the total weld volume and they have the lowest measured-to-specified ratio. The weighting assignments are listed in Table 4.4.

Table 4.4. Welding process weight assignments.

Welding Process	Electrode Classification				
	70 ksi	80 ksi	90 ksi	100 ksi	110 ksi
FCAW-G	50%	50%	50%	60%	30%
GMAW	30%	30%	35%	25%	40%
FCAW-S	10%	10%	10%	0%	0%
SAW	5%	5%	0%	5%	0%
SMAW	5%	5%	5%	10%	30%

Effect of Strain Rate

Filler metal classification strengths are determined using all-weld-metal tensile tests according to AWS B4.0, which specifies the testing procedures in ASTM E8. These test results are reported on product certificates of conformance to document their compliance with the corresponding AWS A5 standard. For tensile strength measurements, ASTM E8 (ASTM, 2016) Section 7.6.5 allows strain rates between 0.05 and 0.5 in./in./min. The maximum value is equal to a strain rate of 0.00833 s^{-1}. Dieter (1986) defined the strain rate range for tensile tests, with static strain rates between10^{-5} and 10^{-1} s^{-1} and dynamic strain rates between 10^{-1} and 10^{2} s^{-1}. Compliance testing by electrode manufacturers is assumed to be performed at the maximum strain rate allowed for the post-yield range. This has been verified for a major electrode manufacturer (Miller, 2022).

Both the yield and tensile strengths measured with all-weld-metal tensile tests vary with strain rate. To obtain static values, yield stresses from mill test reports have been reduced by different amounts by various researchers. For example, mill test values were reduced by 4, 4.25 and 2.44 ksi by Galambos and Ravindra (1978), Schmidt and Bartlett (2002) and Jaques and Frank (1999), respectively.

Although the yield strength reductions are known to be estimates, the determination of appropriate values for weld metal tensile strength is further complicated. Previous research has shown a reduction in strain rate sensitivity with increased strength, and the tensile strength is less dependent on strain rate than yield strength (Dieter, 1986). Using tensile tests on S690QL and S960QL high strength steels, Alabi et al. (2018) found that the properties measured with quasi-static tensile tests are valid up to a maximum strain rate of 4 s^{-1}. Based on the experimental results, the authors observed a lower strain rate sensitivity for steels with finer-grained microstructures. Tensile tests on lower strength specimens of Q355 steel showed that the properties measured with quasi-static tensile tests are valid up to a maximum strain rate of approximately 2 s^{-1} (Chen et al., 2021). At higher strain rates, the tensile strength increased with the log of the strain rate.

Soroushian and Choi (1987) used data found in the literature to formulate empirical equations to estimate steel properties at dynamic loading rates. Because strain rate sensitivity has an inverse relationship with strength, the equation variables were the strain rate and yield strength. For weld metal strengths of 70 and 110 ksi tested at a strain rate of 0.00833 (1/120) s^{-1}, the trend lines show tensile strength increases of approximately 4% and 2%, respectively.

To determine the strength of fillet welds subjected to impact loading, Grismo et al. (2017) tested both longitudinal and transverse fillet weld specimens. The specimen were fabricated by welding S355 plates with a tensile strength of 68.2 ksi (470 MPa) using E70XX SMAW electrodes. For the base metal and the all-weld-metal coupons machined from groove-welded plates, three different strain rates were used to determine the uniaxial properties: 10^{-3} s^{-1}, 10^{-1} s^{-1} and 300 s^{-1}. Although the base metal was more strain-rate sensitive than the weld metal, the strain rate increases from 10^{-3} s^{-1} to 10^{-1} s^{-1} resulted in a weld metal tensile strength increase of 4% and the strain rate increase from 10^{-3} s^{-1} to 300 s^{-1} resulted in a 22% increase.

Chen et al. (2021) Used experimental tests on Q355 steel welded with matching weld metal to study the effect of strain rate on the properties of the base metal, weld metal and HAZ. The measured tensile strengths in Table 4.5 show the expected strength increase for the dynamically

loaded specimens. However, the HAZ and weld metal strengths were higher for the quasi-static specimens.

Table 4.5. Tensile strengths measured by Chen et al. (2021).		
Coupon Location	**Quasi-Static Strain Rate: 10^{-3} s^{-1}**	**Dynamic Strain Rate: 2 to 3 s^{-1}**
Base Metal	76.6 ksi	78.5 ksi
HAZ	78.6 ksi	78.0 ksi
Weld Metal	73.5 ksi	71.9 ksi

Based on the research discussed in this section, a 2.5 ksi reduction was applied to the tensile strengths listed on manufacturer CMTRs and CCs. Because research-oriented specimens are typically tested at quasi-static strain rates, the research-oriented tensile strength data was not reduced.

Effect of Dilution

The extent of admixture is dependent on the welding parameters, welder technique and joint geometry. Miller (1989) discussed the effect of joint geometry using two different preparations, showing that the square butt welds are composed primarily of the base metal and single vee butt welds are composed primarily of the weld metal. Svensson (1994) noted that dilution is typically between 25% and 50%. 25% dilution is in agreement with the design requirements in prEN 1993-1-8 (CEN, 2021) for steel grades higher than S460 with mismatched filler metals. 50% dilution is in agreement with the design method proposed by Lightenburgh (1968), Treiberg (1992) and other researchers.

Effect of Cooling Rate

The microstructures of both the weld metal and heat affected zone are dependent on the welding parameters. For carbon steels, higher cooling rates result in stronger welds with less ductility and reduced impact properties. The cooling rate is dependent on the heat input, preheat level, interpass temperature and the ambient temperature (Miller, 1989). The cooling rate is also affected by the connection geometry. When several thick elements intersect at the welded joint, the heat sink effect is greater than the condition where two thin elements are connected.

Another variable that can affect the strength and ductility is the number of weld passes. Single-pass welds typically cool faster than multi-pass welds. For multi-pass welds without preheat, the first pass will cool faster than subsequent passes (Miller, 1989). Additionally, weld passes can be effectively heat treated by subsequent passes, causing lower strength and higher impact properties (Miller, 1989). However, the data summarized by Callele et al. (2005, 2009) showed that the weld strength is independent of the number of passes.

The effect of cooling rate was clearly shown in the tests by Gresnigt (1992), where the weld metal tensile strengths were measured with coupons extracted from conventional groove welded plate specimens and coupons extracted from fillet welds. The strength ratios, which are listed in Table 3.7, show that the fillet weld coupons are about 9% stronger on average than the groove weld coupons. Similar tests by Grismo et al. (2017) showed an 18% strength increase for the fillet weld coupons compared to the groove weld coupons. Grismo et al. (2017) attributed the difference to the cooling rate during and after welding: “the butt weld was manufactured with several weld

passes, which induced a comparatively low cooling rate. Thus, a coarser ferritic microstructure would develop, and a weaker weld metal was obtained."

Consideration of every possible condition cannot be duplicated in a single standardized all-weld-metal tensile coupon. Miller (1989) noted that the tensile test in AWS B4.0 is for "classification or qualification of a particular product to a specific filler metal type." Because the welding parameters are controlled within the limits of AWS D1.1 and the fabricators Welding Procedure Specification (WPS), the weld metal tensile strength and ductility is expected to be within an acceptable range for properly welded and inspected joints.

Specimen design for welded joints is often limited by the loading capacity of the available testing machine, resulting in single-pass welds for many of the specimens documented in this report. In these cases, the uniaxial tensile strength of the test weld is likely higher than that of the all-weld-metal coupon. For multi-pass welds, the tensile strengths will likely be closer to the measured values.

Relevant Data

For most welds in buildings, the welding parameters deviate significantly from the conditions specified for the tensile test in AWS B4.0. Although, this usually results in strengths that are greater than those measured with the tensile test, the tensile strength variation is considered in the statistical parameters associated with the test-to-predicted strength ratios. For most of the research projects, the tensile strength was measured with tests according to, or similar to AWS B4.0. These tensile strengths were used to calculate the predicted strengths in the test-to-predicted ratios.

Based on the information reviewed in this section, it was concluded that ρ_M can be calculated with the tensile strength data from a combination of Certificates of Conformance (CC), Certified Material Test Reports (CMTR) and research-oriented results. The effect of strain rate was considered by reducing the tensile stress from the CMTRs and CCs by 2.5 ksi. The variation in tensile strength with the welding process was considered by applying the weighting assignments listed in Table 4.4.

The CC data consists of 380 current CCs from three major electrode manufacturers representing each welding process listed in Table 4.4. Table 4.6 lists the statistical parameters, which were based on the tensile strengths listed on the CC (the values were not reduced by 2.5 ksi). A comparison of the ρ_M values in Tables 4.1 and Table 4.6 indicates a mean 4% strength increase for the current data set.

Table 4.6. Statistical parameters for tensile strength from Certificates of Conformance.

Electrode Classification	*n*	ρ_M	V_M
70 ksi	228	1.18	0.0566
80 ksi	87	1.11	0.0526
90 ksi	32	1.10	0.0534
100 ksi	23	1.13	0.0458
110 ksi	10	1.06	0.0131
n = sample size			

The CMTR data consists of 21 CMTRs from a large structural steel fabricator, with dates between 2012 and 2022. This data set includes three CMTRs for the SAW process and 18 CMTRs for the GMAW process with 75% (+) Ar 25% (-) CO2 shielding gas. The electrode classification for two CMTRs was E80C-Ni1-H4, and the remaining CMTRs were for the E70C-6M-H4 electrode classification.

The research-oriented results are listed in Table 4.2. The data set includes all specimens with tensile strengths equal to or greater than 70 ksi.

The final statistical parameters for each electrode strength are listed in Table 4.7. These values were calculated with a 2.5 ksi reduction for the CMTR and CC data. For all electrode strength classifications, 416 data points resulted in on $\rho_M = 1.12$ and $V_M = 0.0543$. These values are similar to those calculated by Lesik and Kennedy (1988, 1990), Li et al. (2007) and Eurocode 3 (CEN, 2005).

Table 4.7. Statistical parameters for tensile strength for the complete data set.

Electrode Classification	*n*	ρ_M	V_M
70 ksi	259	1.14	0.0583
80 ksi	90	1.08	0.0528
90 ksi	33	1.07	0.0532
100 ksi	24	1.10	0.0451
110 ksi	10	1.03	0.0134
n = sample size			

SHEAR-TO-TENSILE STRENGTH RATIO

Although the AISC *Specification* equations are based on the weld shear strength, weld strengths are specified using tensile strengths, which are measured with all-weld-metal tensile tests according to AWS B4.0. The variation in material strength can be considered by separating the tensile strength variation from the shear-to-tensile strength ratio (Fisher et al., 1978; Li et al., 2007). The bias coefficient associated with the shear-to-tensile strength ratio, ρ_{M2}, is discussed in this section of the report. ρ_{M2} is not used in the reliability analysis because the bias and variance associated with the shear-to-tensile strength ratio are included in ρ_P and V_P, respectively. However, the information in this section can be used to determine the accuracy of the 0.6 ratio in AISC *Specification* Equation J2-5. This information can also be used to refine the design method by using a more accurate shear-to-tensile strength ratio if necessary.

Existing Literature

According to Brockenbrough and Johnston (1974), the shear rupture strength of structural steel "ranges from 2/3 to 3/4 of the tensile strength." Gaines (1987) noted that a shear-to-tensile strength ratio of 0.75 has been approved for the design of welds in steel Naval ships.

Kulak (1972) summarized 180 tests on longitudinally loaded fillet weld joints, resulting in a mean shear-to-tensile strength ratio, $(\tau_u/\sigma_{uw})_m$, of 0.769 with a coefficient of variation, V_{M2}, of 0.126.

Based on a similar study with 133 tests, Fisher et al. (1978) calculated $(\tau_u/\sigma_{uw})_m = 0.84$ and $V_{M2} = 0.10$. Using 126 tests, Lesik and Kennedy (1988, 1990) calculated $(\tau_u/\sigma_{uw})_m = 0.749$ and $V_{M2} = 0.121$. Using the results of 304 specimens from eight research projects, Li et al. (2007) calculated $(\tau_u/\sigma_{uw})_m = 0.774$ and $V_{M2} = 0.130$. Li et al. (2007) also determined that the shear-to-tensile strength ratio was not affected by the weld size or the weld metal tensile strength.

Table 4.8 summarizes the various shear-to-tensile strength ratios discussed in Chapter 3 and in this section of the report. For the specification provisions, the ratio ranges from 0.577 to 0.75. Generally, these values are conservative compared to the experimental results, which range from 0.64 to 0.948. However, as discussed in the section on Tensile Strength, a portion of this difference can be attributed to the higher tensile strength of the tested welds compared to the all-weld-metal coupons.

Table 4.8. Shear-to-tensile strength ratios, τ_u/σ_{uw}.

Reference	τ_u/σ_{uw}	Source	Comments
AISC *Specification* (AISC, 2022)	0.60	Specification	
AWS D1.1 (2015)	0.60	Specification	
Canadian Standard CSA (2014)	0.67	Specification	
Eurocode 3 (CEN, 2005)	0.722	Specification	$\beta_w = 0.80$
Eurocode 3 (CEN, 2005)	0.679	Specification	$\beta_w = 0.85$
Eurocode 3 (CEN, 2005)	0.642	Specification	$\beta_w = 0.90$
Eurocode 3 (CEN, 2005)	0.577	Specification	$\beta_w = 1.0$
Eurocode 3 (CEN, 2005)	0.525	Specification	$\beta_w = 1.1$
AIJ (2012)	0.577	Specification	
Naval Ships	0.75	Specification	Gaines (1987)
ISO	0.745	Specification	Ligtenburg (1968)
International Institute of Welding (IIW)	0.745	Specification	Van der Eb (1952)
Freeman (1931)	0.69	Design	For butt welds
Rosenthal and Levray (1939)	0.833	Experimental	
Spraragen and Claussen (1942)	0.64-0.84	Experimental	
Koenigsberger (1951)	0.73	Experimental	
Eb (1952)	0.807	Experimental	
Vreedenburgh (1954)	0.75	Experimental	
Wastlund and Ostlund (1956)	0.692	Experimental	
Swannell (1968)	0.885	Experimental	
Ligtenburg (1968), Strating (1971)	0.83	Experimental	
Kulak (1972)	0.769	Experimental	$V_{M2} = 0.126$
Brockenbrough and Johnston (1974)	0.67-0.75	Experimental	
Fisher et al. (1978)	0.84	Experimental	$V_{M2} = 0.10$
Lesik and Kennedy (1988, 1990)	0.749	Experimental	$V_{M2} = 0.121$
Miazga and Kennedy (1989)	0.764	Experimental	
Li et al. (2007)	0.774	Experimental	$V_{M2} = 0.130$
Gallow (2019)	0.948	Experimental	
Gallow (2019)	0.837	Experimental	Torsion Tests
Dowswell et al. (2021)	0.820	Experimental	$F_{EXX} = 70$ ksi
Dowswell et al. (2021)	0.843	Experimental	$F_{EXX} = 80$ ksi
Dowswell et al. (2021)	0.752	Experimental	$F_{EXX} = 100$ ksi
Chen et al. (2023)	0.807	Experimental	

τ_u = measured weld metal shear rupture stress
σ_{uw} = measured weld metal uniaxial tensile stress

Krumpen and Jordan (1984) developed equations to estimate the shear strength of weld metal as a function of the tensile strength by curve fitting experimental results from the literature with filler metal classification strengths between 60 and 140 ksi. Equations 4.3 and 4.5 were developed for SMAW and GWAM electrodes, respectively. These equations were divided by the tensile strength, σ_{uw}, resulting in the shear-to-tensile strength ratios according to Equations 4.4 and 4.6. These equations were used to calculate the shear-to-tensile strength ratios in Table 4.9.

$$\tau_u = 1.8\sigma_{uw}^{0.80} \tag{4.3}$$

$$\frac{\tau_u}{\sigma_{uw}} = \frac{1.8}{\sigma_{uw}^{0.20}} \tag{4.4}$$

$$\tau_u = 2.5\sigma_{uw}^{0.75} \tag{4.5}$$

$$\frac{\tau_u}{\sigma_{uw}} = \frac{2.5}{\sigma_{uw}^{0.25}} \tag{4.6}$$

Table 4.9. Shear-to-tensile strength ratios calculated with the Krumpen and Jordan (1984) Equations.

F_{EXX} ksi	τ_u/σ_{uw}	
	SMAW	GMAW
60	0.794	0.898
70	0.770	0.864
80	0.749	0.836
90	0.732	0.812
100	0.717	0.791
110	0.703	0.772

Discussion

The experimental shear-to-tensile strength ratios in Table 4.8 and the values in Table 4.9 show the conservatism of the 0.60 ratio in the AISC *Specification*. Although the Eurocode 3 values are also conservative, the general trend in Table 4.9 is captured with the Eurocode equations, where the strength ratio reduces with increasing tensile strength.

Except for the torsion tests by Gallow (2019), the experimental shear-to-tensile strength ratios in Table 4.8 were based on longitudinal PJP and fillet weld tests. Although the tests by Gallow (2019) and Dowswell (2021) had specimens with multi-pass welds, most of the tested welds were single-pass fillet welds. As discussed in the previous section of this report, differences in the cooling rates for the single-pass test welds and the associated all-weld-metal coupons would likely cause higher tensile strengths for the weld metal in the test welds. This effect could be the source for a portion of the disparity. However, with $(\tau_u/\sigma_{uw})_m$ = 0.774 from Li et al. (2007), ρ_{M2} = 1.29, which is significantly greater than the 7 to 18% increase that was documented by Gresnigt (1992) and Grismo et al. (2017).

DIRECTIONAL STRENGTH INCREASE FOR FILLET WELDS

An increase in the load angle, θ, for fillet welds results in a nonlinear strength increase and a decrease in ductility. Based on 18 experimental tests with loading angles of 0°, 30°, 60° and 90°, Clark (1971) showed that the transversely loaded welds were approximately 70% stronger than the longitudinally loaded welds. Gaines (1987) noted that a transverse-to-longitudinal strength ratio of 1.44 has been approved for the design of fillet welds in steel Naval ships. Although the information in this section is not used in the reliability analysis, it can be used to determine the accuracy of equation for k_{ds} and to refine the design method if necessary.

Table 4.10 summarizes the transverse-to-longitudinal strength ratios found in the literature. The experimental values are between 1.12 and 1.70. The theoretical ratios range from 1.30 to 1.48, with a ratio of 1.50 for the semi-empirical equation developed by Miazga and Kennedy (1989). For the various specifications reviewed, the ratios are between 1.13 and 1.50.

Table 4.10. Fillet weld transverse-to-longitudinal strength ratios, k_{ds}, for θ = 90°.

Reference	k_{ds}	Source	Comments
AISC *Specification* (AISC, 2016)	1.50	Specification	
AWS D1.1 (2015)	1.50	Specification	
Canadian Standard CSA (2014)	1.50	Specification	
Eurocode 3 (CEN, 2005)	1.22	Specification	Directional Method
AIJ (2012)	1.40	Specification	
Naval Ships	1.44	Specification	Gaines (1987)
ISO	1.13	Specification	Ligtenburg (1968)
International Institute of Welding (IIW)	1.13	Specification	Van der Eb (1952)
Freeman (1931)	1.60	Design	
Vreedenburgh (1954)	1.12	Experimental	
Archer et al. (1959)	1.56	Experimental	
Preece (1968)	1.57	Experimental	F_{EXX} = 70 ksi
Preece (1968)	1.44	Experimental	F_{EXX} = 110 ksi
Ligtenburg (1968), Strating (1971)	1.60	Experimental	
Butler and Kulak (1971)	1.45	Experimental	
Clark (1971)	1.70	Experimental	
Kato and Morita (1974)	1.46	Theoretical	
Kamtekar (1982), Kamtekar (1987)	1.41	Theoretical	
Kennedy and Kriviak (1985)	1.42	Experimental	
Neis (1985)	1.41	Theoretical	
McClellan (1989)	1.51	Experimental	F_{EXX} = 70 ksi
McClellan (1989)	1.39	Experimental	F_{EXX} = 100 ksi
Miazga and Kennedy (1989)	1.50	Semi-empirical	Lap joints in tension
Miazga and Kennedy (1989)	1.34	Semi-empirical	Lap joints in compression
Bowman and Quinn (1994)	1.20-1.70	Experimental	
Iwankiw (1997)	1.41	Theoretical	
Yasui et al. (2004)	1.26	Theoretical	
Collin and Johansson (2005)	1.41	Semi-empirical	
Lu et al. (2015)	1.48	Theoretical	
Lu and Dong (2020)	1.30	Theoretical	
Luo et al. (2020a)	1.41	Theoretical	
Luo et al. (2020b)	1.34	Experimental	
Dowswell et al. (2021)	1.30	Experimental	

GEOMETRIC PROPERTIES

The bias coefficient and coefficient of variation for the geometric properties, ρ_G and V_G are discussed in this section of the report. ρ_G and V_G address the difference between the nominal throat area based on the specified weld size and the actual throat area. An equal-leg fillet weld with ψ = 90° is shown in Figure 4.1. *w* is the leg size, which is commonly known as the weld size, *E* is the effective throat and *p* is the penetration depth.

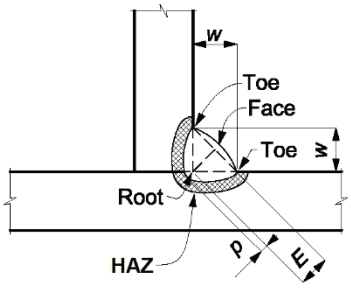

Fig. 4.1. Fillet weld.

A single-bevel PJP weld is shown in Figure 4.2. *S* is the preparation (bevel) size, *E* is the effective throat and *Z* is the Z loss dimension.

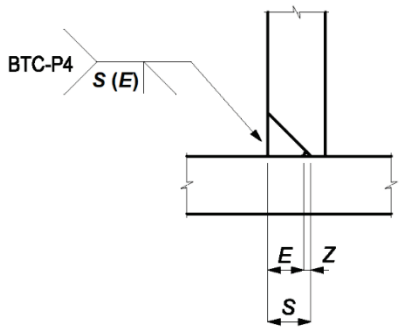

Fig. 4.2. Single-bevel PJP weld.

Tolerances

Profile tolerances for fillet and PJP welds are specified in AWS D1.1 (AWS, 2020) Section 7.23. Fillet weld profile tolerances are specified in Section 7.23.1. The faces of fillet welds may be slightly convex, flat or slightly concave. Convex and concave profiles are shown in Figures 4.3a and b, respectively. The maximum allowable convexity, C_{max}, is specified in D1.1 Table 7.9, where the allowable convexity is dependent on the width of the weld face, *W*, as listed in Table 4.11. There is no limit on concavity if the minimum weld size, considering both leg and throat dimensions, is achieved.

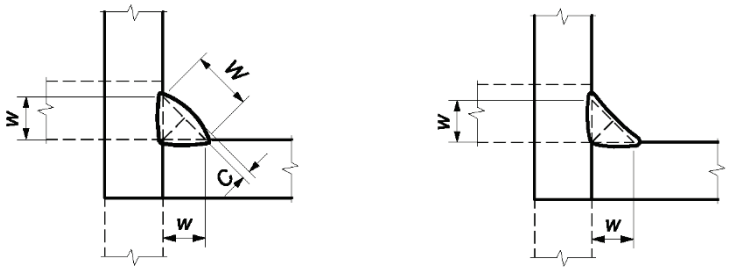

a. Convex *b. Concave*

Fig. 4.3. Fillet weld profiles.

Table 4.11. Fillet weld profile tolerances (from AWS Table 7.9)		
W **(in.)**	w_W **(in.)**	C_{max} **(in.)**
$W \leq 5/16$	$w_W \leq 0.221$	1/16
$5/16 < W < 1$	$0.221 < w_W < 0.707$	1/8
$W \geq 1$	$w_W \geq 0.707$	3/16
C_{max} = maximum allowable convexity W = width of weld face w_W = equivalent weld size corresponding to W for a perfectly triangular weld = $W/\sqrt{2}$		

PJP profile tolerances are specified in AWS D1.1 Section 7.23.3. In all cases, reinforcement must be equal to or greater than 0 in. The maximum allowable reinforcement, R_{max}, for butt and outside corner joints is specified in AWS D1.1 Table 7.9, where the allowable reinforcement is dependent on the effective throat, E, as listed in Table 4.12.

Table 4.12. PJP weld profile tolerances for butt and outside corner joints (from AWS D1.1 Table 7.9)	
E **(in.)**	R_{max} **(in.)**
$E \leq 1$	1/8
$1 < E < 2$	3/16
$E \geq 2$	1/4
E = effective throat R_{max} = maximum allowable reinforcement	

The maximum allowable convexity, C_{max}, for T-joints and inside corner joints is specified in AWS D1.1 Table 7.9, where the allowable convexity is dependent on the effective throat, E, as listed in Table 4.13.

Table 4.13. PJP weld profile tolerances for T and inside corner joints (from AWS D1.1 Table 7.9)	
E **(in.)**	C_{max} **(in.)**
$E < 1$	1/8
$E \geq 1$	3/16
E = effective throat C_{max} = maximum allowable convexity	

Acceptance criteria for visual inspection are specified in AWS D1.1 Section 8.9. The size and length acceptance criteria for fillet welds is specified in AWS D1.1 Table 8.1 Item 6, where the allowable decrease in weld size is dependent on the specified weld size as shown in Table 4.14. AWS D1.1 Table 8.1 Item 6 also requires that the undersize portion of the weld shall not exceed 10% of the weld length. The third column in Table 4.14 lists the strength reduction at the tolerance limit, *r*.

Table 4.14. Fillet weld visual acceptance criteria (from AWS D1.1 Table 8.1)

W **(in.)**	***U*** **(in.)**	***r***
$w \leq 3/16$	1/16	0.933 (at $w = 3/16$)
$w = 1/4$	3/32	0.938
$w \geq 5/16$	1/8	0.940 (at $w = 5/16$)
U = allowable decrease in the weld size r = strength reduction factor = $1 - 0.10(w - U)/(w)$		

Existing Literature

Some of the available specimens had welds that were machined to size after welding; however, most of the specimens were tested in the as-welded condition. Prior to testing, weld dimensions were measured using one of three different methods. The calculated weld strengths were based on the measured effective throats, E_m, which were defined differently for each case. For some research projects, the throat dimension was measured at a 45° angle from the legs, and this value was reported as E_m. When both leg dimensions, w_1 and w_2, were reported, the effective throat was calculated with Equation 4.7.

$$E_m = \frac{w_1 + w_2}{\sqrt{w_1^2 + w_2^2}} \tag{4.7}$$

When both legs were measured, but only the average size was reported, the effective throat was calculated with Equation 4.8.

$$E_m = \frac{w_m}{\sqrt{2}} \tag{4.8}$$

Because the weld strength calculations were based on the pre-test measurements, root penetration was not considered in the calculations. Reinforcement was considered only when the measured throat dimension was reported. Because penetration and reinforcement can significantly affect the weld strength, the geometry of the weld was measured for some of the specimens by sectioning the specimens. These measurements are used to quantify the effects of penetration and reinforcement. The post-test rupture surface widths that were reported by some researchers were also used in this effort.

Statistical data on the geometric properties of welds is available in several documents. Background documentation to Eurocode 3 (CEN, 2005) indicates that the provisions in Section 4 were based

on ρ_G = 1.0 and V_G = 0.10. For butt welds between equal-width rectangular hollow sections, Teh and Rasmussen (2002) used ρ_G = 1.0 and V_G = 0.05. Li et al. (2007) analyzed 1,706 measurements on weld leg or throat dimensions from 12 research projects and determined that the average measured-to-specified ratio, ρ_G, is 1.08 with a coefficient of variation, V_G, of 0.142.

Based on dimensional measurements and electrode consumption for ¼, ⅜, ½, ⅝ and ¾ in. SMAW fillet welds by Freeman (1931), the weld legs were approximately 30% and 20% larger than the specified size for the ¼ and ⅜ in. welds, respectively. The ½, ⅝ and ¾ in. welds were 10 to 13% larger than specified.

Preece (1968) and Higgins and Preece (1969) documented 168 tests on fillet welded specimens with either ¼, ⅜ or ½-in. weld sizes. For the ¼-in. fillet welds, the average measured weld size was 20% greater than the specified size. For the ⅜ and ½-in. fillet welds, the average measured weld sizes were 13 and 5% greater than the specified sizes, respectively.

Several specimens were sectioned by Strating (1971) for penetration measurements. The results are listed in Table 3.1. As expected, the SAW welds had the largest mean penetration depth at 0.130 in. For the combined group of FCAW and GMAW welds, the mean penetration depth is 0.0520 in.

Adequate data was not available in 1978 to obtain the bias coefficient and coefficient of variation for the geometric properties quantitatively. To account for the variability on the weld effective area, Fisher et al. (1978) based their analysis on ρ_G = 1.00 and V_G = 0.15. This assumption, which implies a 50% probability that the actual shear area will be within ± 10% of the nominal area, was believed to be conservative.

Pham (1983) documented a series of 36 tests on transversely-loaded T-joints connected with fillet welds using the FCAW and SAW welding processes. Macro-etches showed that the theoretical throat increased by 30% for FCAW welds and 50% for SAW welds with a coefficient of variation of 0.20 for both processes. Many of the welds ruptured along the fusion zone; however, the experimental loads exceeded the expected strengths due to oversized welds and overstrength weld metals.

Miazga and Kennedy (1986) measured the weld leg sizes using a digital micrometer with a minimum of 44 readings per specimen. For the 5 mm welds, the average measured-to-specified leg ratio, w_m/w, was 1.04 with a coefficient of variation of 0.026. For the 9 mm welds, the average measured-to-specified leg ratio, w_m/w, was 1.03 with a coefficient of variation of 0.027.

To study the effect of penetration, Wilcox (1995) tested 10 transversely loaded fillet weld specimens in cruciform T-joints. The specimens were welded with the FCAW process with 100% CO_2 gas shielding. The penetration was increased by varying the arc voltage, current, wire feed speed and travel speed. As expected, the experimental rupture loads increased significantly with increased penetration.

For the 33 fillet weld specimens tested by Dowswell et al. (2021), the measured-to-specified leg ratio, w_m/w, averaged 1.16 with a coefficient of variation (COV) of 0.101. However, as with the

previous research by Li et al. (2007), ρ_G decreases with increasing weld size according to Table 4.15. ρ_G was also calculated with the effective throat ratio, based on the measured unequal leg dimensions, with almost identical results. Average penetration depths for each specimen varied from – 0.0332 in. to + 0.0621 in., with most of the negative values for the 100 ksi specimens and the larger positive values for the 70 ksi specimens.

Table 4.15. Fillet weld measured-to-specified leg ratios.

w	ρ_G	COV
¼	1.23	0.0802
⅜	1.19	0.0581
½	1.02	0.0542
All Specimens	1.16	0.101

For the PJP welds tested by Dowswell et al. (2021), which had 45° groove angles, the etched sections typically indicated an unfused distance at the root as shown in Figure 4.4. These distances, measured digitally, were typically between 1⁄16 and 3⁄16 in.

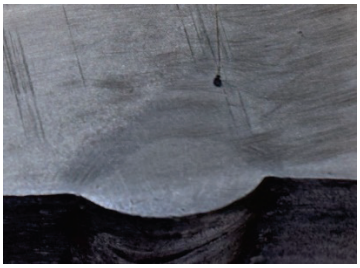

Fig. 4.4. Specimen PL4 Weld 4 (Dowswell, 2021).

Three of the longitudinal PJP Specimens were fabricated with T-joints and the remaining specimens were fabricated with corner joints. For the T-joints, the average measured rupture surface width, E_r, was 1.32 times the depth of preparation, S. This was much larger than for the corner joints, where E_r averaged 0.970S. However, the results indicated that the normalized rupture stress calculated with the measured rupture surface area, f_r/σ_{uw}, was similar for all specimens. Therefore, the T-joints were significantly stronger than the corner joints due to the larger effective throat dimensions. The larger effective throats were caused by the differences in reinforcement geometries for each joint type. The average reinforcement was 0.675S and 0.121S for the T-joints and corner joints, respectively. The reinforcement geometries for corner and T-joints are shown in Figures 4.5a and 4.5b, respectively.

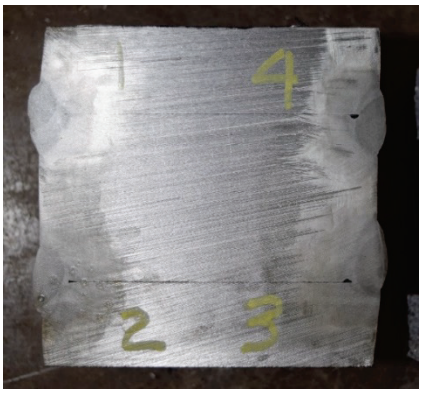

a. Specimen PL2.

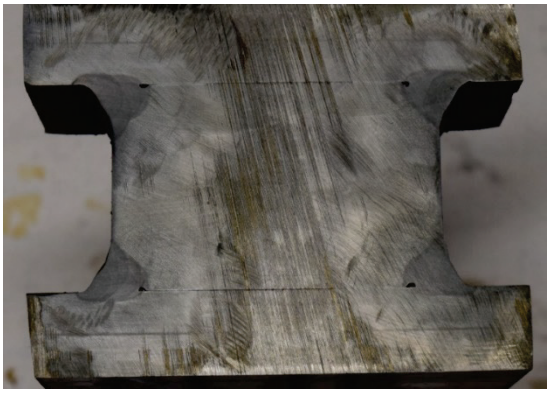

b. Specimen PL15.

Fig. 4.5. PJP sections (Dowswell, 2021).

The rupture surface widths for the transverse PJP specimens with F_{EXX} = 70 ksi were as expected, with an average value of 1.01 times the depth of preparation, *S*. However, for the specimens with F_{EXX} = 80 and 100 ksi, the rupture surface widths averaged only 0.733*S*. This difference was primarily caused by differences in the reinforcement dimensions, which averaged 0.217*S* for the 70 ksi specimens and only 0.0599*S* for the 80 and 100 ksi specimens.

Influence of Welding Parameters

Miller and Funderburk (2001) showed that the fillet weld leg size can be predicted to an accuracy equal to one fillet weld size with Equations 4.9a and b for US customary units and metric units, respectively.

US customary

$$w = \sqrt{\frac{J}{500}} \tag{4.9a}$$

Metric

$$w = 5.5\sqrt{J} \tag{4.9b}$$

where
w = fillet weld leg size, in. (mm)
J = heat input, kJ/in. (kJ/mm)

The heat input is

$$J = \frac{60VI}{1,000S} \tag{4.10}$$

where
I = welding current, amperes
S = arc travel speed, in./min. (mm/min.)
V = arc voltage, volts

Rearranging Equations 4.9, the heat input can be predicted using the fillet weld size with Equations 4.11.

US customary

$$J = 500w^2 \tag{4.11a}$$

Metric

$$J = \frac{w^2}{30.3} \tag{4.11b}$$

Hajro and Tasic (2020) measured macro-etched sections of joints that were fillet welded in either the Flat or Overhead position. Both GMAW (100% CO_2) and Pulsed GMAW (82% Ar + 18% CO_2) were used in specimen fabrication. Compared to the Overhead position, the Flat position resulted in lower penetration and reinforcement. For GMAW (100% CO_2), the weld size and effective throat can be predicted with Equations 4.12 and 4.13, respectively.

US customary

$$w = \frac{\sqrt{J}}{19.9} \tag{4.12a}$$

Metric

$$w = 6.43\sqrt{J} \tag{4.12b}$$

US customary

$$E = \frac{\sqrt{J}}{28.1} \tag{4.13a}$$

Metric

$$E = 4.55\sqrt{J} \tag{4.13b}$$

Rearranging Equations 4.12, the heat input can be predicted using the fillet weld size with Equations 4.14.

US customary

$$J = 396w^2 \tag{4.14a}$$

Metric

$$J = \frac{w^2}{41.3} \tag{4.14b}$$

Rearranging Equations 4.13, the heat input can be predicted using the effective throat with Equations 4.15.

US Customary

$$J = 790E^2 \tag{4.15a}$$

Metric

$$J = \frac{E^2}{20.7} \tag{4.15b}$$

For the flat position, the penetration depth can be estimated with Equations 4.16.

US customary

$$p = \frac{\sqrt{J}}{340} \tag{4.16a}$$

Metric

$$p = 0.38\sqrt{J} \tag{4.16b}$$

For the flat position, the reinforcement can be estimated with Equations 4.17.

US customary

$$C = \frac{\sqrt{J}}{65.0} \tag{4.17a}$$

Metric

$$C = 1.97\sqrt{J} \tag{4.17b}$$

Substituting Equations 4.13 into Equations 4.16 shows that the penetration depth of single-pass welds can be expressed as a portion of the effective throat according to Equation 4.18.

$$p = 0.0826E \tag{4.18}$$

Similarly, by substituting Equations 4.15 into Equations 4.17, the reinforcement of single-pass welds can be expressed as a portion of the effective throat according to Equation 4.19.

$$C = 0.432E \tag{4.19}$$

Several researchers measured the penetration depth from etched cross sections to determine the effect of various welding parameters including current, voltage and travel speed. The data from these projects were combined into a database to determine the expected penetration depth. All specimens were fabricated with mild steel plates using either the SMAW, FCAW-G or SAW process. The welding parameters were typical of those used in the structural steel industry, resulting in a mean heat input of 35 kJ/in. with values between 13 and 88 kJ/in. Some projects also studied the effect of other variables: welding position, electrode angle, arc length, electrode feed rate and base metal thickness. The results of Arya et al. (2015) and Pradhan et al. (2022) showed only a minor reduction in penetration with increased base metal thickness due to the conduction heat loss. Pathak et al. (2021) showed that the electrode angle has only a negligible effect on the penetration. The analysis included data from the following projects:

1. Pathak et al. (2021) measured 18 specimens with butt joints and single-V preparations welded using the SMAW process with E6013 electrodes.
2. Thakur et al. (2020) measured 16 specimens with 10 mm plates welded using the SAW process with EH14 electrodes.
3. Arya et al. (2015) measured 32 specimens with 8 to 16 mm plates welded using the SAW process with F7A2-EH14 electrodes.
4. Pradhan et al. (2022) measured 53 fillet welded T-joint specimens with 3 to 10 mm plates welded using the FCAW-G process with 100% CO_2 shielding gas.

The penetration measurements and the corresponding heat input values from the database are plotted using US customary units in Figure 4.6. Linear curve fit trendlines with a 0,0 intercept are plotted for each welding process.

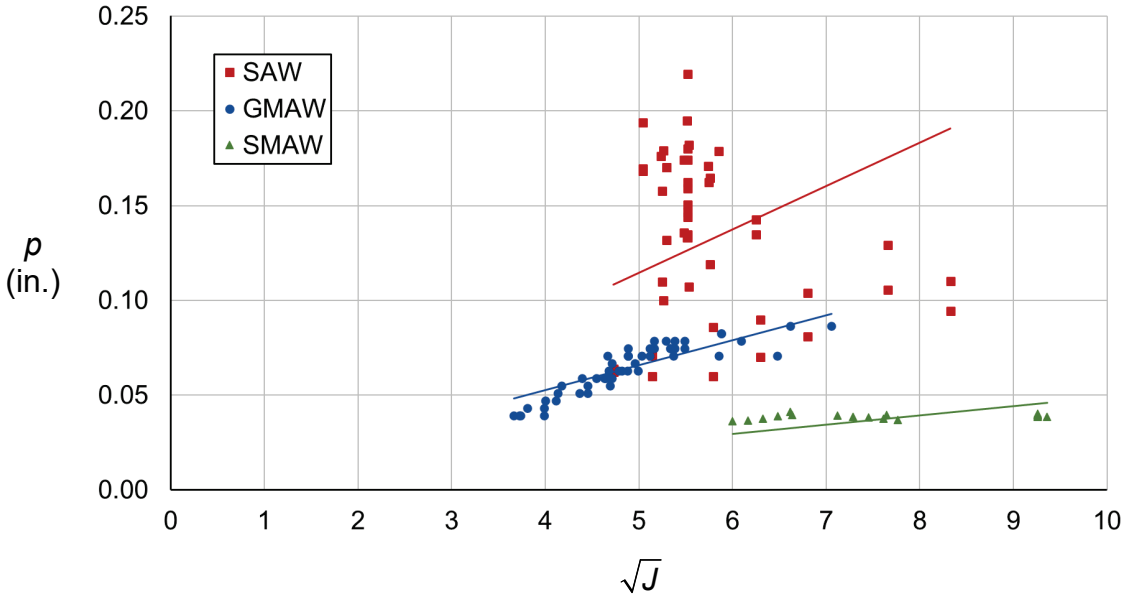

Fig. 4.6. Penetration depth as a function of heat input.

The curve fit equation for the 18 SMAW specimens is defined by Equation 4.20. The minimum penetration depth from this group is 0.0362 in. The mean ratio for the effective throat of a single-pass fillet weld, E_p/E, is 1.16 with a coefficient of variation of 0.0204.

$$p = \frac{\sqrt{J}}{204} \tag{4.20}$$

Substituting Equation 4.15a into Equation 4.20 results in Equation 4.21.

$$p = 0.138E \tag{4.21}$$

The curve fit equation for the 53 FCAW specimens is defined by Equation 4.22. The minimum penetration depth from this group is 0.0394 in. The mean ratio for the effective throat of a single-pass fillet weld, E_p/E, is 1.41 with a coefficient of variation of 0.0300.

$$p = \frac{\sqrt{J}}{75.8} \tag{4.22}$$

Substituting Equation 4.15a into Equation 4.22 results in Equation 4.23.

$$p = 0.371E \tag{4.23}$$

The curve fit equation for the 48 SAW specimens is defined by Equation 4.24. The minimum penetration depth from this group is 0.0598 in. The mean ratio for the effective throat of a single-pass fillet weld, E_p/E, is 1.76 with a coefficient of variation of 0.149.

$$p = \frac{\sqrt{J}}{43.7} \tag{4.24}$$

Substituting Equation 4.15a into Equation 4.24 results in Equation 4.25.

$$p = 0.643E \tag{4.25}$$

Using all 119 specimens, the mean ratio for the effective throat of a single-pass fillet weld, E_p/E, is 1.52 with a coefficient of variation of 0.183. Using only the 71 SMAW and GMAW specimens, the mean increase in the effective throat of a single-pass fillet weld, E_p/E, is 1.35 with a coefficient of variation of 0.0855.

Fillet Welds

Fillet weld geometric measurements were reported in the following research projects, which include specimens fabricated with the SMAW, GMAW, FCAW-G and FCAW-S processes. The filler metal classification strengths were primarily 70 ksi; however, 56, 60, 80, 90, 100, 110 and 140 ksi filler metals were also included. A total of 2,976 data points were reported. Each data point is for a single weld segment, which was typically reported as the average of several measurements along the length of the segment.

1. ABW (1931)
2. Preece (1968)
3. Butler and Kulak (1969)
4. Miazga and Kennedy (1986)
5. McClellan (1989)
6. Bowman and Quinn (1994)
7. Ng et al. (2002)
8. Deng et al. (2003)
9. Callele et al. (2005)
10. Li et al. (2007)
11. Kanvinde et al. (2009a)
12. Sugitani and Mochizuli (2013)
13. Shi and Chen (2018)
14. Reynolds (2020)
15. Luo et al. (2020)
16. Ran et al. (2021)
17. Dowswell et al. (2021)

Generally, the measured fillet weld leg dimensions, w_m, were larger than the specified weld sizes, w. For the 2,976 data points, the measured-to-specified leg ratio, w_m/w, averaged 1.08 with a coefficient of variation (COV) of 0.143. Because ρ_G decreases slightly with increasing weld size, the values for three different weld size ranges are listed in Table 4.16.

Table 4.16. Fillet weld measured-to-specified leg ratios.			
w	***n***	ρ_G	V_G
3⁄16 to 5⁄16	1,048	1.11	0.130
3⁄8 to 9⁄16	1,850	1.07	0.149
5⁄8 to 3⁄4	78	1.09	0.115
All Specimens	2,976	1.08	0.143
n = sample size			

Based on a linear curve fit to all 2,976 measurements, the expected-to-specified leg size ratio can be predicted with Equation 4.26.

$$w_e/w = 1.2 - 0.2w \tag{4.26}$$

where

w = specified leg size, in.
w_e = expected leg size, in.

Fillet weld root penetration measurements were reported in the following research projects, which include specimens fabricated with the SMAW, GMAW, FCAW-G, FCAW-S and SAW processes. A total of 300 data points were reported. The effect of penetration depth is included in ρ_P and V_P; therefore, the penetration ratios are not included in the reliability analysis. However, this data can be used to improve the accuracy of the design equations.

1. Strating (1971)
2. Wilcox (1995)
3. Chen et al. (2001)
4. Deng et al. (2003)
5. Sugitani and Mochizuli (2013)
6. Luo et al. (2020)
7. Pathak et al. (2021)
8. Dowswell et al. (2021)
9. Pradhan et al. (2022)

Because the penetration depth is dependent on the welding process, the values for the four processes are listed in Table 4.17. For the 208 measurements including only the SMAW, GMAW and FCAW processes, the penetration averaged 0.0485 with a standard deviation of 0.0342. Using the weight assignments in Table 4.4, the weighted average is 0.0533 with a standard deviation of 0.0333.

Table 4.17. Fillet weld penetration depths.			
Process	***n***	p_a	***SD***
SMAW	24	0.0331	0.0106
GMAW	45	0.0535	0.0244
FCAW	139	0.0495	0.0387
SAW	92	0.118	0.0463
SMAW, GMAW, FCAW	208	0.0485	0.0343
SD = standard deviation (in.) *n* = sample size p_a = mean penetration depth (in.)			

Using the penetration measurements with the actual weld sizes for each specimen resulted in a mean measured-to-specified throat ratio, E_m/E, of 1.23 with a coefficient of variation of 0.137 based solely on the increase caused by the penetration depth. However, E_m/E decreases with increasing weld size. Because the specimens had smaller weld sizes than is typical in practice, a weighted average value may be more appropriate. The ratios for seven different weld sizes are listed in Table 4.18. These values were calculated with the weighted average penetration depth of 0.0533.

Table 4.18. Fillet weld measured-to-specified throat ratios.

w (in.)	Weight Assignment	E_m/E
3⁄16	0.0	1.40
¼	0.1	1.30
5⁄16	0.5	1.24
⅜	0.1	1.20
½	0.1	1.15
⅝	0.1	1.12
¾	0.1	1.10

Using the weight assignments in Table 4.18, the weighted average E_m/E is 1.21 with a coefficient of variation of 0.125. For transverse fillet welds assumed to rupture at a 22.5° from the loading direction, the weighted average penetration depth along the rupture surface is reduced to (0.765)(0.0533 in.) = 0.0408 in. This results in a mean measured-to-specified throat ratio of 1.16. The expected-to-specified throat ratio can be predicted with Equation 4.27, which provides a reasonable, slightly conservative, estimate based on the weighted penetration measurements.

$$E_e/E = 1.3 - 0.4w \tag{4.27}$$

where

E = throat based on the specified leg size
E_e = expected throat

PJP Welds

PJP root penetration measurements were reported in the following research projects, which include specimens fabricated with the SMAW, GMAW and FCAW processes. All specimens had single- or double-bevel preparations with 45° groove angles. A total of 121 data points were reported. The effect of penetration depth is included in ρ_P and V_P; therefore, the penetration ratios are not included in the reliability analysis. However, this data can be used to improve the accuracy of the design equations.

1. Popov and Stephen (1977)
2. Gagnon and Kennedy (1989)
3. Rasmussen et al. (1999)
4. Luo et al. (2020)
5. Reynolds et al. (2020)
6. Dowswell et al. (2021)

The effective throat is $E = S - Z$, where the relevant values for Z are in AISC *Specification* Table J2.1 based on the welding process, the welding position and the groove type. For FCAW in the flat (F) or horizontal (H) position with a 45° bevel groove, $Z = 0$. For SMAW with a 45° bevel groove, $Z = ⅛$ in. for all positions.

Because the penetration is dependent on the welding process, the values for the three processes are listed in Table 4.19. The mean Z loss dimension, Z_a, for all 121 data points is 0.0358 with a standard deviation of 0.0725.

Table 4.19. PJP weld Z loss dimensions.

Process	*n*	Z_a	*SD*
SMAW	67	+ 0.0711	0.0416
GMAW	19	+ 0.0622	0.0156
FCAW	35	– 0.0460	0.0726
All Specimens	121	+ 0.0358	0.0725

SD = standard deviation (in.)
n = sample size
Z_a = mean measured Z loss dimension (in.)

Using the Z loss measurements with the actual groove depths for each specimen resulted in a mean measured-to-specified throat ratio, E_m/E, of 1.12 with a coefficient of variation of 0.256. However, E_m/E decreases with increasing weld size. Because the specimens had smaller weld sizes than is typical in practice, a weighted average value may be more appropriate. The ratios for eight different weld sizes are listed in Table 4.20. Using the weight assignments in Table 4.20, the weighted average value is 1.06 with a COV of 0.103.

Table 4.20. PJP weld measured-to-specified throat ratios.

S (in.)	Weight Assignment	E_m/E	COV
¼	0.05	1.25	0.304
5⁄16	0.05	1.17	0.230
⅜	0.10	1.13	0.186
½	0.10	1.09	0.136
¾	0.20	1.05	0.0890
1	0.20	1.04	0.0662
2	0.20	1.02	0.0328
3	0.10	1.01	0.0218

TEST-TO-PREDICTED STRENGTH RATIOS

The bias coefficient and coefficient of variation for the test-to-predicted strength ratios, ρ_P and V_P are discussed in this section of the report. Predicted strengths were calculated using the AISC *Specification* equations with the measured weld sizes and the measured (or expected) weld metal tensile strengths. Unless otherwise stated, the parameters were calculated using data from normal strength specimens. For this report, normal strength specimens are those with $F_{EXX} \leq 110$ ksi and $F_u \leq 110$ ksi. Parameters for the following joint types are included:

1. Longitudinal fillet welds
2. Transverse fillet welds
3. Fillet welds with skewed load angles ($0° < \theta < 90°$)
4. Multi-orientation fillet weld groups
5. Longitudinal PJP welds
6. Transverse PJP welds
7. Welds with skewed dihedral angles ($0° < \Psi < 90°$)
8. Single-sided fillet welds
9. High-strength welds
10. Eccentrically loaded fillet weld joints

The strength ratios can vary significantly with the welding processes. This variation is caused primarily by the differences in the root penetration depths. Also, it has been observed that the welding process can affect the shear-to-tensile strength ratio (Krumpen and Jordan, 1984).

Longitudinal Fillet Welds

Longitudinally loaded fillet weld tests were reported in the following research projects, which include specimens fabricated with the SMAW, GMAW, FCAW and SAW processes. A total of 727 experimental tests were reported.

1. ABW (1931)
2. Rosenthal and Levray (1939)
3. Wilson et al. (1949)
4. Wastlund and Ostlund (1956)
5. Bornscheuer and Feder (1966)
6. Higgins and Preece (1968, 1969)
7. Ligtenburg (1968)
8. Strating (1971)
9. Clark (1971)
10. Swannell (1974)
11. Miazga and Kennedy (1986, 1989)
12. McClellan (1989)
13. Bowman and Quin (1994)
14. Deng et al. (2003)
15. Yasui et al. (2004)
16. Callele et al. (2005, 2009)
17. Dowswell et al. (2021)
18. Waite et al. (2022)
19. Gallow (2019)
20. Luo et al. (2020b)

The statistical parameters for all specimens as well as for each welding process are listed in Table 4.21. Using the weight assignments in Table 4.4, $\rho_P = 1.41$ and $V_P = 0.161$.

Table 4.21. Statistical parameters for longitudinal fillet welds.			
Process	***n***	ρ_P	V_P
SMAW	581	1.29	0.151
GMAW	28	1.43	0.132
FCAW	106	1.35	0.186
SAW	12	2.07	0.0970
All Specimens	727	1.32	0.173
n = sample size			

Transverse Fillet Welds

Transversely loaded fillet weld tests were reported in the following research projects, which include specimens fabricated with the SMAW, GMAW, FCAW and SAW processes. A total of 449 experimental tests were reported. The ABW (1931) specimens were excluded from this data set due to inconsistent results that were likely caused by limited ductility and toughness.

1. Wilson et al. (1949)
2. Bornscheuer and Feder (1966)
3. Higgins and Preece (1968, 1969)
4. Ligtenburg (1968)
5. Strating (1971)
6. Clark (1971)
7. Swannell (1974)
8. Kato and Morita (1974)
9. Miazga and Kennedy (1986, 1989)
10. McClellan (1989)
11. Bowman and Quin (1994)
12. Wilcox (1995)
13. Ng et al. (2002, 2004) SER 245
14. Deng et al. (2003) SER 251
15. Yasui et al. (2004)
16. Callele et al. (2005, 2009)
17. Li et al. (2007)
18. Kanvinde et al. (2009a)
19. Sugitani and Mochizuki (2013)
20. Shi and Chen (2018)
21. Dowswell et al. (2021)
22. Gallow (2019)
23. Luo et al. (2020b)

The statistical parameters for all specimens as well as for each welding process are listed in Table 4.22. Using the weight assignments in Table 4.4, $\rho_P = 1.39$ and $V_P = 0.204$.

Table 4.22. Statistical parameters for transverse fillet welds.			
Process	***n***	ρ_P	V_P
SMAW	219	1.40	0.180
GMAW	30	1.38	0.209
FCAW	194	1.34	0.221
SAW	6	2.09	0.0698
All Specimens	449	1.38	0.208
n = sample size			

The ρ_P values are comparable to those of longitudinal fillet welds; however, V_P is higher than for longitudinal welds, at least partially because the strength of transverse welds is dependent on the joint type. Also, the research shows that the strength of transverse welds increases with ductility and toughness. By separating the data by joint type, Table 4.23 clearly shows that lap joints are 15% stronger than T-joints. This strength increase could be caused by a frictional force that develops on the faying surfaces due to the transverse force, *a*, that was discussed by Miazga and Kennedy (1989) and Gallow (2019). Weighting T-joints at 75% and lap joints at 25% and using the process-based weight assignments in Table 3.4, $\rho_P = 1.29$ and $V_P = 0.193$.

Table 4.23. Statistical parameters for transverse fillet welds.			
Joint Type	***n***	ρ_P	V_P
Lap	376	1.41	0.204
T-joint	73	1.23	0.186
n = sample size			

Fillet Welds with Skewed Load Angles, θ

Fillet weld tests with skewed load angles were reported in the following research projects, which include specimens fabricated with the SMAW, GMAW and FCAW processes. The specimens included load angles, θ, of 15°, 30°, 45°, 60° or 75°. A total of 53 experimental tests with normal strength specimens were reported.

1. Butler and Kulak (1969, 1971)
2. Clark (1971)
3. Miazga and Kennedy (1986, 1989)
4. Deng et al. (2003)
5. Yasui et al. (2004)
6. Luo et al. (2020b)

The statistical parameters for all specimens as well as for each welding process are listed in Table 4.24. Using weight assignments of 10% for SMAW, 30% for GMAW and 60% for FCAW, $\rho_P = 1.39$ and $V_P = 0.204$.

Table 4.24. Statistical parameters for fillet welds with skewed load angles.			
Process	***n***	ρ_P	V_P
SMAW	36	1.34	0.132
GMAW	9	1.12	0.0540
FCAW	8	1.47	0.221
All Specimens	53	1.33	0.0947
n = sample size			

The data for the GMAW process in Table 4.24 can be misleading because all nine of the specimens had T-joints, which were shown in the section on transverse fillet welds to have lower strength than double-lap joints. Of the 53 specimens in the data set, only nine have T-joints. All nine of these specimens were welded with the GMAW process and tested by Yasui et al. (2004) and Luo et al. (2020b). The remaining 44 specimens had double-lap joints. By separating the data by joint type, Table 3.25 clearly shows that lap joints are 22% stronger than T-joints. Weighting T-joints at 75% and lap joints at 25% and using the process-based weight assignments in Table 4.4, ρ_P = 1.21 and V_P = 0.0549.

Table 4.25. Statistical parameters for fillet welds with skewed load angles.

Joint Type	*n*	ρ_P	V_P
Lap	44	1.37	0.130
T-joint	9	1.12	0.0540
n = sample size			

The 36 high strength specimens tested by Ran et al. (2021) had double-lap joints that were fabricated using the GMAW process. The mean measured uniaxial weld metal tensile strength was 1,052 MPa (153 ksi). For these specimens, ρ_P = 1.80 and V_P = 0.0806.

Multi-Orientation Fillet Weld Groups

Tests with multi-orientation fillet weld groups were reported in the following research projects, which include specimens fabricated with the SMAW, GMAW and FCAW processes. Eight specimens tested by Callele et al. (2005, 2009) combined skewed (θ = 45°) and transverse (θ = 90°) welds. The remaining 311 specimens had both longitudinal (θ = 0°) and transverse welds. A total of 319 experimental tests with normal strength specimens were reported.

1. ABW (1931)
2. Wilson et al. (1949)
3. Ligtenburg (1968)
4. Strating (1971)
5. Swannell (1974)
6. Gresnigt (1992)
7. Callele et al. (2005, 2009)

The weld strengths were calculated by combining the welds using three methods: 1) sum with $k_{ds} \geq 1.0$, 2) sum with $k_{ds} = 1.0$, 3) AISC *Specification* Equation J2-6. The statistical parameters for all specimens as well as for each welding process are listed in Table 4.26. The weighted values, which were calculated with weight assignments of 10% for SMAW, 30% for GMAW and 60% for FCAW, are also listed.

Table 4.26. Statistical parameters for multi-orientation fillet weld groups.							
Process	n	Sum with $k_{ds} \geq 1.0$		Sum with $k_{ds} = 1.0$		Equation J2-6	
		ρ_P	V_P	ρ_P	V_P	ρ_P	V_P
SMAW	270	1.23	0.132	1.44	0.132	1.34	0.135
GMAW	16	1.36	0.0906	1.63	0.0794	1.48	0.0963
FCAW	33	1.34	0.133	1.65	0.176	1.43	0.121
All Specimens	319	1.24	0.134	1.47	0.145	1.35	0.135
Weighted	319	1.34	0.118	1.63	0.140	1.44	0.113
n = sample size							

The six high strength specimens tested by Bjork et al. (2012) had both longitudinal and transverse welds that were fabricated using the GMAW process. The measured base metal tensile strength is 1,076 MPa (156 ksi) and the measured uniaxial weld metal tensile strengths are 690 MPa (100 ksi) and 1,245 MPa (181 ksi). For these specimens, ρ_P = 1.01, 1.19 and 1.10 when the calculations are based on sum with $k_{ds} \geq 1.0$, sum with $k_{ds} = 1.0$ and Equation J2-6, respectively.

Single-Sided Fillet Welds

Single-sided transverse fillet weld tests were reported in the following research projects. A total of 184 experimental tests were reported. The total includes several different specimen types: round HSS, rectangular HSS, single-lap double-weld and cruciform T-joint.

1. ABW (1931)
2. Zhao and Hancock (1995)
3. Chen et al. (2001)
4. Packer et al. (2016)
5. Tuominen et al. (2018)
6. Torabian et al. (2018)
7. Thomas (2021)

The weld strengths were calculated using *Specification* Equation J2-4 with k_{ds} = 1.0. The statistical parameters for all specimens as well as for each specimen type are listed in Table 4.27.

Table 4.27. Statistical parameters for single-sided fillet welds.			
Specimen Type	n	ρ_P	V_P
Round HSS	6	1.73	0.121
Rectangular HSS	25	1.19	0.161
Single-lap double-weld	115	1.40	0.150
Cruciform T-joint	38	1.29	0.159
All Specimens	184	1.36	0.170
n = sample size			

Longitudinal PJP Welds

Longitudinally loaded PJP weld tests were reported by Luo et al. (2020b), Reynolds et al. (2020) and Dowswell et al. (2021), which include specimens fabricated with the GMAW and FCAW processes. All specimens had single- or double-bevel preparations with 45° groove angles. A total of 19 data points were reported. Because only two specimens were fabricated using the GMAW process, the statistical parameters were not separated based on process. For all 19 specimens, ρ_P = 1.20 and V_P = 0.202.

Transverse PJP Welds

Transversely loaded PJP weld tests were reported in the following research projects, which include specimens fabricated with the SMAW, GMAW and FCAW processes. A total of 92 experimental tests were reported.

1. Satoh et al. (1974)
2. Popov and Stephen (1977)
3. Gagnon and Kennedy (1987, 1989)
4. Rasmussen et al. (1999)
5. Luo et al. (2020b)
6. Reynolds et al. (2020)
7. Dowswell et al. (2021)

The statistical parameters for all specimens as well as for each welding process are listed in Table 4.28. The strengths of the SMAW specimens were calculated with $Z = ⅛$ in., which is conservative compared to the measured values in Table 4.19. This is the primary cause of the high value of ρ_P for the SMAW specimens relative to the GMAW and FCAW specimens. Using weight assignments of 10% for SMAW, 30% for GMAW and 60% for FCAW, $\rho_P = 1.72$ and $V_P = 0.202$.

Table 4.28. Statistical parameters for transverse PJP welds.

Process	*n*	ρ_P	V_P
SMAW	66	2.17	0.337
GMAW	3	1.40	0.0979
FCAW	23	1.80	0.216
All Specimens	92	2.05	0.332
n = sample size			

Longitudinal Welds with Skewed Dihedral Angles, Ψ

Longitudinally loaded welds with skewed dihedral angles were tested by Gallow (2019) and Barry et al. (2023) as part of the same research project. The FCAW-G process was used for all specimens. The dihedral angle, ψ, varied from 30° to 150° in 15° increments. A total of 15 data points were reported.

The weld strengths were calculated using the effective throat dimensions defined in AWS D1.1 Annex A. The Z loss dimensions for the FCAW-G process with welding in either the Horizontal (H) or Flat (F) position are $Z = ¼$ in. when $30° \le \psi < 45°$ and $Z = 0$ in. when $45° \le \psi < 60°$. For all 15 specimens, $\rho_P = 1.73$ and $V_P = 0.310$.

Transverse Welds with Skewed Dihedral Angles, Ψ

Transversely loaded welds with skewed dihedral angles were tested by Gallow (2019). The FCAW-G process was used for all specimens. The dihedral angle, ψ, varied from 30° to 150° in 15° increments. A total of 16 data points were reported.

The weld strengths were calculated using *Specification* Equation J2-4 with $k_{ds} = 1.0$ and the effective throat dimensions defined in AWS D1.1 Annex A. The Z loss dimensions for the FCAW-G process with welding in either the Horizontal (H) or Flat (F) position are $Z = ¼$ in. when $30° \le$

$\psi < 45°$ and $Z = 0$ in. when $45° \le \psi < 60°$. The statistical parameters for all specimens are listed in Table 4.29. Also, the specimens were separated into groups with either acute ($\psi < 90°$) or obtuse ($\psi > 90°$) dihedral angles, with the statistical parameters for each group listed in Table 4.29.

Table 4.29. Statistical parameters for single-sided fillet welds.

Specimen Type	*n*	ρ_P	V_P
$\psi < 90°$	8	1.45	0.286
$\psi > 90°$	8	2.74	0.0893
All Specimens	16	2.10	0.347
n = sample size			

High-Strength Longitudinal Fillet Welds

High-strength longitudinally loaded fillet weld tests were reported by Collin and Johansson (2005), Bjork et al. (2012) and Ran et al. (2021). A total of 33 data points were reported. All specimens were fabricated using high strength base metals with measured weld metal tensile strengths, σ_{uw}, between 79.5 and 181 ksi. The specimens with $\sigma_{uw} = 181$ ksi had overmatching electrodes, with a measured base metal tensile strength, σ_u, of 156 ksi. The specimens with $\sigma_{uw} \le 133$ ksi had undermatched electrodes.

The test-to-calculated ratios for all specimens are plotted against the electrode tensile strength in Figure 4.7. The high variability of P_e/P_c is partially caused by the intermixing of weld and base metal, indicating that the base metal strength is an important variable for mismatched electrodes. For the specimens in the strength range in prEN 1993-1-8 (CEN, 2021), $72.5 \le F_{EXX} \le 136$ ksi, the correlation factors in Table 2.3 capture the downward trend of P_e/P_c with increasing σ_{uw}.

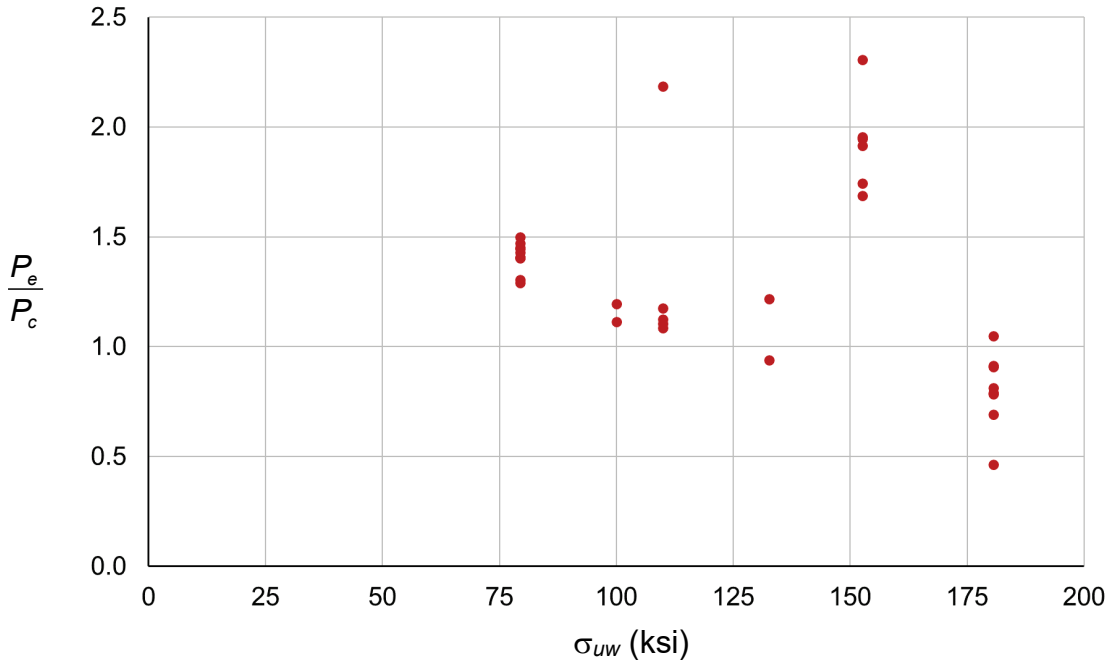

Fig. 4.7. Test-to-calculated ratio vs. electrode tensile strength for high-strength longitudinal fillet welds.

For the 19 specimens with $\sigma_{uw} \leq 133$ ksi, $\rho_P = 1.33$ and $V_P = 0.192$. These values are lower than those for the normal-strength specimens that were welded with the GMAW process. Additionally, intermixing of the weld metal with higher strength base metals likely caused ρ_P to be higher than for the matching condition.

High-Strength Transverse Fillet Welds

High-strength transversely loaded fillet weld tests were reported by Collin and Johansson (2005), Bjork et al. (2012), Sun et al. (2019), Ran et al. (2021) and Ghimire and Wald (2023). A total of 68 data points were reported. All specimens were fabricated using high strength base metals with measured weld metal tensile strengths, σ_{uw}, between 79.5 and 181 ksi. The specimens with $\sigma_{EXX} = 181$ ksi had overmatching electrodes, with a measured base metal tensile strength, σ_u, of 156 ksi. The specimens with $\sigma_{EXX} \leq 133$ ksi had undermatched electrodes.

The test-to-calculated ratios for all specimens are plotted against the electrode tensile strength in Figure 4.8. The high variability of P_e/P_c is partially caused by the intermixing of weld and base metal, indicating that the base metal strength is an important variable for mismatched electrodes. For the specimens in the strength range in prEN 1993-1-8 (CEN, 2021), $72.5 \leq F_{EXX} \leq 136$ ksi, the correlation factors in Table 2.3 capture the downward trend of P_e/P_c with increasing σ_{uw}.

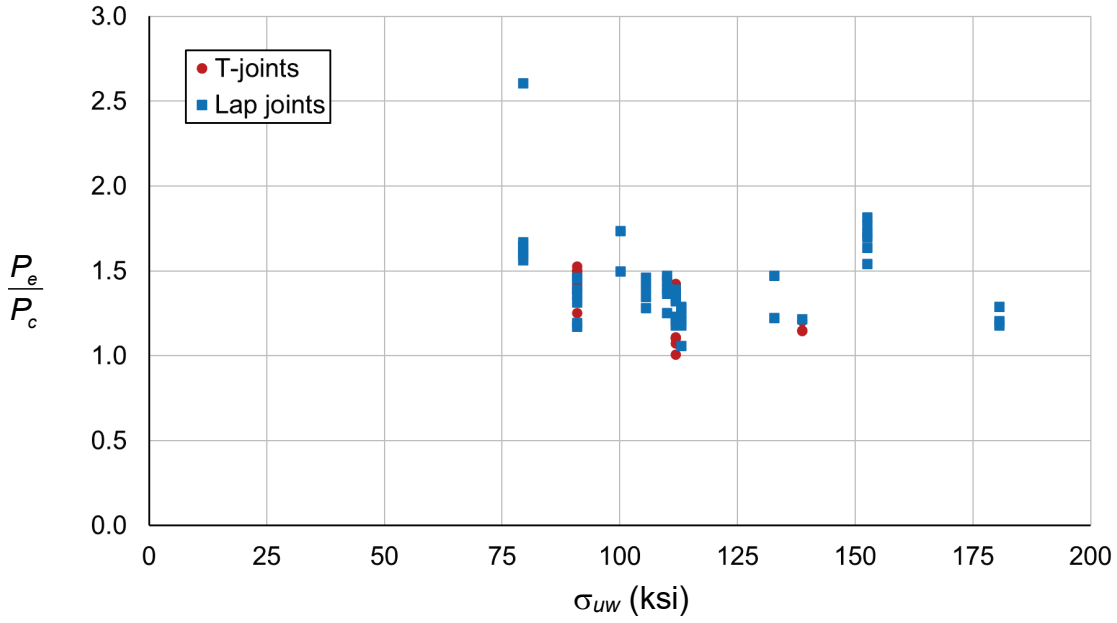

Fig. 4.8. Test-to-calculated ratio vs. electrode tensile strength for high-strength transverse fillet welds.

Unlike the high-strength longitudinal welds P_e/P_c is greater than 1.00 for all specimens, including those with $\sigma_{uw} = 181$ ksi. For all 68 specimens, $\rho_P = 1.39$ and $V_P = 0.170$. For the 53 specimens with $\sigma_{uw} \leq 133$ ksi, $\rho_P = 1.39$ and $V_P = 0.169$. These values are similar to those of the normal-strength specimens that were welded with the GMAW process. However, intermixing of the weld

metal with higher strength base metals likely caused ρ_P to be higher than for the matching condition.

As with normal-strength transverse welds, the strength of high-strength transverse welds is dependent on the joint type. By separating the data by joint type, Table 4.30 clearly shows that lap joints are 11% stronger than T-joints. Weighting T-joints at 75% and lap joints at 25%, $\rho_P = 1.33$ and $V_P = 0.137$.

Table 4.30. Statistical parameters for high-strength transverse fillet welds.

Joint Type	n	ρ_P	V_P
Lap	50	1.43	0.175
T-joint	18	1.29	0.124
n = sample size			

Eccentrically Loaded Fillet Welds

Eccentrically loaded lap joint tests were reported in the following research projects. Specimens with various weld group shapes were used, including rectangular box-shaped, C-shaped and groups with two parallel welds. A total of 78 experimental tests were reported.

1. Schreiner (1935)
2. Koenigsberger (1951)
3. Butler et al. (1972)
4. Swannell and Skewes (1979), Swanell (1981)
5. Kulak and Timler (1984)
6. Sanaei and Kametkar (1988)
7. Soliman et al. (2021)

Of the 24 specimens tested by Schreiner (1935), 17 were fabricated with lightly coated electrodes, which led to brittle weld metal. Because ductility is required for the weld groups to reach their full strength, these specimens ruptured at lower loads compared to the 7 tests with heavily coated electrodes.

Several of the specimen welds were unrestrained against rotation about the longitudinal axis of the weld. This condition can result in a reduced strength compared to the calculations when using a directional strength increase factor, k_{ds}, greater than 1. Because both the ICR method and the optimum plastic method use $k_{ds} \geq 1.0$, the unrestrained specimens ruptured at lower loads compared to the tests with the welds that are restrained against rotation about the longitudinal axis. This included seven of the nine specimens tested by Sanaei and Kametkar (1988), which were double-lap specimens subjected to compression. The 24 single-lap specimens tested by Koenigsberger (1951), Swannell and Skewes (1979) and Swanell (1981) were also unrestrained.

For the out-of-plane specimens, which had the eccentricity perpendicular to the plane of the weld group, the strengths were calculated with three methods: 1) the ICR method, 2) the elastic method, 3) the optimum plastic method. For the in-plane specimens, which had the eccentricity in the plane of the weld group, the strengths were calculated with two methods: 1) the ICR method, 2) the elastic method. The statistical parameters for all specimens are listed in Table 4.31.

Table 4.31. Statistical parameters for eccentrically loaded fillet welds.							
Specimen Group	***n***	**ICR**		**Elastic**		**Plastic**	
		ρ_P	V_P	ρ_P	V_P	ρ_P	V_P
Out-of-plane specimens							
Proper specimens[1]	22	1.40	0.209	2.84	0.225	1.36	0.203
All specimens	47	1.27	0.219	2.59	0.232	1.23	0.214
In-plane specimens							
Proper specimens[1]	8	1.58	0.156	2.67	0.177	–	–
All specimens	31	1.19	0.262	2.00	0.288	–	–
All specimens							
Proper specimens[1]	30	1.45	0.202	2.80	0.216	–	–
All specimens	78	1.24	0.238	2.35	0.279	–	–

n = sample size

[1] This group includes all specimens with normal ductility and restraint against rotation about the longitudinal axis of the weld

CHAPTER 5
RELIABILITY ANALYSIS

A reliability analysis was used to determine the required resistance factor, ϕ, for use with the weld strength provisions in the AISC *Specification*. The statistical parameters were based on the measured material and geometric properties of the experimental specimens. The resistance factor required to obtain a specific reliability level is (Galambos and Ravinda, 1978)

$$\phi = C_R \rho_R e^{-\beta \alpha_R V_R} \tag{5.1}$$

where

C_R = load ratio correction factor
V_R = coefficient of variation
α_R = separation factor
β = reliability index
ρ_R = bias coefficient

Galambos and Ravinda (1973) recommended a separation factor, α_R, of 0.55. For L/D = 3.0, Li et al. (2007) developed Equation 5.2 for calculating the load ratio correction factor.

$$C_R = 1.40 - 0.156\beta + 0.0078\beta^2 \tag{5.2}$$

The bias coefficient and the coefficient of variation are calculated using the statistical parameters for the specific weld type using Equations 4.1 and 4.2, respectively. Equations 4.1, 4.2, 5.1 and 5.2 are accurate only for large sample sizes; however, many of the data sets consist of only a limited number of tests. To consider the effect of small sample sizes, AISI (2016) uses a correction factor applied to V_P, resulting in a coefficient of variation of

$$V_R = \sqrt{V_M^2 + V_G^2 + C_p V_P^2} \tag{5.3}$$

The sample size correction factor for $n \geq 4$ is

$$\begin{aligned} C_P &= \left(1 + \frac{1}{n}\right)\left(\frac{m}{m-2}\right) \\ &= \left(1 + \frac{1}{n}\right)\left(\frac{n-1}{n-3}\right) \end{aligned} \tag{5.4}$$

where

m = degrees of freedom
$= n - 1$
n = number of tests

Equation 5.4 was originally developed by Hall and Pekoz (1988) and revised by Tsai (1992).

For the 1986 AISC LRFD *Specification* with $L/D = 1.0$, reliability indices for concentrically and eccentrically loaded fillet welds were 4.4 and 3.9, respectively (Galambos, 1992). The 2022 AISC *Specification* is calibrated at $L/D = 3.0$, which will result in lower reliability indices. For the 1986 AISC LRFD *Specification* with $L/D = 3.0$, reliability indices for concentrically and eccentrically loaded fillet welds were 4.0 and 3.7, respectively (Galambos, 1985). Based on the Commentary to AISC *Specification* Section B3.1, the reliability indices for members and connections are 2.6 and 4.0, respectively. Therefore, a target reliability index, β_T, of 4.0 is used in this report.

RESULTS

Using the data from Chapter 4, the results of the reliability analysis are presented for each weld type in this section of the report. The bias coefficient, ρ_R, and the coefficient of variation, V_R, are calculated with Equations 4.1 and 5.3, respectively.

Longitudinal Fillet Welds

The calculations for longitudinal fillet welds were based on the statistical parameters in Table 5.1. The values for ρ_P and V_P are process weighted. With $\phi = 0.75$, the resulting reliability index is 5.02, which is significantly greater than the target reliability index of 4.0. With a reliability index, β, of 4.0, $\phi = 0.941$.

Table 5.1. Statistical parameters for longitudinal fillet welds.

Variable	Bias Coefficient	Coefficient of Variation
Geometric	$\rho_G = 1.08$	$V_G = 0.143$
Material	$\rho_M = 1.12$	$V_M = 0.0543$
Test-to-Predicted Strength	$\rho_P = 1.41$	$V_P = 0.161$
	$\rho_R = 1.70$	$V_R = 0.222$

Transverse Fillet Welds

The calculations for transverse fillet welds were based on the statistical parameters in Table 5.2. The values for ρ_P and V_P are weighted by both process and joint type. With $\phi = 0.75$, the resulting reliability index is 4.35, which is greater than the target reliability index of 4.0. With $\beta = 4.0$, $\phi = 0.816$. Analyzing the data with $\beta = 4.0$ by separating the joint types results in $\phi = 0.873$ and 0.783 for lap joints and T-joints, respectively.

Table 5.2. Statistical parameters for transverse fillet welds.

Variable	Bias Coefficient	Coefficient of Variation
Geometric	$\rho_G = 1.08$	$V_G = 0.143$
Material	$\rho_M = 1.12$	$V_M = 0.0543$
Test-to-Predicted Strength	$\rho_P = 1.29$	$V_P = 0.193$
	$\rho_R = 1.56$	$V_R = 0.247$

Fillet Welds with Skewed Load Angles

The calculations for fillet welds with skewed load angles were based on the statistical parameters in Table 5.3. The values for ρ_P and V_P are weighted by both process and joint type. With $\phi = 0.75$, the resulting reliability index is 5.07, which is significantly greater than the target reliability index of 4.0. With a reliability index, β, of 4.0, $\phi = 0.920$.

Table 5.3. Statistical parameters for fillet welds with skewed load angles.		
Variable	**Bias Coefficient**	**Coefficient of Variation**
Geometric	$\rho_G = 1.08$	$V_G = 0.143$
Material	$\rho_M = 1.12$	$V_M = 0.0543$
Test-to-Predicted Strength	$\rho_P = 1.21$	$V_P = 0.0549$
	$\rho_R = 1.46$	$V_R = 0.163$

Multi-Orientation Fillet Weld Groups

The weld strengths for multi-orientation fillet weld groups were calculated by combining the welds using three methods: 1) sum with $k_{ds} = 1.0$, 2) AISC *Specification* Equation J2-6, 3) sum with $k_{ds} \geq 1.0$.

The calculations for multi-orientation fillet weld groups using the sum with $k_{ds} = 1.0$ were based on the statistical parameters in Table 5.4. The values for ρ_P and V_P are process weighted. With $\phi = 0.75$, the resulting reliability index is 5.92, which is significantly greater than the target reliability index of 4.0. With a reliability index, β, of 4.0, $\phi = 1.12$.

Table 5.4. Statistical parameters for multi-orientation fillet weld groups (Sum with $k_{ds} = 1.0$)		
Variable	**Bias Coefficient**	**Coefficient of Variation**
Geometric	$\rho_G = 1.08$	$V_G = 0.143$
Material	$\rho_M = 1.12$	$V_M = 0.0543$
Test-to-Predicted Strength	$\rho_P = 1.63$	$V_P = 0.140$
	$\rho_R = 1.97$	$V_R = 0.208$

The calculations for multi-orientation fillet weld groups using Equation J2-6 were based on the statistical parameters in Table 5.5. The values for ρ_P and V_P are process weighted. With $\phi = 0.75$, the resulting reliability index is 5.57, which is significantly greater than the target reliability index of 4.0. With a reliability index, β, of 4.0, $\phi = 1.03$.

Table 5.5. Statistical parameters for multi-orientation fillet weld groups (AISC *Specification* Equation J2-6)		
Variable	**Bias Coefficient**	**Coefficient of Variation**
Geometric	$\rho_G = 1.08$	$V_G = 0.143$
Material	$\rho_M = 1.12$	$V_M = 0.0543$
Test-to-Predicted Strength	$\rho_P = 1.44$	$V_P = 0.113$
	$\rho_R = 1.74$	$V_R = 0.190$

The calculations for multi-orientation fillet weld groups using the sum with $k_{ds} \geq 1.0$ were based on the statistical parameters in Table 5.6. The values for ρ_P and V_P are process weighted. With ϕ

= 0.75, the resulting reliability index is 5.16, which is significantly greater than the target reliability index of 4.0. With a reliability index, β, of 4.0, ϕ = 0.953.

Table 5.6. Statistical parameters for multi-orientation fillet weld groups (Sum with $k_{ds} \geq 1.0$)		
Variable	**Bias Coefficient**	**Coefficient of Variation**
Geometric	$\rho_G = 1.08$	$V_G = 0.143$
Material	$\rho_M = 1.12$	$V_M = 0.0543$
Test-to-Predicted Strength	$\rho_P = 1.34$	$V_P = 0.118$
	$\rho_R = 1.62$	$V_R = 0.193$

High Strength Multi-Orientation Fillet Weld Groups

The weld strengths for high strength multi-orientation fillet weld groups were calculated by combining the welds using two methods: 1) sum with k_{ds} = 1.0, 2) AISC *Specification* Equation J2-6.

The calculations for high strength multi-orientation fillet weld groups using the sum with k_{ds} = 1.0 were based on the statistical parameters in Table 5.7. This data was based on only six specimens, and Equation J2-6a is valid only for normal strength welds. With ϕ = 0.75, the resulting reliability index is 2.65, which is significantly less than the target reliability index of 4.0. With a reliability index, β, of 4.0, ϕ = 0.480.

Table 5.7. Statistical parameters for high strength multi-orientation fillet weld groups (Sum with $k_{ds} = 1.0$)		
Variable	**Bias Coefficient**	**Coefficient of Variation**
Geometric	$\rho_G = 1.08$	$V_G = 0.143$
Material	$\rho_M = 1.00$	$V_M = 0.05$
Test-to-Predicted Strength	$\rho_P = 1.19$	$V_P = 0.265$
	$\rho_R = 1.28$	$V_R = 0.400$

The calculations for high strength multi-orientation fillet weld groups using Equation J2-6 were based on the statistical parameters in Table 5.8. This data was based on only six specimens, and Equation J2-6 is valid only for normal strength welds. With ϕ = 0.75, the resulting reliability index is 2.62, which is significantly less than the target reliability index of 4.0. With a reliability index, β, of 4.0, ϕ = 0.494.

Table 5.8. Statistical parameters for high strength multi-orientation fillet weld groups (AISC *Specification* Equation J2-6)		
Variable	**Bias Coefficient**	**Coefficient of Variation**
Geometric	$\rho_G = 1.08$	$V_G = 0.143$
Material	$\rho_M = 1.00$	$V_M = 0.05$
Test-to-Predicted Strength	$\rho_P = 1.10$	$V_P = 0.227$
	$\rho_R = 1.19$	$V_R = 0.351$

Single-Sided Fillet Welds

Single-sided fillet welds were analyzed using the complete data set of 184 specimens. Also, each specimen type in Table 4.27 was analyzed separately.

The calculations for the complete data set were based on the statistical parameters in Table 5.9. With $\phi = 0.75$, the resulting reliability index is 4.76, which is greater than the target reliability index of 4.0. With a reliability index, β, of 4.0, $\phi = 0.893$.

Table 5.9. Statistical parameters for single-sided fillet welds.		
Variable	**Bias Coefficient**	**Coefficient of Variation**
Geometric	$\rho_G = 1.08$	$V_G = 0.143$
Material	$\rho_M = 1.12$	$V_M = 0.0543$
Test-to-Predicted Strength	$\rho_P = 1.36$	$V_P = 0.170$
	$\rho_R = 1.64$	$V_R = 0.230$

The calculations for round HSS specimens were based on the statistical parameters in Table 5.10. This data was based on only six specimens. With $\phi = 0.75$, the resulting reliability index is 5.89, which is significantly greater than the target reliability index of 4.0. With a reliability index, β, of 4.0, $\phi = 1.14$.

Table 5.10. Statistical parameters for round HSS specimens		
Variable	**Bias Coefficient**	**Coefficient of Variation**
Geometric	$\rho_G = 1.08$	$V_G = 0.143$
Material	$\rho_M = 1.12$	$V_M = 0.0543$
Test-to-Predicted Strength	$\rho_P = 1.73$	$V_P = 0.121$
	$\rho_R = 2.09$	$V_R = 0.228$

The calculations for rectangular HSS specimens were based on the statistical parameters in Table 5.11. With $\phi = 0.75$, the resulting reliability index is 4.18, which is slightly greater than the target reliability index of 4.0. With a reliability index, β, of 4.0, $\phi = 0.781$.

Table 5.11. Statistical parameters for rectangular HSS specimens		
Variable	**Bias Coefficient**	**Coefficient of Variation**
Geometric	$\rho_G = 1.08$	$V_G = 0.143$
Material	$\rho_M = 1.12$	$V_M = 0.0543$
Test-to-Predicted Strength	$\rho_P = 1.19$	$V_P = 0.161$
	$\rho_R = 1.44$	$V_R = 0.230$

The calculations for single-lap double-weld specimens were based on the statistical parameters in Table 5.12. With $\phi = 0.75$, the resulting reliability index is 5.07, which is significantly greater than the target reliability index of 4.0. With a reliability index, β, of 4.0, $\phi = 0.948$.

Table 5.12. Statistical parameters for single-lap double-weld specimens		
Variable	**Bias Coefficient**	**Coefficient of Variation**
Geometric	$\rho_G = 1.08$	$V_G = 0.143$
Material	$\rho_M = 1.12$	$V_M = 0.0543$
Test-to-Predicted Strength	$\rho_P = 1.40$	$V_P = 0.150$
	$\rho_R = 1.69$	$V_R = 0.216$

The calculations for cruciform T-joint specimens were based on the statistical parameters in Table 5.13. With $\phi = 0.75$, the resulting reliability index is 4.58, which is greater than the target reliability index of 4.0. With a reliability index, β, of 4.0, $\phi = 0.855$.

Table 5.13. Statistical parameters for cruciform T-joint specimens		
Variable	**Bias Coefficient**	**Coefficient of Variation**
Geometric	$\rho_G = 1.08$	$V_G = 0.143$
Material	$\rho_M = 1.12$	$V_M = 0.0543$
Test-to-Predicted Strength	$\rho_P = 1.29$	$V_P = 0.159$
	$\rho_R = 1.56$	$V_R = 0.225$

Longitudinal PJP Welds

The calculations for longitudinal PJP welds were based on the statistical parameters in Table 5.14. This data was based on only 19 specimens (17 FCAW, 2 GMAW). With $\phi = 0.75$, the resulting reliability index is 3.95, which is slightly less than the target reliability index of 4.0. With a reliability index, β, of 4.0, $\phi = 0.742$.

Table 5.14. Statistical parameters for longitudinal PJP welds.		
Variable	**Bias Coefficient**	**Coefficient of Variation**
Geometric	$\rho_G = 1.06$	$V_G = 0.103$
Material	$\rho_M = 1.12$	$V_M = 0.0543$
Test-to-Predicted Strength	$\rho_P = 1.20$	$V_P = 0.202$
	$\rho_R = 1.42$	$V_R = 0.249$

Transverse PJP Welds

The calculations for transverse PJP welds were based on the statistical parameters in Table 5.15. The values for ρ_P and V_P are process weighted. With $\phi = 0.75$, the resulting reliability index is 5.65, which is significantly greater than the target reliability index of 4.0. With $\beta = 4.0$, $\phi = 1.09$.

Table 5.15. Statistical parameters for transverse PJP welds.		
Variable	**Bias Coefficient**	**Coefficient of Variation**
Geometric	$\rho_G = 1.06$	$V_G = 0.103$
Material	$\rho_M = 1.12$	$V_M = 0.0543$
Test-to-Predicted Strength	$\rho_P = 1.72$	$V_P = 0.202$
	$\rho_R = 1.56$	$V_R = 0.247$

Longitudinal Welds with Skewed Dihedral Angles

The calculations for longitudinal fillet welds with skewed dihedral angles were based on the statistical parameters in Table 5.16. This data was based on only 15 specimens that were welded with the FCAW-G process. With $\phi = 0.75$, the resulting reliability index is 4.28, which is slightly greater than the target reliability index of 4.0. With a reliability index, β, of 4.0, $\phi = 0.820$.

Table 5.16. Statistical parameters for longitudinal fillet welds with skewed dihedral angles.		
Variable	**Bias Coefficient**	**Coefficient of Variation**
Geometric	$\rho_G = 1.08$	$V_G = 0.143$
Material	$\rho_M = 1.12$	$V_M = 0.0543$
Test-to-Predicted Strength	$\rho_P = 1.73$	$V_P = 0.310$
	$\rho_R = 2.09$	$V_R = 0.378$

Transverse Welds with Skewed Dihedral Angles

The calculations for the complete data set of only 16 specimens were based on the statistical parameters in Table 5.17. All 16 specimens were welded with the FCAW-G process. With $\phi = 0.75$, the resulting reliability index is 4.62, which is greater than the target reliability index of 4.0. With a reliability index, β, of 4.0, $\phi = 0.920$.

Table 5.17. Statistical parameters for transverse fillet welds with skewed dihedral angles.		
Variable	**Bias Coefficient**	**Coefficient of Variation**
Geometric	$\rho_G = 1.08$	$V_G = 0.143$
Material	$\rho_M = 1.12$	$V_M = 0.0543$
Test-to-Predicted Strength	$\rho_P = 2.10$	$V_P = 0.347$
	$\rho_R = 2.54$	$V_R = 0.413$

For the eight specimens with $\psi < 90°$, the calculations were based on the statistical parameters in Table 5.18. With $\phi = 0.75$, the resulting reliability index is 3.64, which is less than the target reliability index of 4.0. With a reliability index, β, of 4.0, $\phi = 0.669$.

Table 5.18. Statistical parameters for transverse fillet welds with skewed dihedral angles ($\psi < 90°$)		
Variable	**Bias Coefficient**	**Coefficient of Variation**
Geometric	$\rho_G = 1.08$	$V_G = 0.143$
Material	$\rho_M = 1.12$	$V_M = 0.0543$
Test-to-Predicted Strength	$\rho_P = 1.45$	$V_P = 0.286$
	$\rho_R = 1.75$	$V_R = 0.390$

For the eight specimens with $\psi > 90°$, the calculations were based on the statistical parameters in Table 5.19. With $\phi = 0.75$, the resulting reliability index is 9.69, which is significantly greater than the target reliability index of 4.0. With a reliability index, β, of 4.0, $\phi = 1.96$.

Table 5.19. Statistical parameters for transverse fillet welds with skewed dihedral angles ($\psi > 90°$)		
Variable	**Bias Coefficient**	**Coefficient of Variation**
Geometric	$\rho_G = 1.08$	$V_G = 0.143$
Material	$\rho_M = 1.12$	$V_M = 0.0543$
Test-to-Predicted Strength	$\rho_P = 2.74$	$V_P = 0.0893$
	$\rho_R = 3.31$	$V_R = 0.190$

High-Strength Longitudinal Fillet Welds

The calculations for high-strength longitudinal fillet welds were based on the statistical parameters in Table 5.20. This data was based on the 19 specimens with $\sigma_{EXX} \leq 133$ ksi. With $\phi = 0.75$, the resulting reliability index is 3.91, which is slightly less than the target reliability index of 4.0. With a reliability index, β, of 4.0, $\phi = 0.733$.

Table 5.20. Statistical parameters for high-strength longitudinal fillet welds.		
Variable	**Bias Coefficient**	**Coefficient of Variation**
Geometric	$\rho_G = 1.08$	$V_G = 0.143$
Material	$\rho_M = 1.00$	$V_M = 0.05$
Test-to-Predicted Strength	$\rho_P = 1.33$	$V_P = 0.192$
	$\rho_R = 1.44$	$V_R = 0.258$

High-Strength Transverse Fillet Welds

The calculations for high-strength transverse fillet welds were based on the statistical parameters in Table 5.21. The values for ρ_P and V_P are weighted by both process and joint type. With $\phi = 0.75$, the resulting reliability index is 4.42, which is greater than the target reliability index of 4.0. With $\beta = 4.0$, $\phi = 0.821$. Analyzing the data with $\beta = 4.0$ by separating the joint types results in $\phi = 0.828$ and 0.802 for lap joints and T-joints, respectively.

Table 5.21. Statistical parameters for high-strength transverse fillet welds.		
Variable	**Bias Coefficient**	**Coefficient of Variation**
Geometric	$\rho_G = 1.08$	$V_G = 0.143$
Material	$\rho_M = 1.00$	$V_M = 0.05$
Test-to-Predicted Strength	$\rho_P = 1.33$	$V_P = 0.137$
	$\rho_R = 1.44$	$V_R = 0.206$

Fillet Weld Groups with Out-of-Plane Eccentricity

The calculations for fillet welds with out-of-plane eccentricity using the ICR method were based on the statistical parameters in Table 5.22. This data was calculated using the 22 proper specimens. With $\phi = 0.75$, the resulting reliability index is 4.44, which is greater than the target reliability index of 4.0. With a reliability index, β, of 4.0, $\phi = 0.838$. When all 47 specimens were included in the analysis, the resulting reliability index with $\phi = 0.75$ is 4.04.

Table 5.22. Statistical parameters for fillet welds with out-of-plane eccentricity. (ICR method)		
Variable	**Bias Coefficient**	**Coefficient of Variation**
Geometric	$\rho_G = 1.08$	$V_G = 0.143$
Material	$\rho_M = 1.12$	$V_M = 0.0543$
Test-to-Predicted Strength	$\rho_P = 1.40$	$V_P = 0.209$
	$\rho_R = 1.69$	$V_R = 0.272$

The calculations for fillet welds with out-of-plane eccentricity using the elastic method were based on the statistical parameters in Table 5.23. This data was calculated using the 22 proper specimens. With $\phi = 0.75$, the resulting reliability index is 7.21, which is significantly greater than the target reliability index of 4.0. With a reliability index, β, of 4.0, $\phi = 1.65$. When all 47 specimens were included in the analysis, the resulting reliability index with $\phi = 0.75$ is 6.83.

Table 5.23. Statistical parameters for fillet welds with out-of-plane eccentricity. (elastic method)		
Variable	**Bias Coefficient**	**Coefficient of Variation**
Geometric	$\rho_G = 1.08$	$V_G = 0.143$
Material	$\rho_M = 1.12$	$V_M = 0.0543$
Test-to-Predicted Strength	$\rho_P = 2.84$	$V_P = 0.225$
	$\rho_R = 3.43$	$V_R = 0.272$

The calculations for fillet welds with out-of-plane eccentricity using the plastic method were based on the statistical parameters in Table 5.24. This data was calculated using the 22 proper specimens. With $\phi = 0.75$, the resulting reliability index is 4.37, which is greater than the target reliability index of 4.0. With a reliability index, β, of 4.0, $\phi = 0.824$. When all 47 specimens were included in the analysis, the resulting reliability index with $\phi = 0.75$ is 3.95.

Table 5.24. Statistical parameters for fillet welds with out-of-plane eccentricity. (plastic method)		
Variable	**Bias Coefficient**	**Coefficient of Variation**
Geometric	$\rho_G = 1.08$	$V_G = 0.143$
Material	$\rho_M = 1.12$	$V_M = 0.0543$
Test-to-Predicted Strength	$\rho_P = 1.36$	$V_P = 0.203$
	$\rho_R = 1.65$	$V_R = 0.266$

Fillet Weld Groups with In-Plane Eccentricity

The calculations for fillet welds with in-plane eccentricity using the ICR method were based on the statistical parameters in Table 5.25. This data was calculated using the eight proper specimens. With $\phi = 0.75$, the resulting reliability index is 5.20, which is significantly greater than the target reliability index of 4.0. With a reliability index, β, of 4.0, $\phi = 0.996$. When all 31 specimens were included in the analysis, the resulting reliability index with $\phi = 0.75$ is 3.48.

Table 5.25. Statistical parameters for fillet welds with in-plane eccentricity. (ICR method)		
Variable	**Bias Coefficient**	**Coefficient of Variation**
Geometric	$\rho_G = 1.08$	$V_G = 0.143$
Material	$\rho_M = 1.12$	$V_M = 0.0543$
Test-to-Predicted Strength	$\rho_P = 1.58$	$V_P = 0.156$
	$\rho_R = 1.91$	$V_R = 0.219$

The calculations for fillet welds with in-plane eccentricity using the elastic method were based on the statistical parameters in Table 5.26. This data was calculated using the eight proper specimens. With $\phi = 0.75$, the resulting reliability index is 7.23, which is significantly greater than the target reliability index of 4.0. With a reliability index, β, of 4.0, $\phi = 1.61$. When all 31 specimens were included in the analysis, the resulting reliability index with $\phi = 0.75$ is 5.11.

Table 5.26. Statistical parameters for fillet welds with in-plane eccentricity. (elastic method)		
Variable	**Bias Coefficient**	**Coefficient of Variation**
Geometric	$\rho_G = 1.08$	$V_G = 0.143$
Material	$\rho_M = 1.12$	$V_M = 0.0543$
Test-to-Predicted Strength	$\rho_P = 2.67$	$V_P = 0.177$
	$\rho_R = 3.23$	$V_R = 0.234$

All Eccentrically Loaded Fillet Weld Groups

The calculations for all eccentrically loaded fillet weld groups (both in-plane and out-of-plane eccentricity) using the ICR method were based on the statistical parameters in Table 5.27. This data was calculated using the 30 proper specimens. With $\phi = 0.75$, the resulting reliability index is 4.68, which is greater than the target reliability index of 4.0. With a reliability index, β, of 4.0, $\phi = 0.887$. When all 78 specimens were included in the analysis, the resulting reliability index with $\phi = 0.75$ is 3.83.

Table 5.27. Statistical parameters for all eccentrically loaded fillet welds. (ICR method)		
Variable	**Bias Coefficient**	**Coefficient of Variation**
Geometric	$\rho_G = 1.08$	$V_G = 0.143$
Material	$\rho_M = 1.12$	$V_M = 0.0543$
Test-to-Predicted Strength	$\rho_P = 1.45$	$V_P = 0.202$
	$\rho_R = 1.75$	$V_R = 0.253$

The calculations for all eccentrically loaded fillet weld groups (both in-plane and out-of-plane eccentricity) using the elastic method were based on the statistical parameters in Table 5.28. This data was calculated using the 30 proper specimens. With $\phi = 0.75$, the resulting reliability index is 7.37, which is significantly greater than the target reliability index of 4.0. With a reliability index, β, of 4.0, $\phi = 1.68$. When all 78 specimens were included in the analysis, the resulting reliability index with $\phi = 0.75$ is 5.88.

Table 5.28. Statistical parameters for all eccentrically loaded fillet welds. (elastic method)		
Variable	**Bias Coefficient**	**Coefficient of Variation**
Geometric	$\rho_G = 1.08$	$V_G = 0.143$
Material	$\rho_M = 1.12$	$V_M = 0.0543$
Test-to-Predicted Strength	$\rho_P = 2.80$	$V_P = 0.216$
	$\rho_R = 3.39$	$V_R = 0.265$

CHAPTER 6
ANALYSIS AND DISCUSSION

This chapter of the report provides an analysis of the results from Chapter 5. Potential revisions that are intended to improve the reliability of the AISC *Specification* and *Manual* provisions will be discussed.

LONGITUDINAL FILLET WELDS

The reliability index for longitudinal fillet welds is significantly greater than the target reliability index, with $\phi = 0.941$ providing an appropriate reliability level. The shear-to-tensile strength ratio of 0.67 specified by Canadian Standard S16-14 (CSA, 2014) is more accurate than the 0.60 value specified for fillet welds in AISC *Specification* Table J2.5. In lieu of the shear-to-tensile strength ratio of 0.60, a statistically accurate value can be determined using the calculated-to-specified ϕ ratio for longitudinal welds: (0.60)(0.941/0.75) = 0.753. This value is too high because the effect of penetration has not been considered. The reliability analysis was based on the weld size but included the effect of penetration implicitly. From Chapter 5, the mean weld leg size ratio is 1.08 and the mean effective throat ratio is 1.23. Therefore, the adjusted shear-to-tensile strength ratio is (0.753)(1.08/1.23) = 0.661. Replacing $F_{nw} = 0.60F_{EXX}$ with $F_{nw} = 0.67F_{EXX}$ for longitudinal welds results in an appropriate reliability level when $\phi = 0.843$.

TRANSVERSE FILLET WELDS

The reliability index for transverse fillet welds is greater than the target reliability index, with $\phi = 0.816$ providing an appropriate reliability level. At $\theta = 90°$, $k_{ds} = 1.50$ is appropriate only for lap joints, which are 15% stronger than T-joints. A statistically accurate value for k_{ds} for $\theta = 90°$ can be determined using the ratio of the calculated values for ϕ: $k_{ds} = (1.5)(0.816/0.941) = 1.30$. Replacing $F_{nw} = 0.60F_{EXX}$ with $F_{nw} = 0.67F_{EXX}$ and replacing $k_{ds} = 1.5$ with $k_{ds} = 1.3$ for transverse welds results in an appropriate reliability level when $\phi = 0.843$.

FILLET WELDS WITH SKEWED LOAD ANGLES

The reliability index for fillet welds with skewed load angles is significantly greater than the target reliability index, with $\phi = 0.920$ providing an appropriate reliability level. However, AISC *Specification* Equation J2-5 is accurate only for lap joints, which are 22% stronger than T-joints. Equation 6.1 provides an appropriate reliability level for both T-joints and lap joints when $F_{nw} = 0.60F_{EXX}$ is replaced by $F_{nw} = 0.67F_{EXX}$, with $\phi = 0.80$.

$$k_{ds} = 1.0 + 0.30\sin^{1.5}\theta \tag{6.1}$$

The experimental data, which is plotted in Figure 6.1, shows a linear trend with different slopes for T- and lap joints. For the specimens with $\theta = 15°$, the strengths are similar for T- and lap joints.

For the lap-joint specimens, the strength increases with θ at a higher rate than for the T-joint specimens. This trend is similar to the behavior of longitudinal and transverse fillet welds, which showed a strength increase for lap joints relative to T-joints for the specimens with transverse welds.

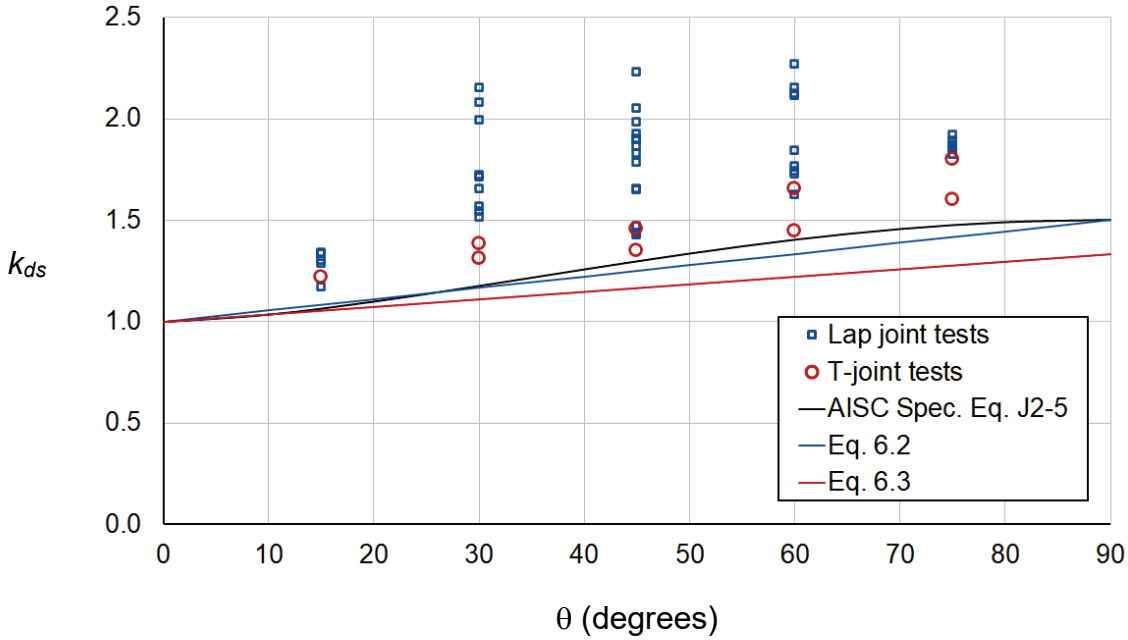

Fig. 6.1. k_{ds} versus θ.

Equations 6.2 and 6.3 are the linear trend lines plotted for lap and T-joints, respectively. The range of validity for both equations is $0° \le \theta \le 90°$.

$$k_{ds} = 1 + \frac{\theta}{180} \tag{6.2}$$

$$k_{ds} = 1 + \frac{\theta}{270} \tag{6.3}$$

For the 44 lap joint specimens, the reliability of Equation 6.2 is similar to that of AISC *Specification* Equation J2-5, with $\phi = 0.976$ required for Equation 6.2 and $\phi = 0.951$ required for Equation J2-5.

For the nine T-joint specimens, the reliability of Equation 6.3 is similar to that of Equation 6.1, with $\phi = 0.922$ required for Equation 6.3 and $\phi = 0.925$ required for Equation 6.1. For these specimens, AISC *Specification* Equation J2-5 requires $\phi = 0.845$, which indicates a non-uniform level of reliability compared to the lap joint specimens.

Although the accuracy increases when different equations are used for T- and lap joints, it is more practical to use either Equation 6.1 or 6.3 for all joints. Because Equation 6.3 is simpler than Equation 6.1, it is recommended that AISC *Specification* Equation J2-5 is replaced by Equation

6.3. To conform with the recommended value of k_{ds} = 1.30 when θ = 90°, Equation 6.3 can be modified slightly to k_{ds} = 1.0 + θ/300. As with the longitudinal and transverse fillet welds, F_{nw} = 0.60F_{EXX} can be replaced by F_{nw} = 0.67F_{EXX} for fillet welds in AISC *Specification* Table J2.5. This revision results in an appropriate reliability level when ϕ = 0.905.

MULTI-ORIENTATION FILLET WELD GROUPS

Normal Strength Weld Groups

When multi-orientation fillet weld groups are summed using k_{ds} = 1.0 for all welds, the reliability index is significantly greater than the target reliability index. In this case, ϕ = 1.12 provides an appropriate reliability level.

Using *Specification* Equation J2-6 to combine the welds increases the accuracy, but results in a conservative solution. In this case, ϕ = 1.03 provides an appropriate reliability level.

When the joint strengths are calculated by summing the individual weld strengths with $k_{ds} \geq 1.0$, V_P is similar to that of *Specification* Equation J2-6. However, ρ_P is reduced to a level that eliminates much of the conservatism associated with the other two methods. In this case, ϕ = 0.953 provides an appropriate reliability level. This is similar to the ϕ = 0.941 for longitudinal fillet weld joints that forms the baseline value for all fillet welds.

It is recommended that *Specification* Equation J2-6 is deleted. The strength of welds can be combined directly, without special reduction factors. As with the longitudinal and transverse fillet welds, F_{nw} = 0.60F_{EXX} can be replaced by F_{nw} = 0.67F_{EXX} for fillet welds in AISC *Specification* Table J2.5. This revision results in an appropriate reliability level when ϕ = 0.853.

High Strength Weld Groups

With only six specimens, which had a base metal strength of 156 ksi, the results for combining high-strength welds are inconclusive. However, these preliminary results indicated that the available methods that were discussed in this report are non-conservative, requiring ϕ ≈ 0.50 to obtain an appropriate reliability level.

SINGLE-SIDED FILLET WELDS

For the complete data set with all 184 single-sided fillet welds, the reliability index is greater than the target reliability index only when the weld strengths were calculated with k_{ds} = 1.0. In this case, ϕ = 0.893 provides an appropriate reliability level. As with the longitudinal and transverse fillet welds, F_{nw} = 0.60F_{EXX} can be replaced by F_{nw} = 0.67F_{EXX} for fillet welds in AISC *Specification* Table J2.5. This revision results in an appropriate reliability level when ϕ = 0.800.

With k_{ds} = 1.0, the reliability index for the round HSS specimens is significantly greater than the target reliability index. In this case, ϕ = 1.14 provides an appropriate reliability level. With k_{ds} = 1.50, ϕ = 0.760 is required. Although this is greater than the ϕ = 0.75 that is specified in AISC

Specification Table J2.5, the reliability analysis was based on only six specimens. Therefore, using k_{ds} = 1.0 for round HSS may be appropriate until further experimental results are available.

With k_{ds} = 1.0, the reliability index for the rectangular HSS specimens is slightly greater than the target reliability index. In this case, ϕ = 0.781 provides an appropriate reliability level.

As with the transverse double fillet weld specimens, the transverse single-sided specimen strengths varied with the joint type, with the strength of lap joints exceeding that of T-joints by 11%. Appropriate reliability levels with k_{ds} = 1.0 are provided by ϕ = 0.948 and ϕ = 0.855 for lap and T-joints, respectively.

Tension Joints with a = 0

Double-lap fillet weld joints with a = 0 that are loaded in transverse tension behave in a similar manner to single-sided welds. The strength is reduced when the restraining transverse force, a, that was discussed by Miazga and Kennedy (1989) and Gallow (2019) is not present.

The analysis by Gallow (2019) resulted in a ratio of transverse compression strength to transverse tension strength equal to 0.921. The analysis by Miazga and Kennedy (1986, 1989), Lesik and Kennedy (1990) and Kennedy et al. (1990) resulted in a ratio of transverse compression strength to transverse tension strength equal to 0.893.

A gapped T-joint specimen designed by Kist (1936) to eliminate the transverse force had only 64% of the strength of a double-lap transverse tension specimen with similar welds. Hankins and Brown (see Spraragen and Claussen, 1942) tested double-lap specimens with a cutout in the middle plate to eliminate any contact between the outer plates and the inner plates. Compared to otherwise identical specimens without the cutouts, the specimens with the cutouts had a 25% reduction in strength. Tests by Eb (1952) on specimens that were similar to those of Kist (1936) showed a 39% strength reduction compared to otherwise identical double-lap specimens.

Double-Lap Compression Joints

Double-lap fillet weld joints that are loaded in transverse compression behave in a similar manner to single-sided welds. Transverse welds are stronger in tension than compression because the restraining transverse force, a, that was discussed by Miazga and Kennedy (1989) and Gallow (2019) is not present for compression loading.

Kist (1936) tested a double-lap joint in transverse compression, showing that the compression joint had only 78% of the strength of a similar double-lap transverse tension specimen. The experimental results of Swannell and Skewes (1979) resulted in a ratio of transverse compression strength to transverse tension strength equal to 0.829. Experimental tests by Vandeperre and Joukoff (see Spraragen and Claussen, 1942) and Sanaei and Kametkar (1988) showed similar reductions. The experimental results of Chen and Chen (2022) resulted in a mean ratio of transverse compression strength to longitudinal shear strength equal to 0.940.

LONGITUDINAL PJP WELDS

The reliability index for longitudinal PJP welds is slightly less than the target reliability index, with $\phi = 0.742$ providing an appropriate reliability level. As with the longitudinal and transverse fillet welds, $F_{nw} = 0.60F_{EXX}$ can be replaced by $F_{nw} = 0.67F_{EXX}$ for PJP welds subjected to shear in AISC *Specification* Table J2.5. This revision results in an appropriate reliability level when $\phi = 0.665$.

TRANSVERSE PJP WELDS

The reliability index for transverse PJP welds is significantly greater than the target reliability index, with $\phi = 1.09$ providing an appropriate reliability level. $F_{nw} = 0.60F_{EXX}$ can be replaced by $F_{nw} = F_{EXX}$ for PJP welds subjected to tension in AISC *Specification* Table J2.5. This revision results in an appropriate reliability level when $\phi = 0.654$.

WELDS WITH SKEWED DIHEDRAL ANGLES

Longitudinal Welds with Skewed Dihedral Angles

The reliability index for longitudinal fillet welds with skewed dihedral angles is slightly greater than the target reliability index, with $\phi = 0.820$ providing an appropriate reliability level. Replacing $F_{nw} = 0.60F_{EXX}$ with $F_{nw} = 0.67F_{EXX}$ results in an appropriate reliability level when $\phi = 0.734$.

The experimental-to-calculated strength ratios, P_e/P_c, for all specimens are plotted against the dihedral angles in Figure 6.2. For uniform reliability, P_e/P_c should be approximately equal for all specimens, with a value of approximately 1.35, which is ρ_P for longitudinal welds fabricated with the FCAW process from Table 4.21. However, the variability of P_e/P_c in Figure 6.2 is indicative of non-uniform reliability with respect to ψ.

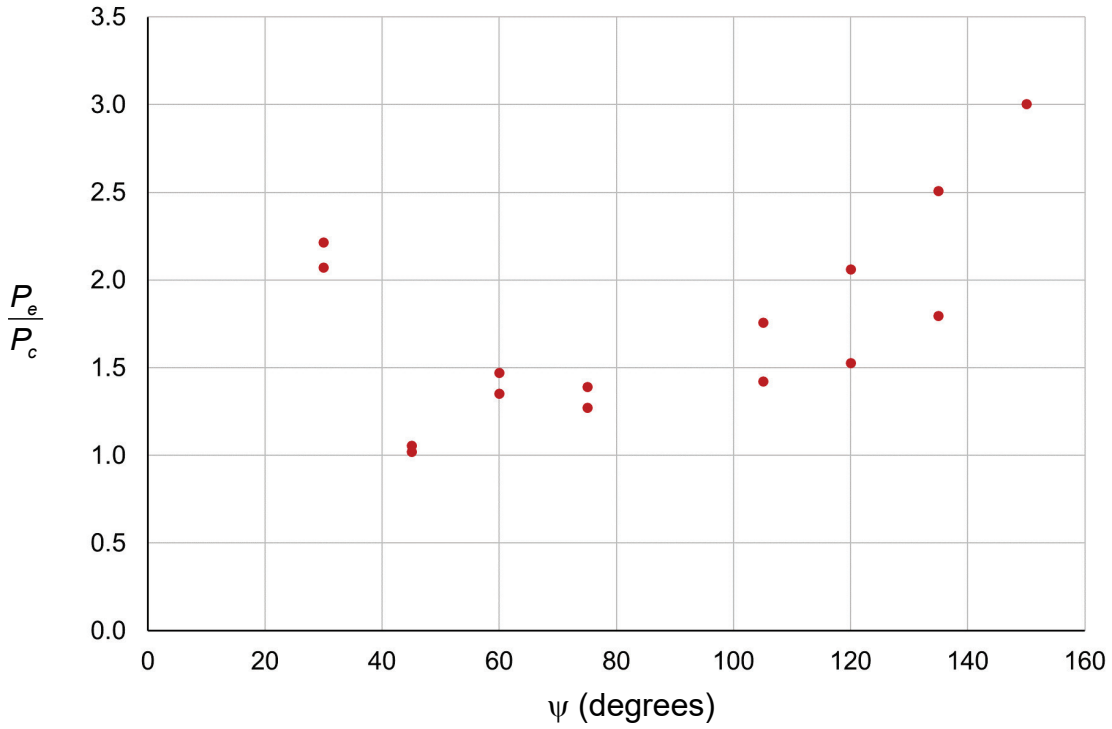

Fig. 6.2. Test-to-calculated ratio vs. dihedral angle for longitudinal welds.

The stress ratios, τ_r/σ_{EXX}, are plotted against the dihedral angles in Figure 6.3, where τ_r is the shear stress at the maximum experimental load on the measured rupture surface of the weld and σ_{EXX} is the measured uniaxial tensile strength of the weld metal. Compared to the P_e/P_c ratios in Figure 6.2, the τ_r/σ_{EXX} ratios are uniform, with a mean value of 0.938 and a coefficient of variation of 0.0732. This indicates that the primary cause of the high variability of P_e/P_c is the difference between the calculated effective throat dimension and the actual rupture surface width.

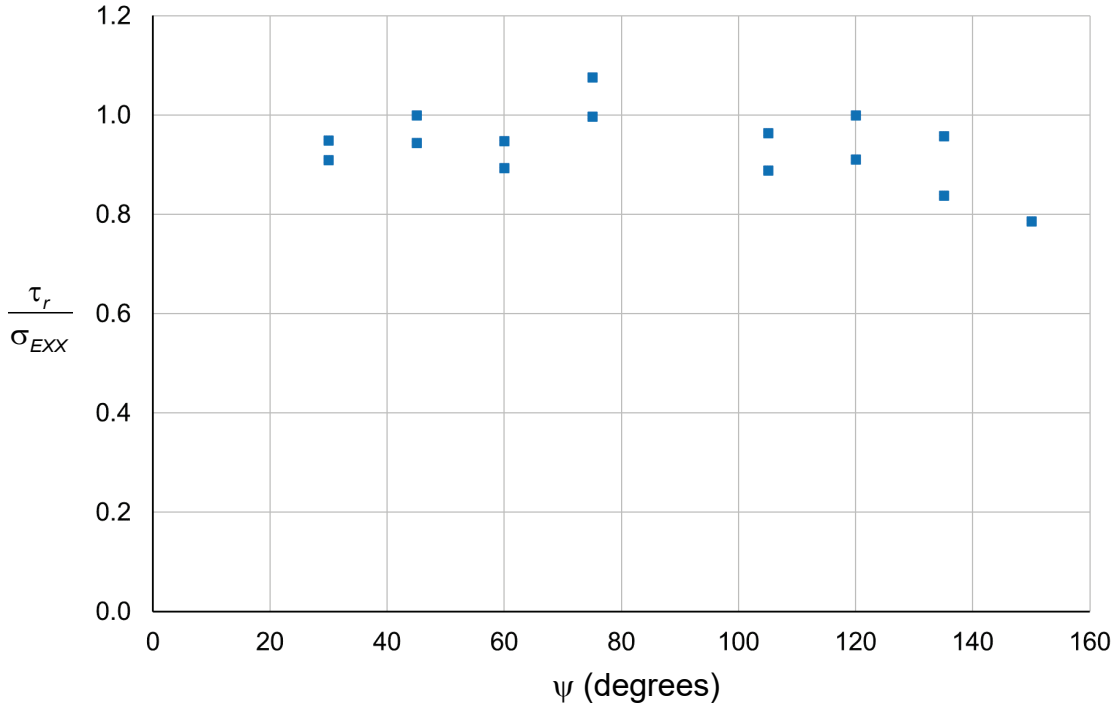

Fig. 6.3. Stress ratio vs. dihedral angle for longitudinal welds.

The high variability of P_e/P_c for the specimens with $\psi < 90°$ is likely caused by inaccuracy in the specified values for the Z loss dimension. For the specimens with $\psi = 30°$, $P_e/P_c = 2.07$ and 2.22. Because these values are significantly greater than $\rho_P = 1.35$, $Z = ¼$ in. may be too conservative for this condition. For the specimens with $\psi = 45°$, $P_e/P_c = 1.02$ and 1.06. Because these values are significantly less than $\rho_P = 1.35$, Z may need to be greater than 0 for this condition. For the specimens with $\psi = 60°$ and 75°, P_e/P_c is approximately equal to $\rho_P = 1.35$. Therefore, $Z = 0$ is appropriate for these conditions.

For the specimens with $\psi > 90°$, the increase in P_e/P_c with ψ is primarily caused by shear rupture areas that were larger than the calculated effective throats. Because the effective throats were calculated using the measured weld leg sizes, both penetration and reinforcement could have contributed to the overstrength of these welds.

Transverse Welds with Skewed Dihedral Angles

The reliability analysis for transverse fillet welds with skewed dihedral angles was based on weld strengths that were calculated using *Specification* Equation J2-4 with $k_{ds} = 1.0$. Using the data set with all 16 specimens, the reliability index is greater than the target reliability index, with $\phi = 0.920$ providing an appropriate reliability level. Replacing $F_{nw} = 0.60F_{EXX}$ with $F_{nw} = 0.67F_{EXX}$ results in an appropriate reliability level when $\phi = 0.824$.

For the eight specimens with $\psi < 90°$, the resulting reliability index is 3.64, which is less than the target reliability index. In this case, $\phi = 0.669$ provides an appropriate reliability level.

For the eight specimens with $\psi > 90°$, the resulting reliability index is 9.69, which is significantly greater than the target reliability index. In this case, $\phi = 1.96$ provides an appropriate reliability level.

The experimental-to-calculated strength ratios, P_e/P_c, for all specimens are plotted against the dihedral angles in Figure 6.4. For uniform reliability, P_e/P_c should be approximately equal for all specimens, with a value of approximately 1.34, which is ρ_P for transverse welds fabricated with the FCAW process from Table 4.22. However, the variability of P_e/P_c in Figure 6.4 is indicative of non-uniform reliability with respect to ψ.

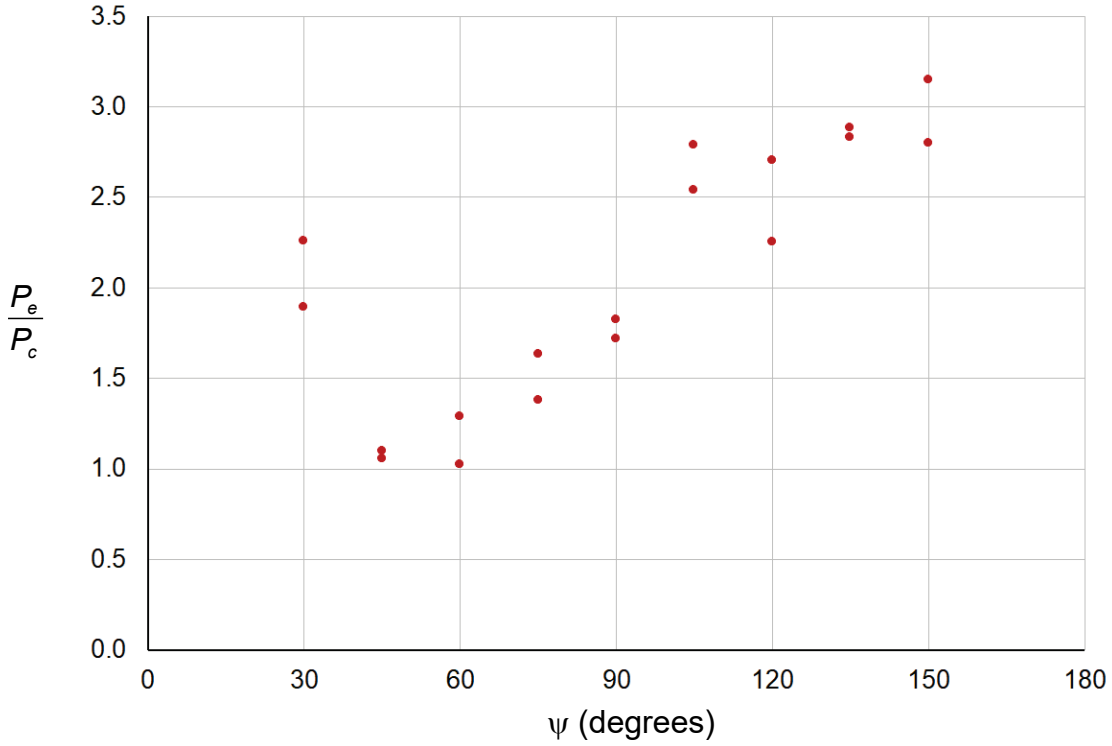

Fig. 6.4. Test-to-calculated ratio vs. dihedral angle for transverse welds.

The stress ratios, τ_r/σ_{EXX}, are plotted against the dihedral angles in Figure 6.5, where τ_r is the stress at the maximum experimental load on the measured rupture surface of the weld and σ_{EXX} is the measured uniaxial tensile strength of the weld metal. Compared to the P_e/P_c ratios in Figure 6.4, the τ_r/σ_{EXX} ratios are more uniform; however, the data shows an increase in the stress ratio with the dihedral angle. Therefore, only a portion of the variability of P_e/P_c in Figure 6.4 can be attributed to the difference between the calculated effective throat dimension and the actual rupture surface width.

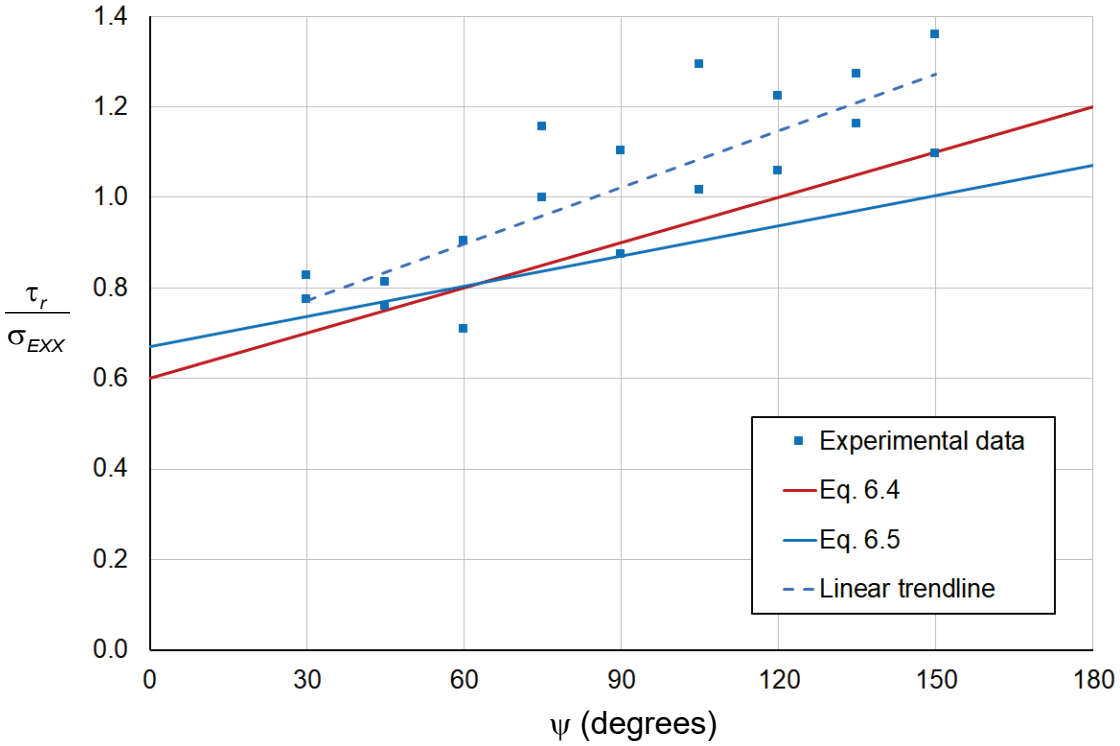

Fig. 6.5. Stress ratio vs. dihedral angle for transverse welds.

The data in Figure 6.5 indicates that ten of the specimens with $\psi > 60°$ ruptured at stresses greater than the measured uniaxial tensile stress of the weld metal. The PJP specimens tested by Gagnon and Kennedy (1987, 1989) had similar results. Due to the transverse constraint of the weld metal by the base metal, the weld strength can be significantly greater than the measured uniaxial tensile stress of the weld metal. The well-known effect of multiaxial stresses on the rupture strength has been extensively documented by Bridgman (1964), Schafer et al. (2000) and many others.

The linear trendline in Figure 6.5 shows an increase in the stress ratio with the dihedral angle. The equation for this trendline is $\tau_r/\sigma_{EXX} = 0.65 + \psi/240$. This is expected because, as the dihedral angle changes from 0° to 180°, the stress state at the effective throat changes from shear to tension. Similar to joints with skewed load angles, a directional strength increase factor can be developed for joints with skewed dihedral angles. This factor should be compatible with the current design provisions for the extreme cases (the impractical geometries $\psi = 0°$ and $\psi = 180°$) and at $\psi = 90°$. To meet this requirement, the following constraints were used to develop linear equations for the directional strength increase factor at joints with skewed dihedral angles.

1. When $\psi = 0°$ k_ψ should equal 1.00. Although $\psi = 0°$ is not a practical condition, this lower bound value is the condition where the effective throat is in shear.
2. When $\psi = 90°$ k_ψ should equal k_{ds} for $\theta = 90°$. This is the condition where the weld is loaded transversely.
3. When $\psi = 180°$ k_ψ should result in a nominal stress that is approximately equal to F_{EXX}. This occurs when k_ψ is equal to the inverse of the shear-to-tensile strength. Although $\psi = 180°$ is not a practical condition, this upper bound value is the condition where the effective throat is in tension.

Equation 6.4 is a linear equation that meets the requirements for the AISC *Specification* equations, where $F_{nw} = 0.60F_{EXX}$ and $k_{ds} = 1.50$ when $\theta = 90°$.

$$k_{\psi} = 1 + \frac{\psi}{180} \leq \frac{1}{0.60} \tag{6.4}$$

Equation 6.5 complies with the requirements for the proposed method, where $F_{nw} = 0.67F_{EXX}$ and $k_{ds} = 1.30$ when $\theta = 90°$.

$$k_{\psi} = 1 + \frac{\psi}{300} \leq \frac{1}{0.67} \tag{6.5}$$

The range of validity for both equations is $0° \leq \psi \leq 180°$; however, the practical range for these joints is $30° \leq \psi \leq 150°$. Until a refined design method is available for acute-angle welds, including a reevaluation of the Z loss factor, proper reliability for these welds can be obtained by using $k_{\psi} = 0.669/0.75 = 0.892$ for acute welds. In this case, both Equations 6.4 and 6.5 should be limited to the range $80° \leq \psi \leq 150°$.

The calculations for the complete data set of 16 specimens were based on the statistical parameters in Table 6.1. The weld strengths were calculated using k_{ds} according to Equation 6.4 when $80° \leq \psi \leq 150°$ and $k_{\psi} = 0.85$ when $0° \leq \psi < 80°$. With $\phi = 0.75$, the resulting reliability index is greater than the target reliability index. With a reliability index, β, of 4.0, $\phi = 0.989$.

Table 6.1. Statistical parameters for transverse fillet welds with skewed dihedral angles. ($k_{\psi} = 0.85$ for $0° \leq \psi < 80°$. k_{ψ} calculated according to Equation 6.4 for $80° \leq \psi \leq 150°$)

Variable	Bias Coefficient	Coefficient of Variation
Geometric	$\rho_G = 1.08$	$V_G = 0.143$
Material	$\rho_M = 1.12$	$V_M = 0.0543$
Test-to-Predicted Strength	$\rho_P = 1.69$	$V_P = 0.214$
	$\rho_R = 2.04$	$V_R = 0.282$

For the eight specimens with $\psi < 90°$, the calculations were based on the statistical parameters in Table 6.2. With $\phi = 0.75$, the resulting reliability index is greater than the target reliability index. With a reliability index, β, of 4.0, $\phi = 0.789$.

Table 6.2. Statistical parameters for transverse fillet welds with skewed dihedral angles ($\psi < 90°$) ($k_{\psi} = 0.85$)

Variable	Bias Coefficient	Coefficient of Variation
Geometric	$\rho_G = 1.08$	$V_G = 0.143$
Material	$\rho_M = 1.12$	$V_M = 0.0543$
Test-to-Predicted Strength	$\rho_P = 1.71$	$V_P = 0.286$
	$\rho_R = 2.07$	$V_R = 0.390$

For the eight specimens with $\psi > 90°$, the calculations were based on the statistical parameters in Table 6.3. With $\phi = 0.75$, the resulting reliability index is significantly greater than the target reliability index. With a reliability index, β, of 4.0, $\phi = 1.20$.

Table 6.3. Statistical parameters for transverse fillet welds with skewed dihedral angles ($\psi > 90°$) (k_ψ calculated according to Equation 6.4)

Variable	Bias Coefficient	Coefficient of Variation
Geometric	$\rho_G = 1.08$	$V_G = 0.143$
Material	$\rho_M = 1.12$	$V_M = 0.0543$
Test-to-Predicted Strength	$\rho_P = 1.67$	$V_P = 0.0871$
	$\rho_R = 2.02$	$V_R = 0.188$

HIGH-STRENGTH FILLET WELDS

For the high strength fillet weld specimens, the relationship between the weld rupture strength and the weld metal tensile strength is nonlinear. The correlation factors in Table 2.3, which were taken from CEN (2021), properly capture the data trends in this report. It may be appropriate to include a strength reduction factor to increase the reliability index for these joints. These reduction factors can be based on ratios of the correlation factors in Table 2.3. Replacing $F_{nw} = 0.60F_{EXX}$ with $F_{nw} = 0.67F_{EXX}$ results in adequate reliability only when a strength reduction factor of approximately 0.85 is used.

High-Strength Longitudinal Fillet Welds

The data for high-strength longitudinal fillet welds was based on the 19 specimens with $\sigma_{EXX} \leq$ 133 ksi. The resulting reliability index is slightly less than the target reliability index. $\phi = 0.733$ provides an appropriate reliability level.

High-Strength Transverse Fillet Welds

For high-strength transverse fillet welds, the resulting reliability index is greater than the target reliability index. $\phi = 0.822$ provides an appropriate reliability level. Analyzing the data by separating the joint types results in $\phi = 0.848$ and 0.802 for lap joints and T-joints, respectively.

ECCENTRICALLY LOADED FILLET WELD JOINTS

Fillet Weld Groups with Out-of-Plane Eccentricity

For fillet welds with out-of-plane eccentricity using the ICR method, the resulting reliability index is greater than the target reliability index. In this case, $\phi = 0.838$ provides an appropriate reliability level. The elastic method is overly conservative, with $\phi = 1.65$ providing an appropriate reliability level. When the plastic method is used, the resulting reliability index is greater than the target reliability index. In this case, $\phi = 0.824$ provides an appropriate reliability level.

Fillet Weld Groups with In-Plane Eccentricity

For fillet welds with in-plane eccentricity using the ICR method, the resulting reliability index is significantly greater than the target reliability index. In this case, $\phi = 0.996$ provides an appropriate reliability level. The elastic method is overly conservative, with $\phi = 1.61$ providing an appropriate reliability level.

All Eccentrically Loaded Fillet Weld Groups

For all eccentrically loaded fillet weld groups (both in-plane and out-of-plane eccentricity) using the ICR method, the resulting reliability index is greater than the target reliability index. In this case, $\phi = 0.877$ provides an appropriate reliability level. The elastic method is overly conservative, with $\phi = 1.68$ providing an appropriate reliability level.

CHAPTER 7
SUMMARY AND CONCLUSIONS

SUMMARY

This report used data from existing research to calculate appropriate resistance factors for various welded joints using a first-order reliability analysis.

DESIGN RECOMMENDATIONS

This section provides suggested revisions that are intended to improve the reliability of the AISC *Specification* and *Manual* provisions.

Longitudinal and Transverse Fillet Welds

The *Specification* provisions for both longitudinal and transverse fillet welds result in appropriate, but nonuniform, reliability. More uniform reliability can be achieved by replacing $F_{nw} = 0.60F_{EXX}$ with $F_{nw} = 0.67F_{EXX}$, replacing $k_{ds} = 1.5$ with $k_{ds} = 1.3$ and replacing $\phi = 0.75$ with $\phi = 0.80$.

Fillet Welds with Skewed Load Angles

The *Specification* provisions for fillet welds with skewed load angles result in appropriate, but nonuniform, reliability. Equation 7.1 provides an appropriate reliability level when $F_{nw} = 0.60F_{EXX}$ is replaced by $F_{nw} = 0.67F_{EXX}$, with $\phi = 0.80$. The range of validity for Equation 7.1 is $0° \le \theta \le 90°$.

$$k_{ds} = 1 + \frac{\theta}{300} \tag{7.1}$$

Multi-Orientation Fillet Weld Groups

The *Specification* provisions for multi-orientation fillet weld groups result in appropriate, but overly conservative, reliability. It is recommended that *Specification* Equation J2-6 is deleted. The strength of welds can be combined directly, without special reduction factors. Less conservative results can be achieved, while maintaining appropriate reliability, by replacing $F_{nw} = 0.60F_{EXX}$ with $F_{nw} = 0.67F_{EXX}$, replacing $\phi = 0.75$ with $\phi = 0.80$ and combining the weld strengths directly.

Single-Sided Fillet Welds

The *Specification* provisions for single-sided fillet welds result in appropriate reliability when the weld strengths are calculated with $k_{ds} = 1.0$. Less conservative results can be achieved, while maintaining appropriate reliability, by replacing $F_{nw} = 0.60F_{EXX}$ with $F_{nw} = 0.67F_{EXX}$ and replacing $\phi = 0.75$ with $\phi = 0.80$. $k_{ds} = 1.0$ is applicable to the following transverse fillet welds subjected to tension:

- Round HSS

- Rectangular HSS
- Single-lap double-weld joints
- Cruciform T-joints

Additionally, k_{ds} = 1.0 is applicable to double-lap fillet weld joints that are loaded in transverse compression.

Longitudinal and Transverse PJP Welds
The *Specification* provisions for both longitudinal and transverse PJP welds result in acceptable, but nonuniform, reliability. The reliability of longitudinal welds is slightly less than the target reliability, and the reliability of transverse welds is significantly greater than the target reliability. More uniform reliability can be achieved by replacing $F_{nw} = 0.60F_{EXX}$ with $F_{nw} = 0.67F_{EXX}$ for longitudinal welds and replacing $F_{nw} = 0.60F_{EXX}$ with $F_{nw} = F_{EXX}$ for transverse welds. In both cases, the specified ϕ (0.75 or 0.80) should be replaced with $\phi = 0.65$.

Welds with Skewed Dihedral Angles
It is recommended that a new section on welds with skewed dihedral angles be added to the *Manual*. The *Specification* and AWS D1.1 provisions result in acceptable, but nonuniform, reliability because the reliability of acute welds is significantly less than that of obtuse welds. This is caused primarily by inaccuracies in the throat calculations. Also, for transverse welds, the stress state at the throat changes with ψ. This effect, which causes the strength to increase with ψ, is not considered in the current design provisions.

For transverse welds with skewed dihedral angles, a more uniform reliability is achieved with a directional strength factor, k_{ψ}. When the current *Specification* provisions are used, the weld strengths should be calculated using k_{ψ} according to Equation 6.4 when $80° \le \psi \le 150°$ and k_{ψ} = 0.85 when $0° \le \psi < 80°$. Equation 6.5 complies with the requirements for the proposed method, where $F_{nw} = 0.67F_{EXX}$ and $k_{ds} = 1.30$ when $\theta = 90°$.

High-Strength Fillet Welds
The *Specification* provisions for both longitudinal and transverse high-strength fillet welds result in acceptable, but nonuniform, reliability. For high-strength longitudinal fillet welds, the reliability index is slightly less than the target reliability index. For high-strength transverse fillet welds, the resulting reliability index is greater than the target reliability index.

For the high strength fillet weld specimens, the relationship between the weld rupture strength and the weld metal tensile strength is nonlinear. The correlation factors in Table 2.3, which were taken from CEN (2021), properly capture the data trends in this report. It may be appropriate to include a strength reduction factor to increase the reliability index for these joints. These reduction factors can be based on ratios of the correlation factors in Table 2.3. Replacing $F_{nw} = 0.60F_{EXX}$ with $F_{nw} = 0.67F_{EXX}$ results in adequate reliability only when a strength reduction factor of approximately 0.85 is used.

Eccentrically Loaded Fillet Weld Joints
For eccentrically loaded fillet welds, the elastic method is conservative by more than 100%. The ICR method and the plastic method result in similar strengths, with both design methods providing

reliabilities that are greater than the target reliability. Although the plastic method is simpler and slightly more accurate than the ICR method, it is currently used only for welds with out-of-plane eccentricity.

FUTURE RESEARCH

The following research needs were identified:

1. More accurate Z loss factors are needed for both PJP welds and acute fillet welds.
2. A design method is needed for calculating the plastic strength of fillet weld groups with in-plane eccentricities.
3. For transversely loaded double fillet weld joints with skewed dihedral angles, there is a ductility differential between the acute and obtuse welds. A design method based on deformation compatibility is needed for combining the weld strengths.

The following joint types were not evaluated in this report. Although the test data are limited for many of these joints, a reliability analysis using the existing data may be beneficial.

1. Fillet welds at elevated temperatures
2. Fillet welds at low temperatures
3. Long longitudinal fillet welds
4. Fillet welds with root openings
5. Single-sided PJP welds
6. PJP welds with skewed load angles ($0° < \theta < 90°$)
7. Flare-bevel groove welds
8. PJP welds with reinforcing fillet welds
9. Weld size requirement to develop the connected element

Although the effect of potential weld defects was not explicitly included in the reliability analysis of this report, it is believed that an analysis that includes the inspection statistics could result in inspection factors. These factors could potentially increase the efficiency of welds with nondestructive testing, helping to offset the testing cost. This analysis would include the determination of the maximum acceptable defect size and evaluating the probability of detection (POD) for that size of defect. However, there are several obstacles to this type of analysis, including the impact of defect directionality on the strength and inaccuracies in the defect rate estimations.

SYMBOLS

A_{we} = effective area of the weld, in.^{2}
A_{wel} = effective area of longitudinally loaded fillet welds, in.^{2}
A_{wet} = effective area of transversely loaded fillet welds, in.^{2}
C = reinforcement, in. (mm)
C_P = sample size correction factor
C_R = load ratio correction factor
C_{max} = maximum allowable convexity, in.
E = specified effective throat, in. (mm)
E = effective throat, in. (mm)
E_e = expected throat dimension, in. (mm)
E_m = measured throat dimension, in.
E_p = actual weld throat defined as the penetration depth plus the effective throat, in.
F_c = nominal tension rupture stress considering constraint, ksi
F_c = rupture stress that considers the effect of base metal dilution, ksi
F_{EXX} = filler metal classification strength, ksi
F_{nw} = nominal stress of the weld metal, ksi
F_u = specified minimum tensile strength of the base metal, ksi
F_{vi} = allowable stress of the weld metal, ksi
F_y = specified minimum yield strength, ksi
I = welding current, amperes
J = heat input, kJ/in. (kJ/mm)
K_{at} = empirical coefficient for transversely loaded double-lap fillet weld joints
L = weld length, in.
M_w = coefficient that accounts for differences in the weld deformation capacity.
P_e = experimental rupture load, kips
P_n = nominal strength calculated with the AISC *Specification* equations, kips
P_c = strength calculated with the measured weld size and the measured weld metal tensile strength, kips
R_i = strength at deformation Δ_i, kips
R_{max} = maximum allowable reinforcement, in.
R_n = root opening, in.
S = PJP weld preparation groove depth, in.
S = arc travel speed, in./min. (mm/min.)
T_u = plastic rupture torsion, kip-in.
U = allowable decrease in the weld size, in.
V = arc voltage, volts
V_G = coefficient of variation for the geometric properties, addressing the difference between the nominal throat area based on the specified weld size and the actual throat area
V_L = longitudinal load, kips
V_M = coefficient of variation for the material properties, addressing the difference between specified and actual weld metal tensile strengths
V_{M2} = coefficient of variation for the material properties, addressing the difference between the nominal and actual shear-to-tensile strength ratios
V_P = coefficient of variation for the test-to-predicted strength ratios

V_T = transverse load, kips
V_u = weld strength at $\theta = 0°$, kips
V_R = coefficient of variation
W = width of the weld face, in.
Z = Z loss dimension, in.
Z_a = mean measured Z loss dimension, in.
a = the portion of P that defines the transverse force on the weld cross section
d = diameter, in.
f_r = experimental rupture stress calculated with the measured rupture surface area, ksi
k = constraint factor
k_{ds} = directional strength increase factor
l = actual length of end-loaded weld, in.
m = degrees of freedom
n = sample size (number of experimental tests)
n = strain-hardening exponent
p = penetration ratio
p = penetration depth, in. (mm)
p_a = mean penetration depth, in. (mm)
r = radius, in.
r = strength reduction factor at the tolerance limit
r_{crit} = distance from the instantaneous center of rotation to the weld element with the minimum Δ_u/r_i ratio, in.
r_i = distance from the instantaneous center of rotation to element i, in.
w = specified fillet weld leg size, in. (mm)
w = fillet weld leg size, in. (mm)
w_1 = size of fillet weld Leg 1, in.
w_2 = size of fillet weld Leg 2, in.
w_e = expected fillet weld leg size, in.
w_m = measured fillet weld leg size, in.
w_W = equivalent weld size corresponding to W for a perfectly triangular weld, in.
Δ_m = deformation of weld element at maximum stress, in.
Δ_u = deformation of weld element at ultimate stress (rupture), in.
Δ_i = deformation of weld element at intermediate stress levels, in.
α = angle between the loading direction and the rupture plane, degrees
α_d = angle between the weld longitudinal axis and the weld displacement direction
α_R = separation factor
β = reliability index
β = length reduction factor
β_T = target reliability index
β_w = correlation factor
β_{wm} = modified correlation factor
δ_i = Δ_i/w
δ_u = Δ_u/w
ε_u = uniaxial engineering tensile rupture strain
γ_{M2} = partial safety factor

θ = angle between the line of action of the required force and the weld longitudinal axis, degrees

θ_1 = angle between the line of action of the required force and the weld longitudinal axis for the weld segment under consideration, degrees

θ_2 = angle between the line of action of the required force and the weld longitudinal axis for the weld segment in the group that is nearest to 90°

θ_p = groove angle measured from the load direction, degrees

ρ_G = bias coefficient for the geometric properties, addressing the difference between the nominal throat area based on the specified weld size and the actual throat area. ρ_G is the mean value of E_m/E.

ρ_M = bias coefficient for the material properties, addressing the difference between the specified and actual weld metal tensile strengths. ρ_{M1} is the mean value of σ_{uw}/F_{EXX}.

ρ_{M2} = bias coefficient for the material properties, addressing the difference between the nominal and actual shear-to-tensile strength ratios. ρ_{M2} is the mean value of $\tau_u/(0.6\sigma_{uw})$.

ρ_P = bias coefficient for the test-to-predicted strength ratios. Mean value of the professional factor calculated with the measured geometric and material properties

ρ_R = bias coefficient

σ_T = normal stress perpendicular to the plane of the throat, ksi.

σ_{tu} = true tensile rupture stress, ksi

σ_{uw} = uniaxial engineering tensile rupture stress of the weld metal, ksi

τ_L = shear stress in the plane of the throat, parallel to the weld axis, ksi.

τ_T = shear stress in the plane of the throat, perpendicular to the weld axis, ksi

τ_u = shear rupture stress, ksi

ψ = dihedral angle, degrees

REFERENCES

ABW (1931), *Report of Structural Steel Welding Committee*, American Bureau of Welding, American Welding Society.

AIJ (2012), *Recommendations for Design of Connections in Steel Structures*, The Architectural Institute of Japan.

AISC (2023), *Steel Construction Manual*, Sixteenth Edition, American Institute of Steel Construction, Chicago, IL.

AISC (2022), *Specification for Structural Steel Buildings*, ANSI/AISC 360-22, August 1, American Institute of Steel Construction, Chicago, IL.

AISC (1986), *Load and Resistance Factor Design Specification for Structural Steel Buildings*, September 1, American Institute of Steel Construction, Chicago, IL.

AISI (2016), *North American Specification for the Design of Cold-Formed Steel Structural Members*, American Iron and Steel Institute, Washington, D.C.

Alabi, A.A., Moore, P.L., Wrobel, L.C., Campbell, J.C. and He, W. (2018), "Tensile Behaviour of S690QL and S960QL Under High Strain Rate," *Journal of constructional steel research*, Vol.150.

Ales, J.M. (1990), *The Design of Shear Tabs Welded to Tubular Columns*, Master's Thesis, The University of Wisconsin at Milwaukee, December.

Archer, F.E., Fischer, H.K. and Kitchen, E.M. (1959), "Fillet Welds Subjected to Bending and Shear," *Civil Engineering and Public Works Review*, Vol. 54, pp. 455-458.

Archer, F.E., Fischer, H.K. and Kitchen, E.M. (1964), *The Strength of Fillet Welds*, University of New South Wales.

Arya, H.K., Singh, K. and Saxena, R.K. (2015), "Effect of Welding Parameters on Penetration and Bead Width for Variable Plate Thickness in Submerged Arc Welding," *International Journal of Mechanical and Mechatronics Engineering*, Vol. 9, No. 9.

ASTM (2020), *Standard Test Methods and Definitions for Mechanical Testing of Steel Products*, ASTM A370-20, ASTM International, West Conshohocken, PA.

ASTM (2016), *Standard Test Methods for Tension Testing of Metallic Materials*, ASTM E8-16, ASTM International, West Conshohocken, PA.

AWS (2020), *Structural Welding Code-Steel*, AWS D1.1:2020, American Welding Society, Miami, FL.

AWS (2020), *Specification for Low-Alloy Steel Electrodes and Rods for Gas Shielded Arc Welding*, AWS A5.28/A5.28M, American Welding Society, Miami, FL.

AWS (2019), *Specification for Carbon Steel Electrodes and Fluxes for Submerged Arc Welding*, AWS A5.17/A5.17M, American Welding Society, Miami, FL.

AWS (2017), *Specification for Carbon Steel Electrodes and Rods for Gas Shielded Arc Welding*, AWS A5.18/A5.18M, American Welding Society, Miami, FL.

AWS (2016), *Standard Methods for Mechanical Testing of Welds*, AWS B4.0:2016, American Welding Society, Miami, FL.

AWS (2015), *Structural Welding Code-Steel*, AWS D1.1:2015, American Welding Society, Miami, FL.

AWS (2015), *Specification for Carbon Steel Electrodes for Flux Cored Arc Welding*, AWS A5.20/A5.20M, American Welding Society, Miami, FL.

AWS (2014), *Specification for Low-Alloy Steel Electrodes for Shielded Metal Arc Welding*, AWS A5.5/A5.5M, American Welding Society, Miami, FL.

AWS (2012), *Specification for Carbon Steel Electrodes for Shielded Metal Arc Welding*, AWS A5.1/A5.1M, American Welding Society, Miami, FL.

AWS (2011), *Specification for Low-Alloy Steel Electrodes and Fluxes for Submerged Arc Welding*, AWS A5.23/A5.23M, American Welding Society, Miami, FL.

AWS (1998), *Specification for Low-Alloy Steel Electrodes for Flux Cored Arc Welding*, AWS A5.29/A5.29M, American Welding Society, Miami, FL.

AWS (1937), "Stress Distribution in Fillet Welds," *Welding Research Supplement*, May, American Welding Society, Miami, FL.

Beaulieu, D. and Picard, A. (1985), "Resultats d'essais sur des assemblages soudes excentriques en flexion," *Canadian Journal of Civil Engineering*, Vol. 12, pp. 494-506.

Barry, A., Dowswell, B., Cox, C. and Fouad, F. (2023), *Skewed Welds with Gaps*, Unpublished Draft, The University of Alabama at Birmingham.

Biggs, M.S., Crofts, M.R., Higgs, J.D. Martin, L.H. and Tzogius, A. (1981), "Failure of Fillet Weld Connections Subject to Static Loading," *Joints in Structural Steelwork, Proceedings of the Conference held at Teeside Polytechnic*, Pentech Press, London, England.

Bjork, T., Ahola, A. and Tuominen, N. (2018), "On the Design of Fillet Welds Made of Ultra-High-Strength Steel," *Welding in the World*, Vol. 62.

Bjork, T., Penttila, T. and Nykanen, T. (2014), “Rotation Capacity of Fillet Weld Joints Made of High-Strength Steel,” *Welding in the World*, Vol. 58.

Bjork, T., Toivonen, J. and Nykanen, T. (2012), “Capacity of Fillet Welded Joints Made of Ultra High-Strength Steel,” *Welding in the World*, Vol. 56.

Blackwood, R.R. (1931), “Strength of Fillet Welds in Structural Mild Steel II,” *Commonwealth Engineer*, Vol. 18, No. 3, pp. 89-97.

Blackwood, R.R. (1930), “Strength of Fillet Welds in Structural Mild Steel,” *Commonwealth Engineer*, Vol. 18, No. 2, pp. 50-55.

Bornscheuer, F.W. and Feder, D. (1966), *Tests on Welded Connections with Long or Thick Fillet Welds*, IIW Document No. XV-214-66, International Institute of Welding.

Bowman, M.D. and Quinn, B.P. (1994), "Examination of Fillet Weld Strength," *Engineering Journal*, American Institute of Steel Construction, Vol. 31, No. 3, pp. 98-108.

Bridgman, W.P. (1964), *Studies in Large Plastic Flow and Fracture with Special Emphasis on the Effects of Hydrostatic Pressure*, Harvard University Press.

Brockenbrough, R.L. and Johnston, B.G. (1974), *Steel Design Manual*, United States Steel Corporation.

Butler, L.J., Pal, S. and Kulak, G.L. (1972), “Eccentrically Loaded Welded Connections,” *Journal of the Structural Division*, American Society of Civil Engineers, Vol. 98, No. ST5, May.

Butler, L.J., and Kulak, G.L. (1971), "Strength of Fillet Welds as a Function of Direction of Load," *Welding Research Supplement*, American Welding Society, Miami, FL., pp. 231-234.

Butler, L.J., and Kulak, G.L. (1969), "Behavior of Eccentrically loaded Welded Connection," *Studies in Structural Engineering No. 7*, Nova Scotia Technical College, Halifax, Canada.

Callele, L.J., Driver, .G. and Grondin, G.Y. (2009), "Design and Behavior of Multi-Orientation Fillet Weld Connections," *Engineering Journal*, American Institute of Steel Construction, Fourth Quarter, pp. 257-272.

Callele, L.J., Grondin, G.Y. and Driver, .G. (2005), *Strength and Behavior of Multi-Orientation Fillet Weld Connections*, Structural Engineering Report No. 255, University of Alberta, February.

CEN (2021), *Eurocode 3: Design of Steel Structures—Part 1–8: Design of Joints*, prEN 1993-1-8, Draft, Brussels, Belgium.

CEN (2007), *Eurocode 3: Design of Steel Structures—Part 1–12: Additional Rules for the Extension of EN 1993 up to Steel Grades S700*, EN 1993-1-12, Brussels, Belgium.

CEN (2005), *Eurocode 3: Design of Steel Structures-Part 1-8: Design of Joints*, EN 1993-1-8, European Committee for Standardization, May, Brussels, Belgium.

Chan, S.W.K. and Ogle, M.H. (1992), "Elastic-Plastic Behavior of a Simulated Transverse Fillet-Welded Lap Joint Subjected to In-Plane Tensile Loading," *Low Cycle Fatigue and Elasto-Plastic Behavior of Materials-3*, Elsevier Applied Science.

Chen, Y., Huo, J., Hao, H., Zhou, X. and Chen, W. (2023), "Dynamic Behaviors of Butt Welds and Fillet Welds Under Intermediate Strain Rate," *Journal of constructional steel research*, Vol. 201.

Chen, Y. and Chen, Y. (2022), "Residual Shearing Strength of Fillet Weld Connections After Exposure to Elevated Temperature," *Journal of constructional steel research*, Vol. 188.

Chen, Y., Hao, H., Chen, W., Cui, J., Hao, Y. and Hua, C. (2021), "Dynamic Tensile Behaviors of Welded Steel Joint Material," *Journal of constructional steel research*, Vol. 183.

Chen, Y., Shen, Z., Zheng, Q., and Chen, C. (2001), "Experimental Study on the Performance of Single Weld Joints in H-Shaped Steel Members," *Steel Structures*, Vol. 1, pp. 201-211.

Clark, P.J. (1971), "Basis of Design for Fillet-Welded Joints Under Static Loading," Conference on Welding Product Design, Cambridge, England.

Collin, P.P. and Johansson, P.B. (2005), "Design of Welds in High Strength Steel," Proceedings of the Fourth European Conference on Steel and Composite Structures.

CSA (2014), *Design of Steel Structures*, S16-14, Canadian Standards Association, Toronto, Canada.

Dawe, J.L. and Kulak, G.L. (1974), "Welded Connections under Combined Shear and Moment," *Journal of the Structural Division*, American Society of Civil Engineers, Vol. 100, No. ST4, April.

Deng, K.L., Grondin, G.Y. and Driver, R.G. (2003), *Effect of Loading Angle on the Behavior of Fillet Welds*, Structural Engineering Report No. 251, University of Alberta, June.

Dieter, G.E. (1986), *Mechanical Metallurgy*, Third Edition, McGraw-Hill.

Douwen, A.A.V. and Witteveen, J. (1966), "Proposed Modification of the ISO Formula for the Calculation of Welded Joints," *Lastechniek*, Vol. 32, No. 6.

Dowswell, B., Cox, C., Gallow, M.S. and Fouad, F.H. (2021), *Fillet and PJP Welds*, Final Report Submitted to American Institute of Steel Construction, January 8.

Dowswell, B. (2003), "Connection Design for Steel Structures," American Society of Civil Engineers, two-day seminar that was presented in nine U.S. cities.

Dubina, D. and Stratan, A. (2002), “Behavior of Welded Connections of Moment Resisting Frames Beam-to-Column Joints,” *Engineering Structures*, Vol. 24.

Eb, W.J. (1952), “The Testing of End Fillet Welds,” IABSE Congress Report, International Association of Bridge and Structural Engineers.

Faltus, F. (1988), *Joints with Fillet Welds*, Elsevier.

Feder, D.K. (1994), “Recommendations for the Design of Long Fillet Welds,” *Welding in the World*, Vol. 33, No. 5.

Fisher, J.W., Galambos, T.V., Kulak, G.L. and Ravinda, M.K. (1978), “Load and Resistance Factor Design Criteria for Connectors,” *Journal of the Structural Division*, American Society of Civil Engineers, Vol. 104, No. ST9, September.

Freeman, F.R. (1931), “The Strength of Arc-Welded Joints,” *Proceedings of the Institution of Civil Engineers*, Paper No. 4808, January 27.

Galambos, T.V. (1992), “Chapter 3-Design Codes,” *Engineering Safety*, Ed.: Blockley, D., McGraw-Hill.

Galambos, T.V. (1985), *Reliability of Connections, Joints and Fasteners*, Structural Engineering Report No. 85-05, University of Minnesota, December.

Galambos, T.V. and Ravinda, M.K. (1978), “Properties of Steel for Use in LRFD,” *Journal of the Structural Division*, American Society of Civil Engineers, Vol. 104, No. ST9, September, pp. 1459-1468.

Galambos, T.V. and Ravinda, M.K. (1973), *Tentative Load and Resistance Factor Design Criteria for Steel Buildings*, Research Report No. 18, Department of Civil and Environmental Engineering, Washington University, September.

Gagnon, D.P. and Kennedy, D.J.L. (1989), “Behavior and Ultimate Tensile Strength of Partial Joint Penetration Groove Welds,” *Canadian Journal of Civil Engineering*, Vol. 16.

Gagnon, D.P. and Kennedy, D.J.L. (1987), *The Behavior and Ultimate Strength of Partial Joint Penetration Groove Welds*, Structural Engineering Report 151, University of Alberta, July.

Gaines, E. (1987), "Reduced Fillet Weld Sizes for Naval Ships," *Journal of Ship Production*, Vol. 3, No. 4, pp. 247-255.

Gallow, M.S. (2019), *Behavior of Fillet Welds in Skewed Joints*, Ph.D. Dissertation, The University of Alabama at Birmingham.

Ghimire, A. and Wald, F. (2023), “Deformation Behavior of High-Strength Steel Welds Using DIC,” Proceedings of Eurosteel, CE/Papers, Vol. 6, No. 3-4.

Ginn, M., Pate, M. and Wilkinson, T. (2011), "Fillet Weld Connections to High Strength Steel," *Advances in Steel and Aluminum Structures*, Research Publishing.

Godfrey, H.J. and Mount, E.H. (1940), "Pilot Tests on Covered Electrode Welds," *Welding Research Supplement*, Vol. 19, No. 4, April, American Welding Society.

Gomez, I.R., Kwan, Y.K. Kanvinde, A.M. and Grondin, G.Y. (2008), *Strength and Ductility of Welded Joints Subjected to Out-of-Plane Bending*, Draft Report, American Institute of Steel Construction, June.

Gresnigt, A.M. (1992), "Strength and Deformtion Capacity of Fillet Welds in Fe E 460," *Connections in Steel Structures II: Behavior, Strength, and Design*, Proceedings of the Second International Workshop, American Institute of Steel Construction.

Grismo, E.L., Clausen, A.H., Aalberg, A. and Langseth, M. (2017), "Fillet Welds Subjected to Impact Loading-an Experimental Study," *International Journal of Impact Engineering*, Vol. 108.

Hajro, I. and Tasic, P. (2020), "Influence of Heat Input and Welding Position on Geometrical Properties of GMAW Fillet Welds of Unalloyed Steel," *TEM Journal*, Vol. 9, No. 2.

Hall, B.W. and Pekoz, T. (1988), "Probabilistic Evaluation of Test Results," *Ninth International Specialty Conference on Cold-Formed Steel Structures*.

Higgins, T.R. and Preece, F.R. (1969), "Proposed Working Stresses for Fillet Welds," *Engineering Journal*, American Institute of Steel Construction, January.

Higgs, J.D. (1981), "A Failure Criterion for Fillet Welds," Ph.D Dissertation, The University of Aston.

IIW (1976), *Design Rules for Arc-Welded Connections in Steel Submitted to Static Loads*, International Institute of Welding.

Jaques, T.K. and Frank, K.H. (1999), *Characterization of the Material Properties of Rolled Sections*, Technical Report, SAC Joint Venture, University of Texas at Austin.

Jensen, C.D. and Crispen, R.E. (1938), "Stress Distribution in Welds Subject to Bending," *Welding Research Supplement*, October, pp. 22-24.

Kamtekar, A.G. (1987), "The Strength of Inclined Fillet Welds," *Journal of Constructional Steel Research*, Vol. 7.

Kamtekar, A.G. (1982), "A New Analysis of the Strength of Some Simple Fillet Welded Connections," *Journal of Constructional Steel Research*, Vol. 2, No. 2.

Kanvinde, A.M., Gomez, I.R., Roberts, M., Fell, B.V. and Grondin, G.Y. (2009a), "Strength and Ductility of Fillet Welds with Transverse Root Notch," *Journal of Constructional Steel Research*, Vol. 65, No. 4, pp. 948-958.

Kanvinde, A.M., Grondin, G.Y., Gomez, I.R. and Kwan, Y. (2009b), "Experimental Investigation of Fillet-Welded Joints Subjected to Out-of-Plane Eccentric Loads," *Engineering Journal*, American Institute of Steel Construction, Third Quarter, pp. 197-211.

Kato, B. and Morita, K. (1974), "Strength of Transverse Fillet Welded Joints," *Welding Journal*, Vol. 53, No. 2, pp. 59s-64s.

Kennedy, D.J.L. and Kriviak, G.J. (1985), "The Strength of Fillet Welds Under Longitudinal and Transverse Shear: A Paradox," *Canadian Journal of Civil Engineering*, Vol. 12, pp. 226-231.

Kennedy, D.J.L., Miazga, G.S. and Lesik, D.F. (1990), "Discussion of Fillet Weld Shear Strength," *Welding Journal*, May.

Khanna, C.K. (1969), *Strength of Long Fillet Welds*, Master's Thesis, Nova Scotia Technical College.

Khurshid, M., Barsoum, Z. and Barsoum, I. (2015), "Load Carrying Capacities of Butt Welded Joints in High Strength Steels," *Journal of Engineering Materials and Technology*, Vol. 137, October.

Kist, N.C. (1936), "Calculation of Welds Under Consideration of Constant Deformation Energy," IABSE Congress Report, International Association of Bridge and Structural Engineers.

Koenigsberger, F. (1951), "Design Stresses in Fillet Weld Connections," *Proceedings of the Institution of Mechanical Engineers*, Vol. 164.

Krumpen, R.P. and Jordan, C.R. (1984), *Updating of Fillet Weld Strength Parameters for Commercial Shipbuilding*, Report No. SSC-323, Ship Structure Committee, April.

Kuhlmann, U., Gunther, H.P. and Rasche, C. (2008), "High-Strength Steel Fillet Welded Connections," *Steel Construction*, Issue 1.

Kulak, G.L. (1972), "Statistical Aspects of Strength of Connections," *Specialty Conference on Safety and Reliability of Metal Structures*, American Society of Civil Engineers, November.

Kulak, G.L. and Timler, P.A. (1984), *Tests on Eccentrically Loaded Fillet Welds*, Structural Engineering Report No. 124, The University of Alberta, December.

Lawrence, F.V. and Cox, E.P. (1976), "Influence of Inadequate Joint Penetration on Tensile Behavior of A514 Steel Welds," *Welding Research Supplement*, May.

Lesik D.F, and Kennedy, D.J.L. (1990), "Ultimate Strength of Fillet Welded Connections Loaded

in Plane," *Canadian Journal of Civil Engineering*, Vol. 17, No 1, pp. 55-67.

Lesik, D.F. and Kennedy, D.J.L. (1988), *Ultimate Strength of Eccentrically Loaded Fillet Welded Connections*, Structural Engineering Report 159, University of Alberta, May.

Li, G.Q and Wang, Y.B. (2021), *Behavior and Design of High-Strength Constructional Steel*, Woodhead Publishing.

Li, C., Grondin, G.Y. and Driver, R.G. (2007), *Reliability Analysis of Concentrically Loaded Fillet Welded Joints*, Structural Engineering Report No. 271, University of Alberta, October.

Ligtenburg, F.K. (1968), *International Test Series-Final Report*, IIW Document XV-242-68, International Institute of Welding.

Lord, O.S. and Schutz, F.W. (1963), *Tensile Strengths of Steel Connections Having Transverse and Longitudinal Fillet Welds*, Final Report-Project No. A-566, Engineering Experiment Station, Georgia Institute of Technology.

Ltaief, M. and Mensinger, M. (2023), "The Effect of Temperature Actions on Single-Sided Fillet Welds in Small-Sized Box Girders of Bridges," Proceedings of Eurosteel 2023, CE/Papers.

Lu, H. and Dong, P. (2020), "An Analytical Shear Strength Model for Load-Carying Fillet-Welded Connections Incorporating Nonlinear Effects," *Journal of Structural Engineering*, Vol. 146, No. 3.

Lu, H., Dong, P. and Boppudi. S. (2015), "Strength Analysis of Fillet Welds Under Longitudinal and Transverse Shear Conditions," *Marine Structures*, Vol. 43, pp. 87-106.

Luo, P., Asada, H. and Tanaka, T. (2020a), "Limit Analysis for Partial-Joint-Penetration Weld T-Joints with Arbitrary Loading Angles," *Engineering Structures*, Vol. 213.

Luo, P., Asada, H., Uang, C.M., and Tanaka, T. (2020b), "Directionality Effect on Strength of Partial-Joint Penetration Groove Weld Joints," *Journal of Structural Engineering*, Vol. 146, No. 4.

McClellan, R.W. (1989), "Evaluation of Fillet Weld Shear Strength of FCAW Electrodes," *Welding Journal*, American Welding Society, Miami, Florida, August.

Melchers, R.E. (1999), *Structural Reliability Analysis and Prediction*, Second Edition, John Wiley & Sons.

Mellor, B.G., Rainey, R.C.T. and Kirk, N.E. (1999), "The Static Strength of End and T Fillet Weld Connections," *Materials & Design*, Vol. 20, No. 4, pp. 193-205.

Miazga, G.S., and Kennedy, D.J.L. (1989), "Behavior of Fillet Welds as a Function of the Angle of Loading," *Canadian Journal of Civil Engineering*, Vol. 16, No. 4, pp. 583-599.

Miazga, G.S., and Kennedy, D.J.L. (1986), *Behavior of Fillet Welds as a Function of the Angle of Loading*, Structural Engineering Report No. 133, University of Alberta, March.

Miller, D.K. (2022), Personal Communication.

Miller, D.K. (2017), *Welded Connections-A Primer for Engineers*, Design Guide 21, Second Edition, American Institute of Steel Construction.

Miller, D.K. and Funderburk, R.S. (2001), "Tools for Reviewing Weld Procedures," *Welding Journal*, American Welding Society, July.

Miller, D.K. (1989), "What Structural Engineers and Fabricators Need to Know About Weld Metal," *Engineering Journal*, American Institute of Steel Construction, Third Quarter.

Mocanu, D. and Buga, M. (1970), "Stress Distribution Along Side Fillet Welds and in the Plates of Lap Joints," *Experimental Stress Analysis*, The Institution of Mechanical Engineers, Paper 42.

Moon, A.R. (1948), *The Design of Welded Steel Structures*, Isaac Pitman and Sons.

Neis, V.V. (1985), "New Constitutive Law for Equal Leg Fillet Welds," *Journal of Structural Engineering*, Vol. 111, No. 8.

Ng, A.K.F., Driver, R.G. and Grondin, G.Y. (2004), "Behavior of Transverse Fillet Welds: Parametric and Reliability Analysis," *Engineering Journal*, Second Quarter, American Institute of Steel Construction.

Ng, A.K.F., Driver, R.G. and Grondin, G.Y. (2002), *Behavior of Transverse Fillet Welds*, Structural Engineering Report No. 245, The University of Alberta, October.

NSRP (1989), *Evaluation of the Fillet Weld Shear Strength of Flux Cored Arc Welding Electrodes*, NSRP No. 0297, The National Shipbuilding Research Program, September.

Packer, J.A., Sun, M. and Tousignant, K. (2016), "Experimental Evaluation of Design Procedures for Fillet Welds to Hollow Structural Sections," *Journal of Structural Engineering*, American Society of Civil Engineers, Vol. 142, No. 5.

Pathak, D., Singh, R.P., Gaur, S. and Balu, V. (2021), "To Study the Influence of Process Parameters on Weld Bead Geometry in Shielded Metal Arc Welding," *Materials Today: Proceedings*, Vol. 44.

Pham, L. (1983), "Co-ordinated Testing of Fillet Welds Part 1-Cruciform Specimens-AWRA Contract 94, AWRA Document P6-35-82," *Australian Welding Research*, December.

Popov, E.P. and Stephen, R.M. (1977), "Tensile Capacity of Partial Penetration Groove Welds," *Journal of the Structural Division*, Vol. 103, No. ST9, September.

Pradhan, R., Joshi, A.P., Sunny, M.R. and Sarkar, A. (2022), "Performance of Predictive Models to Determine Weld Bead Shape Parameters for Shielded Gas Metal Arc Welded T-Joints," *Marine Structures*, Vol. 86.

Preece, F.R. (1968), *AWS-AISC Fillet Weld Study: Longitudinal and Transverse Shear Tests*, Testing Engineers Incorporated, AISC Research Report RR-731, May 31.

Ran, M.M., Zhao, C. Sun, F.F., Li, G.Q., Wang, Y.B. and Lyu, Y.F. (2021), "Experimental Study on the Strength and Fracture Behavior of Fillet Welded Joints Made of High Strength Steel Under Multiple Loading Angles," *Thin-Walled Structures*, Vol. 169.

Ran, M.M., Sun, F.F., Li, G.Q., Kanvinde, A., Wang, Y.B. and Xiao, R. (2019), "Experimental Study on the Behavior of Mismatched Butt Joints of High-Strength Steel," *Journal of Constructional Steel Research*, Vol. 153.

Rasche, C. and Kuhlmann, U. (2009), "Investigations on Longitudinal Fillet Welded Lap Joints of HSS," Nordic Steel Construction Conference, Malmö, Sweden, September.

Rasmussen, K.J.R., Ha, J. and Lam, K.Y. (1999), "Strength of Eccentrically Loaded Incomplete Penetration Butt Welds," *Mechanics of Structures and Materials*, Balkema.

Reynolds, M., Huynh, Q., Rafezy, B.and Uang, C.M. (2020), "Strength of Partial-Joint-Penetration Groove Welds as Affected by Root Opening, Reinforcing and Loading Direction," *Journal of Structural Engineering*, Vol. 146, No. 8.

Rosenthal, D. and Levray, P. (1939), "Elastic Behavior and Strength of Side Fillet Welds," *Welding Research Supplement*, Vol. 18, No. 4, April, American Welding Society.

Sanaei, E. and Kamtekar, A.G. (1988), "Experiments on Some Arbitrarily Loaded Fillet Welds," *Welding Research Supplement*, American Welding Society, May.

Satoh, K., Seo, K., Higuchi, G. and Yatagai, T. (1974), "Experimental Study on the Mechanical Behavior and the Tensile Strength of Partial Penetration Groove Welded Joint," *Transactions of the Japan Welding Society*, Vol. 5, No. 2, September.

Schafer, B.W., Ojdrovic, R.P. and Zarghamee, M.S. (2000), "Triaxiality and Fracture of Steel Moment Connections," *Journal of Structural Engineering*, American Society of Civil Engineers, Vol. 125, No. 10, October, pp. 1131-1139.

Schmidt, B.J. and Bartlett, F.M. (2002), "Review of Resistance Factor for Steel: Data Collection," *Canadian Journal of Civil Engineering*, Vol. 29, pp. 98-108.

Schreiner, N.G. (1935), *The Behavior of Fillet Welds When Subjected to Bending Stresses*, Structural Steel Welding Committee Report, American Bureau of Welding, September.

Soliman, M., Russell, B.W., Waite, C., Shen, L. and Stringer, E. (2021), *Understanding the Behavior of Steel Connections with Bolts and Welds in Combination*, Final Report, March 1.

Soroushian, P. and Choi, K.B. (1987), "Steel Mechanical Properties at Different Strain Rates," *Journal of Structural Engineering*, American Society of Civil Engineers, Vol. 113, No. 4.

Spraragen, W. and Claussen, G.E. (1942), "Static Tests of Fillet and Plug Welds-A Review of Literature from 1932 to January 1, 1940," *Welding Research Supplement*, American Welding Society, April.

Strating, J. (1971), *The Strength of Fillet Welds Made by Automatic and Semi-Automatic Welding Processes*, Stevin Laboratory Report 6-71-6-HL 13, Delft University of Technology, March.

Sugitani, D. and Mochizuki, M. (2013), "Experimental Study on Effects of Root Gap and Fillet Size of Welds on Joint Strength," *Quarterly Journal of the Japan Welding Society*, Vol. 31, No. 4.

Sun, F.F., Ran, M.M. and Wang, Y.B. (2019), "Mechanical Behavior of Transverse Fillet Welded Joints of High Strength Steel Using Digital Image Correlation Techniques," *Journal of Constructional Steel Research*, Vol. 162.

Svensson, L.E. (1994), *Control of Microstructures and Properties in Steel Arc Welds*, CRC Press.

Swanell, P. (1981), "Rational Design of Fillet Welds," *Journal of the Structural Division*, American Society of Civil Engineers, Vol. 107, No. ST5, May.

Swannell, P. and Skewes, I.C. (1979), "The Design of Welded Brackets Loaded In-Plane: Elastic and Ultimate Load Techniques-AWRA Report P6-8-77," *Australian Welding Research*, January.

Swannell, P. (1974), "The Load-Carrying Capacity of Combined Longitudinal and Transverse Fillet Welds," *Australian Welding Journal*, September/October.

Swannell, P. (1968), "Deformation of Longitudinal Fillet Welds Subjected to a Uniform Shearing Intensity," *British Welding Journal*, March.

Teh, L.H. and Rasmussen, K.J.R. (2002), *Strength of Butt Welded Connections Between Equal-Width Rectangular Hollow Sections*, Research Report No. R817, The University of Sydney.

Thakur, S., Goga, G. and Singh, A. (2020), "Influence of Welding Parameter on Bead Geometry of Weld Metal in Submerged Arc Welding," *International Conference of Advance Research and Innovation*.

Thomas, J.H. and Tousignant, K. (2022), "Design of Single-Sided Fillet Welds Under Transverse Load," *Journal of Structural Engineering*, American Society of Civil Engineers, Vol. 98, No. ST5, May.

Thomas, J.H. (2021), *Design of Single-Sided Fillet Welds Under Transverse Loading*, Master of Applied Science Thesis, University of Toronto.

Thornton, W.A. (2020), Personal Communication.

Tide, R.H.R. (2020), Personal Communication.

Tide, R.H.R. (1980), "Eccentrically Loaded Weld Groups-AISC Design Tables," *Engineering Journal*, Fourth Quarter, American Institute of Steel Construction.

Torabian, S., Xiao, F., Haws, R.B. and Schafer, B.W. (2018), "Design of Transverse Fillet Welds in the Lapped Joints of Steel Plates," *International Journal of Steel Structures*, Vol. 18, No. 1.

Tousignant, K. and Packer, J.A. (2017), "Numerical Investigation of Fillet Welds in HSS-to-Rigid End-Plate Connections," *Journal of Structural Engineering*, Vol. 143, No. 12.

Treiberg, T. (1992), "Influence of Base and Weld Metal Strength on the Strength of Welds," *Connections in Steel Structures II: Behavior, Strength, and Design*, Proceedings of the Second International Workshop, American Institute of Steel Construction.

Troelsch, H.W. (1932), "Distribution of Shear in Welded Connections," *Proceedings of the American Society of Civil Engineers*, November.

Tsai, M. (1992), *Reliability Models of Load Testing*, Ph.D. Dissertation, University of Illinois at Urbana-Champaign.

Tuominen, N., Bjork, T. and Ahola, A. (2018), "Effect of Bending Moment on Capacity of Fillet Weld," *Tubular Structures XVI*, Taylor and Francis.

Vreedenburgh, C.G.J. (1954), "New Principles for the Calculation of Welded Joints," *Welding Journal*, Vol. 33, pp. 743-751.

Waite, C.D., Shen, L., Soliman, M. and Russel, B.W. (2022), "Experimental Investigation into the Capacity of Concentrically Loaded Steel Connections with Pretensioned High-Strength Bolts and Longitudinal Fillet Welds in Combination," *Engineering Journal*, American Institute of Steel Construction, Third Quarter.

Wastlund, G. and Ostlund, L. (1956), "Stress Distribution in Fillet Welds," IABSE Congress Report, International Association of Bridge and Structural Engineers.

Wheatley, J.M. and Baker, R.G. (1962), "Mechanical Properties of a Mild Steel Weld Metal Deposited by the Metal-Arc Process," *British Welding Journal*, Vol. 9.

Wilcox, R.C. (1995), *The Effect of Weld Penetration on the Tensile Strength of Fillet Welded Joints*, Master's Thesis, Massachusetts Institute of Technology, May.

Wilson, W.M., Munse, W.H. and Bruckner, W.H. (1949), *Fatigue Strength of Fillet-Weld, Plug-Weld, and Slot-Weld Joints Connecting Steel Structural Members*, Bulletin Series No. 380, Vol. 46, No. 68, The University of Illinois, May.

Yabe, Y., Sakamoto, S. and Yakushiji, K. (1994), "Structural Behavior of Steel Columns with Partial-Penetration Welded Joints," *Welding in the World*, Vol. 33, No. 5.

Zhao, X.L. and Hancock, G.J. (1995), "Butt Welds and Transverse Fillet Welds in Thin Cold-Formed RHS Members," *Journal of Structural Engineering*, American Society of Civil Engineers, Vol. 121, No. 11.

130 E Randolph St, Ste 2000
Chicago, IL 60601
312.670.2400
www.aisc.org

Research Report No. 02